

Lawrence Berkeley National Laboratory

Recent Work

Title

THE PHOTOCHEMISTRY OF NO₃ and THE KINETICS OF THE N₂O₅-O₃ SYSTEM

Permalink

<https://escholarship.org/uc/item/5dd1s385>

Author

Graham, Richard Allan.

Publication Date

1975-11-01

0 0 0 0 4 4 0 0 1 7 0

LBL-4147
c.1

THE PHOTOCHEMISTRY OF NO₃ AND THE
KINETICS OF THE N₂O₅-O₃ SYSTEM

Richard Allan Graham
(Ph. D. thesis)

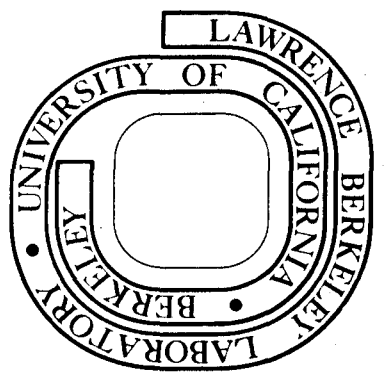
RECEIVED
LIBRARY
JAN 16 1976

November 1975

LIBRARY
PHYSICS DEPARTMENT

Prepared for the U. S. Energy Research and
Development Administration under Contract W-7405-ENG-48

For Reference
Not to be taken from this room



LBL-4147
c.1

DISCLAIMER

This document was prepared as an account of work sponsored by the United States Government. While this document is believed to contain correct information, neither the United States Government nor any agency thereof, nor the Regents of the University of California, nor any of their employees, makes any warranty, express or implied, or assumes any legal responsibility for the accuracy, completeness, or usefulness of any information, apparatus, product, or process disclosed, or represents that its use would not infringe privately owned rights. Reference herein to any specific commercial product, process, or service by its trade name, trademark, manufacturer, or otherwise, does not necessarily constitute or imply its endorsement, recommendation, or favoring by the United States Government or any agency thereof, or the Regents of the University of California. The views and opinions of authors expressed herein do not necessarily state or reflect those of the United States Government or any agency thereof or the Regents of the University of California.

THE PHOTOCHEMISTRY OF NO_3 AND THE KINETICS
OF THE N_2O_5 - O_3 SYSTEM

Contents

Abstract	v
I. Introduction	1
A. Absorption Cross Sections	1
B. N_2O_5 - O_3 Kinetics	3
C. NO_3 Photochemistry	11
II. Experimental	14
A. Methods	14
B. Apparatus	30
1. Reaction Cells and Temperature Control	30
2. Spectroscopic Signals	33
3. Electronics	35
4. Photolysis Lamps	46
C. Gases and Flow System	47
III. Experimental Procedure and Data	50
A. Absorption Cross Sections	50
1. Ultraviolet Region	51
2. Visible Region	64
3. Infrared Region	72
B. Static Cell Decays	79
1. NO_2 - O_3 Reaction	79
2. N_2O_5 - O_3 Reaction	90
3. Effects of Reactant Self-Heating	97

C.	NO_3 Steady State Concentrations	99
D.	Photolysis Lamp Calibration	103
	1. Spectral Distribution	105
	2. Light Flux Calibration	109
E.	Modulation Experiments	112
	1. Identification of Reaction Species	112
	2. NO_3 Absorption Cross Sections	115
	3. NO_3 Quantum Yields	116
	4. Oxygen Atom Reactions	120
IV.	Kinetic Results	122
	A. N_2O_5 - O_3 Kinetics	122
	B. NO_3 Photochemistry	127
	C. Oxygen Atom Reactions	133
	D. NO_3 Phase Shifts	135
V.	Discussion	140
	A. Absorption Cross Sections	140
	B. N_2O_5 - O_3 Kinetics	142
	C. NO_3 Photochemistry	144
VI.	Conclusions	146
	Acknowledgements	148
	Appendices	149
	References	172

-v-

THE PHOTOCHEMISTRY OF NO_3 AND THE KINETICS
OF THE $\text{N}_2\text{O}_5\text{-O}_3$ SYSTEM

Richard Allan Graham

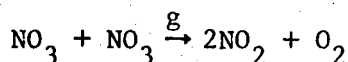
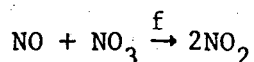
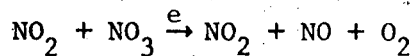
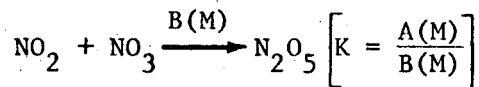
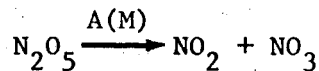
Materials and Molecular Research Division, Lawrence Berkeley Laboratory
and Department of Chemistry, University of California,
Berkeley, California 94720

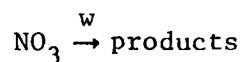
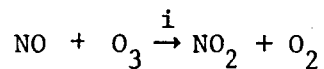
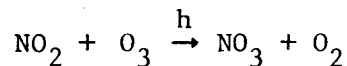
ABSTRACT

This investigation examined the kinetics of the $\text{N}_2\text{O}_5\text{-O}_3$ system and the photochemistry of the NO_3 free radical. Visible and ultraviolet absorption cross sections for NO_2 , NO_3 , HNO_2 and HNO_3 were also determined.

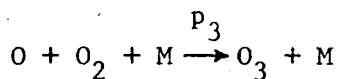
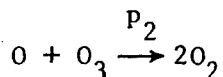
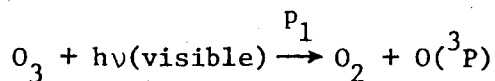
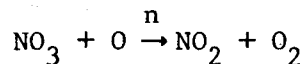
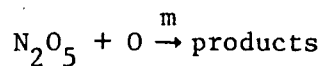
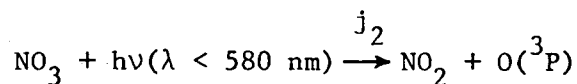
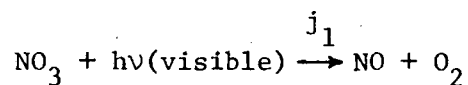
The kinetics of the $\text{N}_2\text{O}_5\text{-O}_3$ system were studied by monitoring the reactants with ultraviolet, visible, and infrared spectroscopic techniques. The techniques included steady state concentration determinations, reactant decay profiles, and molecular modulation of the reactants with intermittent photolytic illumination. The spectroscopic measurements were used to calculate rate constants for the important reactions in the system and to determine quantum yields and products for NO_3 photolysis with visible light.

The $\text{N}_2\text{O}_5\text{-O}_3$ kinetics followed the accepted mechanism²² with the addition of a first order NO_3 loss reaction that is probably heterogeneous (reaction w):





Illumination of the reactants with visible light leads to additional reactions:



Rate constants obtained for the $\text{N}_2\text{O}_5\text{-O}_3$ system were:

$$231 \text{ to } 298^\circ\text{K} \quad h = (1.34 \pm 0.11) \times 10^{-13} e^{-(4900 \pm 60)/RT} \text{ cm}^3 \text{ molecule}^{-1} \text{ sec}^{-1}$$

$$298 \text{ to } 329^\circ\text{K} \quad K = (8.4 \pm 1.8) \times 10^{26} e^{-(22210 \pm 200)/RT} \text{ molecules cm}^{-3}$$

$$298 \text{ to } 329^\circ\text{K} \quad g = (8.5 \pm 2.8) \times 10^{-13} e^{-(4870 \pm 200)/RT} \text{ cm}^3 \text{ molecule}^{-1} \text{ sec}^{-1}$$

where $R = 1.987 \text{ calorie mole}^{-1} \text{ } ^\circ\text{K}^{-1}$. The equilibrium constant K was combined with thermodynamic data to calculate

$$\Delta H_{f,300^\circ\text{K}}(\text{NO}_3) = 17.6 \pm 0.2 \text{ kcal/mole}$$

-vii-

Literature values^{40,49} for Ke and Kf were used to calculate

$$298 \text{ to } 329^\circ\text{K} \quad e = (2.5 \pm 0.5) \times 10^{-14} e^{-(2440 \pm 200)/RT} \text{ cm}^3 \text{ molecule}^{-1} \text{ sec}^{-1}$$

$$297^\circ\text{K} \quad f = (1.87 \pm 0.41) \times 10^{-11} \text{ cm}^3 \text{ molecule}^{-1} \text{ sec}^{-1}$$

The rate constants for reactions e, f and i⁵⁰ were used for second-order corrections in the calculation of K and g.

Experiments using red, gold and green photolysis lamps revealed two sets of products from the strong visible absorption spectrum of NO₃:

$$j_1: \text{ quantum yield} = 0.24 \pm 0.05 \quad 520 \leq \lambda \leq 640 \text{ nm}$$

$$j_2: \text{ quantum yield} = 0.85 \pm 0.17 \quad 470 \leq \lambda \leq 600 \text{ nm}$$

Using Leighton's tabulation¹ of the solar flux in the lower atmosphere, these quantum yields gave $j_1 = 0.040 \pm 0.008 \text{ sec}^{-1}$ and $j_2 = 0.099 \pm 0.020 \text{ sec}^{-1}$ for a solar zenith angle of 0°. Rate constants for reactions m and n were obtained by using the above rate constants and quantum yields:

$$298^\circ\text{K} \quad m \leq 2 \times 10^{-14} \text{ cm}^3 \text{ particle}^{-1} \text{ sec}^{-1}$$

$$298 \text{ to } 329^\circ\text{K} \quad n = (1.0 \pm 0.2) \times 10^{-11} \text{ cm}^3 \text{ particle}^{-1} \text{ sec}^{-1}$$

A quantum yield of one was used for the visible photolysis of ozone.^{54,55}

The rate constants for reactions p₂ and p₃ were taken from the survey by the National Bureau of Standards.⁵⁰ The rate constants calculated for reactions m and n are directly proportional to the rate constant used for reaction p₃ since the calculation of the oxygen atom concentration depended mainly on this reaction. The upper limit for the rate constant for reaction m is applicable if the reaction leads to only one set of products (NO₂+NO₂+O₂ or NO₃+NO₃); otherwise, the above value is the difference of the rate constants for the two reaction paths.

Schott and Davidson¹⁸ used their high temperature shock tube data to calculate 300°K Arrhenius expressions for e, g and K; the results of the present research had a much higher precision at this temperature and disagreed substantially with their expressions for e and g. The activation energy reported here for K is a kilocalorie higher than that of their study. The rate constant h reported here agrees well with the recent studies of Davis and co-workers³⁵ and of Herron and Huie,³⁶ but disagrees with the value reported by Johnston and Yost²⁷ in 1949. The infrared absorption band (1325 to 1375 cm^{-1}) attributed to NO_3 by Cramarossa and Johnston²⁰ was identified as N_2O_5 in the present study. A computer simulation using the Gear⁵⁶ method for coupled differential equations was used to verify that the measured rate constants accurately describe the $\text{N}_2\text{O}_5\text{-O}_3$ system under visible illumination.

I. INTRODUCTION

The oxides of nitrogen and the oxyacids of nitrogen are known to be important constituents in photochemical smog in the lower atmosphere.¹ Their role in determining the ozone balance in the stratosphere has recently become a subject of much interest: it has been proposed that the emission of oxides of nitrogen into the stratosphere by supersonic aircraft could cause damage to the ozone that shields the earth's surface against dangerous ultraviolet radiation.² Unfortunately, some of the photolytic rates and elementary reaction rates important for predicting the atmospheric effects of these species have not been well characterized. The purpose of this research was to determine some of the kinetic parameters needed to better understand atmospheric photochemistry.

A. Absorption Cross Sections

Nitric acid vapor is a by-product of photochemical smog in the lower atmosphere,¹ and it has been identified as an important trace constituent in the stratosphere.³ Absorption cross sections for nitric acid vapor have been reported by Dalmon⁴ for the 230 to 300 nm region. Schmidt et al.⁵ published a 170 to 440 nm spectrum of nitric acid with cross sections 40% higher than Dalmon's and with a strong absorption between 320 and 440 nm. Subsequent to the present work,⁶ Biaume⁷ reported nitric acid cross sections for the 185 to 325 nm region in agreement with Dalmon, and no absorption was observed at higher wavelengths. Beddard, Giachardi, and Wayne⁸ have reported cross sections from 120 to 170 nm in the vacuum ultraviolet.

Nitrous acid is known to have weak absorption bands in the 300 to 400 nm wavelength region.^{9,10} The absorption spectrum of nitrous acid was analyzed with isotopic substitution by King and Moule,¹¹ who found that the absorption bands remained diffuse under high dispersion. Although studies of the ultraviolet photochemistry of nitrous acid have been reported,^{12,13} no values for the absorption cross sections have been published.

Nitrogen dioxide absorption cross sections have been reported for the 240 to 500 nm region at 298°K by Hall and Blacet;¹⁴ they were able to separate the absorption due to the N_2O_4 dimer from their spectrum. Measurements in the 108 to 270 nm region at 300°K were reported by Nakayama¹⁵ and co-workers; no corrections for N_2O_4 were made in this work, but some concentration dependence was observed in the 185 to 240 nm region. These two studies agree within their stated error limits in the region of overlap.

Jones and Wulf¹⁶ used photographic spectroscopy to obtain the weak absorption cross sections of nitrogen pentoxide between 285 and 390 nm at room temperature. They observed no N_2O_5 absorption in the 450 nm region, but the absorption continued to increase from 285 nm to shorter wavelengths with no maximum as far as 240 nm.

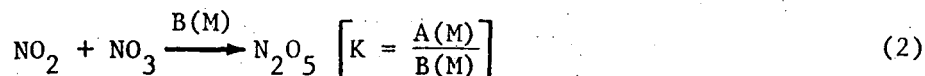
Sprenger¹⁷ monitored the intense visible absorption of the NO_3 free radical as a function of the ozone and nitrogen pentoxide in his cell, but no cross sections could be determined. Visible cross sections for NO_3 were measured by Schott and Davidson¹⁸ at high temperatures in a shock tube. They extrapolated their results to 300°K and obtained a cross section of $8.4 \times 10^{-19} \text{ cm}^2 \text{ molecule}^{-1}$ (base e)

at 652 nm. Ramsay¹⁹ studied the visible NO_3 spectrum under high dispersion and concluded that the observed diffuseness indicates predissociation. He identified a short progression in the symmetric stretching vibration of NO_3 beginning with the strong 0-0 band at 662 nm and extending to shorter wavelengths with approximately 950 cm^{-1} intervals to 559 nm. At least 15 other bands in the visible are unassigned. The only report of an infrared NO_3 absorption is a weak 1325 to 1375 cm^{-1} band observed in an $\text{N}_2\text{O}_5\text{-O}_3$ system by Cramarossa and Johnston.²⁰

The above substances all play important parts in models of the atmosphere's photochemistry. One aspect of the present research was to supply the need for quantitative absorption cross sections for these substances so that their photochemical effects could be evaluated.

B. $\text{N}_2\text{O}_5\text{-O}_3$ Kinetics

The nitrogen pentoxide catalyzed decomposition of ozone was first studied by Schumacher and Sprenger²¹ over 40 years ago. The mechanism for this process can be derived in terms of the following elementary reactions:





For conditions where the ozone concentration is much greater than that of N_2O_5 , reactions e, f and i are usually neglected.²² The remaining four reactions constitute the mechanism first proposed by Sprenger.¹⁷ By making steady state assumptions for NO_2 and NO_3 , the rate expression becomes

$$-\frac{1}{2} \frac{d[\text{O}_3]}{dt} = \frac{1}{2} (\text{Kh})^{2/3} (2g)^{1/3} (\text{O}_3)^{2/3} (\text{N}_2\text{O}_5)^{2/3} \quad (8)$$

This four-thirds order rate law was observed by Schumacher and Sprenger²¹ manometrically over a large range of conditions; their results were confirmed by other workers.^{23,24} The steady state concentration of NO_3 given by this mechanism is

$$[\text{NO}_3] = (\text{Kh}/2g)^{1/3} (\text{O}_3)^{1/3} (\text{N}_2\text{O}_5)^{1/3} \quad (9)$$

The optical densities of visible absorption bands of NO_3 were observed by Sprenger¹⁷ to have this one-third power dependence on ozone and nitrogen pentoxide.

The actual ozone destruction step in the mechanism is the reaction of ozone with nitrogen dioxide. This reaction is also the most important one involving oxides of nitrogen in the stratosphere at night. Reactions h and B(M) are responsible for converting a significant portion of stratospheric NO_2 to N_2O_5 during the night.²⁵ In 1922 Wulf, Daniels, and Karrer²⁶ titrated NO_2 with O_3 and concluded that the

observed reaction stoichiometry was two molecules of NO_2 per molecule of O_3 . This corresponds to a mechanism consisting of reactions h and B(M). The rate constant for reaction h was first reported by Johnston and Yost²⁷ in 1949. They used a stopped-flow method to study this reaction from 286 to 302°K. The disappearance of NO_2 was followed photometrically, and a reaction stoichiometry of 2.0 was measured.²⁸ Reaction B(M) was assumed to be much faster than reaction h, and the observed rate law was

$$-d[\text{NO}_2]/dt = 2h[\text{NO}_2][\text{O}_3] \quad (10)$$

Most of the other kinetic data reported for reaction h were measured near room temperature;²⁹⁻³³ Wu et al.³³ have summarized the work of these investigators. Wu et al.³³ measured the stoichiometry of the reaction in a 45 liter bell jar on a teflon coated stainless steel base plate using chemiluminescent detectors. A stoichiometry of 1.88 ± 0.15 was measured with excess ozone present and 1.68 ± 0.15 with excess nitrogen dioxide. Including reactions e, f and i in their calculations³³ resulted in a predicted stoichiometry of 1.95. The other investigators²⁹⁻³² assumed a stoichiometry of two in their data analysis.

Subsequent to the present study,³⁴ rate constants for the ozone-nitrogen dioxide reaction were reported by Davis and co-workers³⁵ using a time-of-flight mass spectrometer and by Herron and Huie³⁶ using a beam sampling mass spectrometer. Both studies monitored ozone and assumed a stoichiometry of two for their data analysis. The literature values for reaction h are summarized in Table I.

Table I. A summary of the literature values for the rate constant h .
(E_a is in calories/mole).

T(K)	h ($\text{cm}^3 \text{molecule}^{-1} \text{sec}^{-1}$)	Reference
286-302	$9.8 \times 10^{-12} \exp(-7000 \pm 600/RT)$	27
298	3.3×10^{-17}	29
298	$(6.5 \pm 3.2) \times 10^{-17}$	30
298	$(3.2 \pm 0.5) \times 10^{-17}$	31
298	1.3×10^{-17}	32
299	$(4.4 \pm 0.6) \times 10^{-17}$	33
260-343	$(9.76 \pm 0.54) \times 10^{-14} \exp(-4824 \pm 280/RT)$	35
259-362	$(1.57 \pm 0.41) \times 10^{-13} \exp(-4985 \pm 150/RT)$	36

The only experimentally determined value for the equilibrium constant K , relating $A(M)$ and $B(M)$, was measured by Schott and Davidson¹⁸ using the shock pyrolysis of N_2O_5 between 450 and 550°K. The concentrations of NO_2 and NO_3 were monitored in their experiments by visible spectroscopy. Rate constants for reactions e and g were measured in the 550 to 1100°K region using the same techniques. These results were extrapolated to 300°K with the collision theory formula¹⁸

$$E_{act} = E_o + 1/2 RT \quad (11)$$

and are listed in Table II.

Studies of other kinetic systems involving nitrogen pentoxide provide additional information about the elementary reactions in the mechanism. The thermal decomposition of N_2O_5 was first investigated by Daniels and Johnston³⁷ in 1921. The accepted mechanism for this process was proposed by Ogg^{38,39} and consists of reactions $A(M)$, $B(M)$, e, and f. The experimentally observed quantity is K_e , and the results of Johnston and Tao⁴⁰ for this product are entered in Table II. The decomposition of N_2O_5 in the presence of NO consists of reactions $A(M)$ and f, the former being rate determining.⁴¹ This reaction has been studied over an extensive range of pressure and foreign gases by Johnston and co-workers.⁴²⁻⁴⁵ Data by Mills⁴⁶ for the reaction at 300°K and one atmosphere of N_2 has been combined with an estimate⁴⁷ of the activation energy at one atmosphere and entered in Table II. Hisatsune, Crawford, and Ogg⁴⁸ used a fast-scanning infrared spectrometer to follow NO_2 and N_2O_5 in this reaction and obtained a value for the product K_f . The value for this quantity

Table II. A summary of literature values for various rate constants in the $N_2O_5-O_3$ system.

Temp. Range of Data ($^{\circ}K$)	Reaction	Pre-Exponential Factor	E_a (calories) 300 $^{\circ}K$	Reference
450-550	K	2.0×10^{26} molecules cm^{-3}	21,000 \pm 1000*	18
550-1100	e	2.8×10^{-13} cm^3 molecule $^{-1}$ sec $^{-1}$	3,900 \pm 1000	18
550-1100	g	3.2×10^{-12} cm^3 molecule $^{-1}$ sec $^{-1}$	7,100 \pm 1000	18
338-396	Ke	2.05×10^{13} sec $^{-1}$	24,650*	40
300	A	1.24×10^{14} sec $^{-1}$	20,500	46,47
297	Kf	0.71×0.014 sec $^{-1}$		49
198-330	i	$9. \times 10^{-13}$ cm^3 molecule $^{-1}$ sec $^{-1}$	2,380	50

*The energy change of the equilibrium constant with temperature is included in E_a .

recently obtained by Harker and Johnston⁴⁹ from NO_2 photolysis is included in Table II. The rate constant for the reaction of ozone with nitric oxide is taken from the NBS survey.⁵⁰ Rate constants for the remaining reactions in the mechanism, B and f, can be calculated from the information in Table II.

The rate constants in Tables I and II can be used to calculate the quantities observed by Sprenger,¹⁷ and a comparison is made in Table III between the calculated and observed quantities. The first quantity in Table III is the rate constant for the N_2O_5 catalyzed decomposition of ozone from Eq. (8), and the second quantity is from Eq. (9) for the steady state NO_3 concentration. The agreement of the reaction rates and the activation energies in the table is good, but Sprenger¹⁷ had no way to determine the absolute concentration of NO_3 in his system. Sprenger¹⁷ made his experimental observations over 40 years ago and the uncertainties are large. Since the predicted quantities depend on an extrapolation of Schott and Davidson's¹⁸ high temperature shock tube data, the uncertainties in these quantities are also large and the close agreement with Sprenger could be fortuitous.

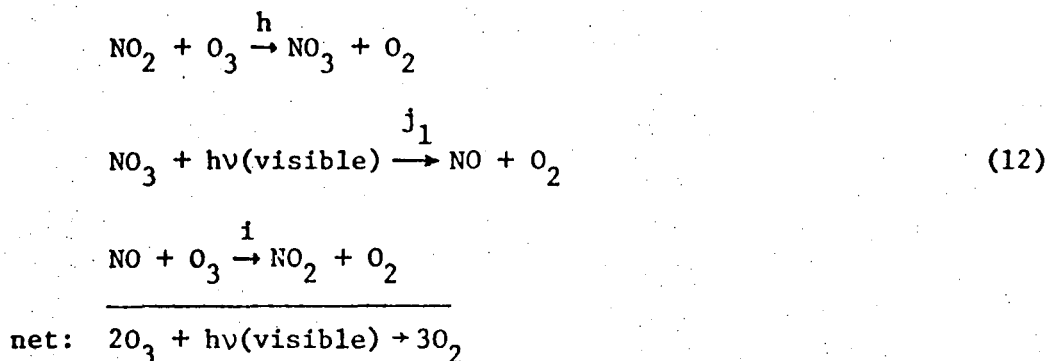
Although $\text{N}_2\text{O}_5\text{-O}_3$ kinetics have often been cited as an example of a well understood complex mechanism,^{22,51} further study of these reactions is needed due to their importance in atmospheric chemistry. The present study combines information from several experimental methods in order to reinvestigate the $\text{N}_2\text{O}_5\text{-O}_3$ system.

Table III. Summary of data on the N₂O₅ catalyzed decomposition of ozone.

Quantity	k _{300 K}	E _a (calories/mole)	Reference
$\frac{1}{2}(\text{Kh})^{\frac{2}{3}}(2\text{g})^{\frac{1}{3}}$	5.8×10^{-10} cm molecule ^{-$\frac{1}{3}$} sec ⁻¹	20,700±1000	Sprenger ¹⁷
$\frac{1}{2}(\text{Kh})^{\frac{2}{3}}(2\text{g})^{\frac{1}{3}}$	6.9×10^{-10} cm molecule ^{-$\frac{1}{3}$} sec ⁻¹	21,000±1400	18, 27
$\left(\frac{\text{Kh}}{2\text{g}}\right)^{\frac{1}{3}}$		6,400±800	Sprenger ¹⁷
$\left(\frac{\text{Kh}}{2\text{g}}\right)^{\frac{1}{3}}$	5.7×10^3 molecules ^{$\frac{1}{3}$} cm ⁻¹	7,000±1000	18, 27

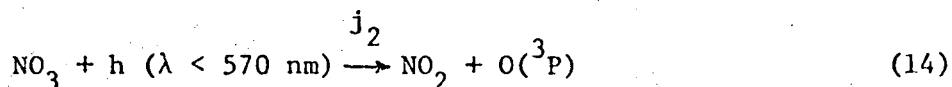
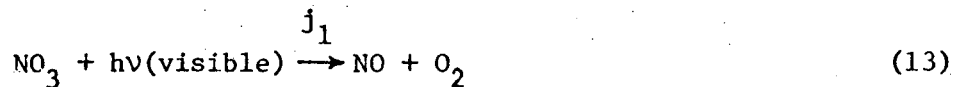
C. NO₃ Photochemistry

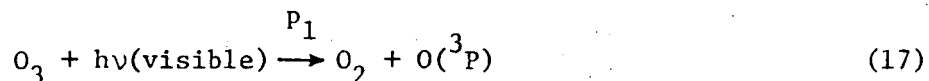
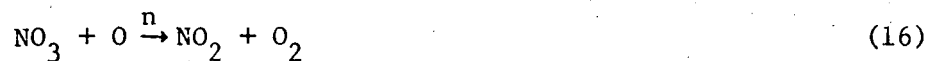
Nitrogen trioxide photolysis in the lower stratosphere has been proposed as part of a significant catalytic cycle that could destroy ozone with visible light:²



Nitrogen dioxide and ground-state oxygen atom are energetically possible products for light of wavelengths less than 570 nm; this is calculated from the enthalpy of formation for NO₃ of Schott and Davidson¹⁸ and other thermodynamic information.⁵² These alternate products would lead to no ozone destruction since the oxygen atom would react with oxygen molecule to reform ozone. No information is currently available on the quantum yields or products of NO₃ photolysis.

The N₂O₅-O₃ system provides a convenient steady state source of NO₃, but the complex interactions of reaction species in this system make it difficult to determine the primary processes in NO₃ photolysis. Several other reactions must also be considered when the system is illuminated with visible light.





Davis, as reported by Garvin and Hampson,⁵⁰ has obtained $m < 2 \times 10^{-13} \text{ cm}^3 \text{ particle}^{-1} \text{ sec}^{-1}$ with the reservations that reaction n may be causing interference and that reaction products could not be identified. Murphy⁵³ derived an upper limit for reaction m of $8 \times 10^{-14} \text{ cm}^3 \text{ particle}^{-1} \text{ sec}^{-1}$ from NO_2 photolysis in the presence of N_2O_5 . No rate constant has been reported for the reaction of oxygen atom with NO_3 . Reaction p_1 has been studied by Castellano and Schumacher^{54,55} with light in the 570 to 630 nm wavelength range. Since the highest quantum yield observed in this study was 2.0, no energy chains were formed from possible excited oxygen molecule products. Rate constants for reactions p_2 and p_3 have been reviewed by Garvin and Hampson.⁵⁰ The preferred values are:

$$p_2 = 1.9 \times 10^{-11} \exp(-2300/T) \text{ cm}^3 \text{ particle}^{-1} \text{ sec}^{-1} \quad (20)$$

$$p_3 = 6.6 \times 10^{-35} \exp(510/T) \text{ cm}^6 \text{ molecule}^{-2} \text{ sec}^{-1}, \text{ M} = \text{Ar}$$

$$\text{M: Ar}(1.0), \text{N}_2(1.6), \text{O}_2(1.7), \text{O}_3(4.0)$$

0 0 0 0 4 4 0 0 1 8 0

-13-

The interpretation of the observed photochemistry of NO_3 by visible light depends upon a combination of the above light-induced reactions and the reinvestigation of $\text{N}_2\text{O}_5\text{-O}_3$ kinetics in this research.

II. EXPERIMENTAL

A. Methods

Conventional spectroscopic methods were used to obtain absorption cross sections for the various oxides and oxyacids of nitrogen. The section on spectroscopic data (Section III-A) will contain a description of the method employed for each substance.

To carry out a more comprehensive analysis of the $N_2O_5-O_3$ system than previous investigators, this research derives information from several experimental techniques. The techniques include measurement of reactant decay profiles, determination of steady state concentrations, and molecular modulation studies of NO_3 and N_2O_5 . Combining the data from these investigations leads to values of the rate constants important in the $N_2O_5-O_3$ system and to information on the photochemistry of NO_3 .

Under the conditions of this study, the kinetics of the $N_2O_5-O_3$ system under illumination by visible light can be well described by the rate constants for reactions A through p_3 and a probably heterogeneous reaction w:



The products of reaction w were not identified, and the consequences of an analysis based on the products in Eq. (21) will be examined in the section on kinetic results (Section IV-A). The wavelength integrated products of absorption cross section, quantum yield, and light intensity for NO_3 and O_3 are also needed for the red, gold and green fluorescent lamps used in this research. The experimentally measured quantities are:

1. The rate constant h for the reaction of NO_2 with O_3 .
2. The quantity $(Kh)^{2/3} (2g)^{1/3}$ from the N_2O_5 catalyzed decomposition of O_3 either with or without photolytic illumination.
3. The quantity $(Kh/2g)^{1/3}$ from concentration measurements of N_2O_5 , O_3 and NO_3 over a broad range of concentrations.
4. The amplitude of the molecular modulation of NO_3 with oxygen or nitrogen as buffer gas and with different colored fluorescent lamps.
5. The visible absorption cross section for NO_3 from the ratio of the molecular modulation amplitudes for N_2O_5 and NO_3 .

These results can be combined with literature values of K_e , K_f , A and i to derive rate constants for reactions B through h as well as the quantum yields for NO_3 photolysis. Using literature values for p_2 and p_3 then gives approximate rate constants for reactions m and n.

Nitrogen dioxide reacts rapidly with ozone to give nitrogen trioxide; this is reaction h in our mechanism. Since reaction B(M) is orders of magnitude more rapid than reaction h under most conditions, a mechanism consisting of reactions h and B is expected for mixtures of NO_2 and O_3 . The measured reaction stoichiometry S , however, is less than two and leads to the following rate law:

$$\frac{d[\text{O}_3]}{dt} = \frac{1}{S} \frac{d[\text{NO}_2]}{dt} = -h[\text{NO}_2][\text{O}_3] \quad (22)$$

If the low stoichiometry is caused by reaction w or some other reaction that competes with reaction B for the NO_3 , data analysis based on Eq. (22)

will give a correct rate constant for reaction h, the rate determining reaction.

The kinetics of unilluminated systems containing O_3 and N_2O_5 can be well represented by reactions A through i and w. Writing steady state expressions for the low concentration intermediates NO, NO_2 and NO_3 gives:

$$\frac{d[NO]}{dt} = e[NO_2][NO_3] - f[NO][NO_3] - i[NO][O_3] = 0 \quad (23)$$

$$\begin{aligned} \frac{d[NO_2]}{dt} = & A[N_2O_5] - B[NO_2][NO_3] + 2f[NO][NO_3] \quad (24) \\ & + 2g[NO_3][NO_3] - h[NO_2][O_3] \\ & + i[NO][O_3] + w[NO_3] = 0 \end{aligned}$$

$$\begin{aligned} \frac{d[NO_3]}{dt} = & A[N_2O_5] - B[NO_2][NO_3] - e[NO_2][NO_3] - f[NO][NO_3] \\ & - 2g[NO_3][NO_3] + h[NO_2][O_3] - w[NO_3] = 0 \quad (25) \end{aligned}$$

Adding Eq. (23) to Eq. (24) and subtracting Eq. (25) leads to:

$$2e[NO_2][NO_3] + 2f[NO][NO_3] + 4g[NO_3]^2 - 2h[NO_2][O_3] + 2w[NO_3] = 0 \quad (26)$$

Equation (23) can be used for [NO], and the first two terms of Eq. (26) can be combined to give

$$\alpha e[NO_2][NO_3] + 2g[NO_3]^2 - h[NO_2][O_3] + w[NO_3] = 0 \quad (27)$$

where

$$\alpha = \frac{2f[NO_3] + i[O_3]}{f[NO_3] + i[O_3]} \quad (28)$$

Another relation can be obtained by adding Eqs. (23), (24) and (25):

$$2A[N_2O_5] - 2B[NO_2][NO_3] = 0 \quad (29)$$

This relation is solved for $[NO_2]$ with $K = A/B$ and substituted in Eq. (27):

$$\alpha Ke[N_2O_5] + 2g[NO_3]^2 - Kh \frac{[N_2O_5][O_3]}{[NO_3]} + w[NO_3] = 0 \quad (30)$$

Rearrangement gives an expression for $[NO_3]$ that must be solved iteratively:

$$[NO_3]_i = \left(\frac{Kh}{2g}\right)^{1/3} [O_3]^{1/3} [N_2O_5]^{1/3} \quad (31)$$

$$\left(1 - \frac{\alpha e}{h} \frac{[NO_3]_{i-1}}{[O_3]} - \frac{w}{Kh} \frac{[NO_3]_{i-1}^2}{[O_3][N_2O_5]}\right)^{1/3}$$

(If reactions e, f, i and w are neglected, this reduces to Eq. (9), the relation used by Sprenger.¹⁷)

In the N_2O_5 catalyzed destruction of O_3 , reaction h is the actual ozone destruction step:

$$-\frac{1}{2} \frac{d[O_3]}{dt} = \frac{1}{2} h [O_3] [NO_2] \quad (32)$$

The ozone depletion by reaction i can be neglected for the present experimental conditions since it is always less than 0.2% of that due to reaction h. Using Eqs. (29) and (31) for $[NO_2]$ and $[NO_3]$ leads to:

$$-\frac{1}{2} \frac{d[O_3]}{dt} = \frac{1}{2} h K \frac{[O_3][N_2O_5]}{[NO_3]} \quad (33)$$

and

$$-1/2 \frac{d[O_3]}{dt} = \frac{1/2(Kh)^{2/3}(2g)^{1/3}(O_3)^{2/3}(N_2O_5)^{2/3}}{\left(1 - \frac{e}{h} \alpha \frac{[NO_3]}{[O_3]} - \frac{w}{Kh} \frac{[NO_3]^2}{[O_3][N_2O_5]}\right)^{1/3}} \quad (34)$$

The equation for the second experimental quantity is

$$1/2(Kh)^{2/3}(2g)^{1/3} = \frac{-1/2 \frac{d[O_3]}{dt}}{[O_3]^{2/3}[N_2O_5]^{2/3}} \quad (35)$$

$$\left(1 - \frac{e}{h} \alpha \frac{[NO_3]}{[O_3]} - \frac{w}{Kh} \frac{[NO_3]^2}{[O_3][N_2O_5]}\right)^{1/3}$$

Since ozone and nitrogen pentoxide are measured directly, the NO_3 concentration can be calculated from Eq. (31) and Eq. (35) can then be evaluated. If the effects of reactions e, f, i and w are neglected, Eq. (35) reduces to Eq. (8), the expression derived by Sprenger.¹⁷

The third quantity, $(Kh/2g)^{1/3}$, is obtained from concentration measurements of N_2O_5 , O_3 , and NO_3 in a steady state flow system.

Equation (30) can be rearranged to give:

$$\frac{[NO_3]^3}{[O_3][N_2O_5]} = \frac{Kh}{2g} - \frac{Kh}{2g} \frac{e}{h} \alpha \frac{[NO_3]}{[O_3]} - \frac{w}{2g} \frac{[NO_3]^2}{[O_3][N_2O_5]} \quad (36)$$

By using known values for e and h, this expression can be evaluated as a linear relation:

$$\underbrace{\left(\frac{[NO_3]^3}{[O_3][N_2O_5]} + \left(\frac{Kh}{2g}\right)_{i-1} \frac{e}{h} \alpha \frac{[NO_3]}{[O_3]}\right)}_{\beta} = \left(\frac{Kh}{2g}\right)_i - \frac{w}{2g} \frac{[NO_3]^2}{[O_3][N_2O_5]} \quad (37)$$

Plotting β (the left side of Eq. (37)) vs $[\text{NO}_3]^2/[\text{O}_3][\text{N}_2\text{O}_5]$ gives $w/2g$ as the slope, and the value of the intercept, $(\text{Kh}/2g)_1$, can be solved for iteratively.

These first three quantities-- h , $(\text{Kh})^{2/3}(2g)^{1/3}$ and $(\text{Kh}/2g)$ -- can be solved simultaneously to give values for K and g . The equilibrium constant K is then used with literature values^{40,49} for K_e and K_f to calculate the rate constants e and f . These improved values for e and f are used in the recalculation of $(\text{Kh})^{2/3}(2g)^{1/3}$ and $(\text{Kh}/2g)$ from the experimental data. Since the effect of reactions e and f on the data evaluation is typically less than 10%, this process of recalculation quickly converges on final values for all of the experimentally determined rate constants.

The enthalpy of formation of NO_3 can be calculated from the van't Hoff energy E_v for the equilibrium constant K . The net change in enthalpy (all quantities at 300°K) for the equilibrium is:

$$\Delta H = \Delta H_f(\text{NO}_2) + \Delta H_f(\text{NO}_3) - \Delta H_f(\text{N}_2\text{O}_5) \quad (38)$$

and

$$\Delta H = E_v + \Delta nRT$$

Since $\Delta H_f(\text{NO}_2)$ and $\Delta H_f(\text{N}_2\text{O}_5)$ are known⁵² (7.93 and 2.7 kcal/mole), $\Delta H_f(\text{NO}_3)$ can be calculated. The energetic threshold wavelength for photolysis of NO_3 to give NO_2 and $\text{O}(^3\text{P})$ can then be calculated:

$$\Delta H = \Delta H_f(\text{NO}_2) + \Delta H_f(\text{O}^3\text{P}) - \Delta H_f(\text{NO}_3) \quad (39)$$

$$\lambda = N_0 hc/\Delta E = N_0 hc/(\Delta H - RT) \quad (40)$$

where N_0 = Avogadro's number.

The last two experimental quantities are derived from the behavior of a $N_2O_5-O_3$ steady state flow system with the photolysis lamps being turned on and off by a low frequency square wave. Since the concentrations of the chemical species vary periodically in time due to the photolysis lamps, they can be described by a Fourier series of the form

$$F(\omega t) = a_0 + \sum_{n=1}^{\infty} [a_n \sin(n\omega t) + b_n \cos(n\omega t)]$$

where $\omega = 2\pi f$ and $f =$ flashing frequency. This can also be written as

$$F(\omega t) = C_0 + \sum_{n=1}^{\infty} C_n \sin(n\omega t + \delta_n) \quad (41)$$

where $C_n = (a_n^2 + b_n^2)^{1/2}$ and $\delta_n = \tan^{-1}(b_n/a_n)$. The C_n are the amplitudes and the δ_n are the phase shifts. The flashing lamps are represented by a square wave

$$L(\omega t) = \frac{I}{2} + \frac{2I}{\pi} \sum_{\substack{\text{odd} \\ n}}^{\infty} \frac{1}{n} \sin(n\omega t) \quad (42)$$

and thus $\delta_n = 0$. The values of δ_n for other chemical species are their phase shifts relative to the photolysis lamps.

A system using red lamps for photolysis will be used for an illustrative calculation. Red light has insufficient energy for reaction j_2 to occur, and the importance of the oxygen atom reactions n and m can be suppressed by using oxygen as the carrier gas. Reactions e , f , i and w have less than a 10% effect on the NO_3 concentration and will be neglected in order to simplify the reaction set. The differential equation for NO_3 is then given by:

$$\frac{d[\text{NO}_3]}{dt} = A[\text{N}_2\text{O}_5] - B[\text{NO}_2][\text{NO}_3] - 2g[\text{NO}_3]^2 + h[\text{NO}_2][\text{O}_3] \quad (43)$$

$$+ \frac{F}{V} ([\text{NO}_3]_{\text{in}} - [\text{NO}_3]_{\text{out}}) - [\text{NO}_3] \left(\frac{j_1}{2} + \frac{2j_1}{\pi} \sum_{\substack{\text{odd} \\ n}}^{\infty} \frac{1}{n} \sin(n\omega t) \right)$$

where F = flow rate

V = volume of cell

$[\text{NO}_3]_{\text{in}}$ = concentration of NO_3 flowing into the cell

$[\text{NO}_3]_{\text{out}}$ = concentration of NO_3 flowing out of the cell

j_1 = wavelength integrated product of the light intensity,
 NO_3 absorption cross section, and primary quantum yield.

The low quantum yield of red light photolysis results in periodic changes in $[\text{NO}_3]$ that are much less than 1%. In this system NO_2 is a low concentration, fast intermediate compared to NO_3 , and an approximate steady state expression for NO_2 is

$$[\text{NO}_2] = \frac{1}{B[\text{NO}_3] + h[\text{O}_3]} \left\{ A[\text{N}_2\text{O}_5] + 2g[\text{NO}_3]^2 + [\text{NO}_3] \left[\frac{j_1}{2} + \frac{2j_1}{\pi} \sum_{\substack{\text{odd} \\ n}}^{\infty} \frac{1}{n} \sin(n\omega t) \right] \right\} \quad (44)$$

This expression is substituted into Eq. (43) to give:

$$\frac{d[\text{NO}_3]}{dt} = \frac{2}{B[\text{NO}_3] + h[\text{O}_3]} \left\{ A[\text{N}_2\text{O}_5] h[\text{O}_3] - B[\text{NO}_3] 2g[\text{NO}_3]^2 - B[\text{NO}_3]^2 \left(\frac{j_1}{2} + \frac{2j_1}{\pi} \sum_{\substack{\text{odd} \\ n}}^{\infty} \frac{1}{n} \sin(n\omega t) \right) \right\} + \frac{F}{V} ([\text{NO}_3]_{\text{in}} - [\text{NO}_3]_{\text{out}}) \quad (45)$$

Under typical experimental conditions at 298°K and one atmosphere, $B[\text{NO}_3] \geq 10 h[\text{O}_3]$ and neglecting the $h[\text{O}_3]$ term in the denominator of Eq. (45) leads to

$$\frac{d[\text{NO}_3]}{dt} = 2 \left[\frac{Kh[\text{N}_2\text{O}_5][\text{O}_3]}{[\text{NO}_3]} - 2g[\text{NO}_3]^2 \right] \quad (46)$$

$$- 2[\text{NO}_3] \left(\frac{j_1}{2} + \frac{2j_1}{\pi} \sum_{\substack{\text{odd} \\ n}}^{\infty} \frac{1}{n} \sin(n\omega t) \right) + \frac{F}{V} ([\text{NO}_3]_{\text{in}} - [\text{NO}_3]_{\text{out}})$$

For a system at steady state with respect to products and reactants, the unmodulated terms in Eq. (46) cancel out. Only the modulated or AC terms are left, and the expression for the modulation of the NO_3 concentration by the flashing lamps is:

$$\frac{d[\text{NO}_3]}{d\theta}_{\text{AC}} = -2[\text{NO}_3] \left[\frac{j_1}{\pi^2 f} \sum_{\substack{\text{odd} \\ n}}^{\infty} \frac{1}{n} \sin(n\theta) \right] \quad (47)$$

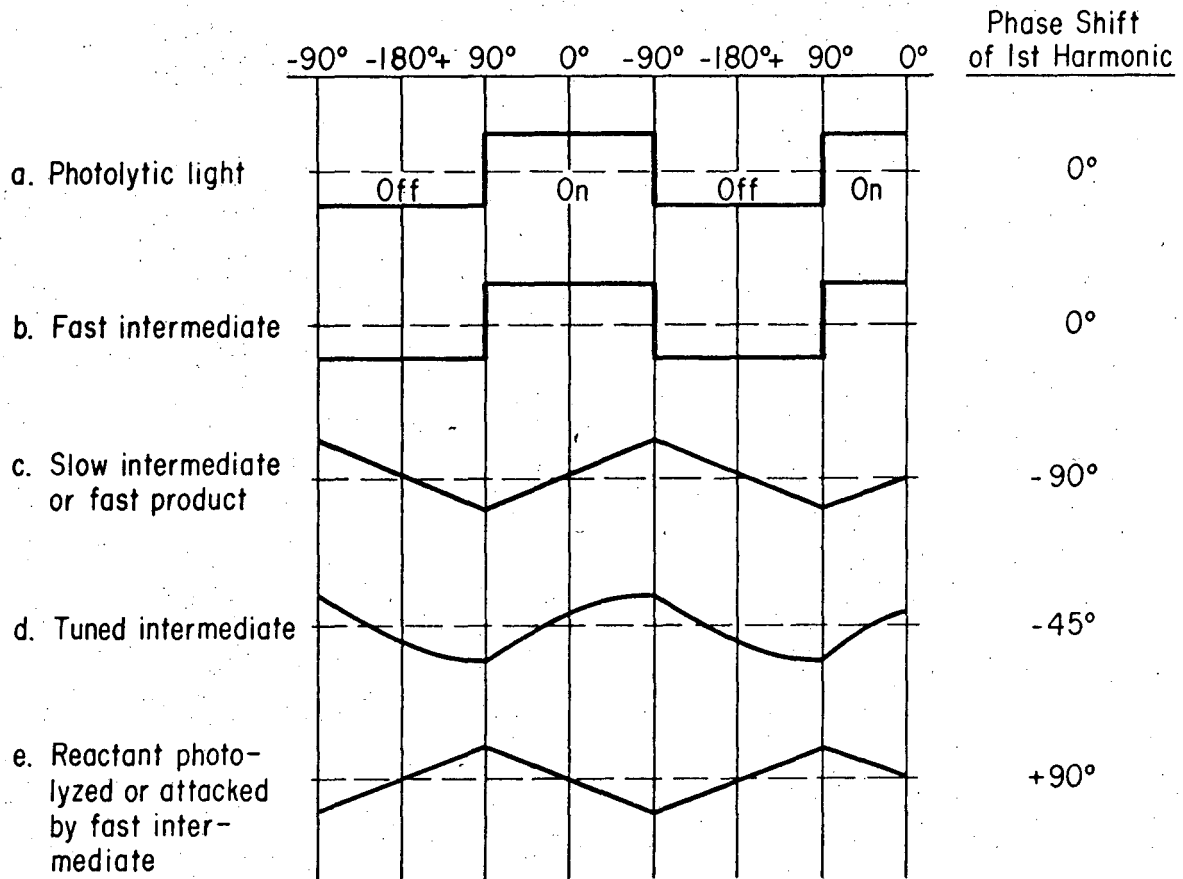
where $\theta = \omega t = 2\pi f t$. Since the modulation of the NO_3 concentration is less than 1%, $[\text{NO}_3]$ will be essentially constant and Eq. (47) integrates in closed form to give:

$$[\text{NO}_3]_{\text{AC}} = 2[\text{NO}_3] \left[\frac{j_1}{\pi^2 f} \sum_{\substack{\text{odd} \\ n}}^{\infty} \frac{1}{n^2} \cos(n\theta) \right] \quad (48)$$

Hence, the concentration modulation of NO_3 is a triangular wave with a phase shift of +90° referred to the flashing lamps (Eq. (42)). The modulation amplitude is directly proportional to the light intensity and the primary quantum yield. Only the first term of the series

in Eq. (48) is used since the experimentally measured quantities are the phase shift and amplitude of the first harmonic of the modulation signal. The above mathematical treatment has been approximate; the actual data analysis uses the complete kinetic mechanism and is performed by a computer program using the Gear method.⁵⁶

The molecular modulation method used in this study is similar to the phase shift method of obtaining fluorescence life times. The response of various reaction species to the modulation of the photolysis lamps is depicted in Fig. 1. Figure 1b is for an intermediate with a very short lifetime relative to the flashing frequency. This "fast" intermediate quickly reaches its steady state concentration when the light is on and quickly decays to zero as soon as the light is switched off. In the $N_2O_5-O_3$ system, the oxygen atom concentration meets these criteria and would have a phase shift of 0° relative to the exciting light. If the intermediate has a long lifetime relative to the flashing frequency, its concentration will increase at a constant rate while the light is on since the relative change in its concentration will be small (Fig. 1c). The resulting triangular waveform lags the exciting light by 90° . For cases where the intermediate's lifetime is comparable to the flashing frequency, the concentration profile will show exponential behavior and the phase shift will be between 0° and -90° (Fig. 1d). A reactant being photolyzed or being attacked by a fast intermediate will decay at a constant rate since the relative change in its concentration is small. Since the system is at a steady state, the reactant's concentration is slowly replenished in the dark by kinetic or flow processes. In the



XBL 759-7271

Fig. 1. Periodic response of reaction species to square wave excitation.

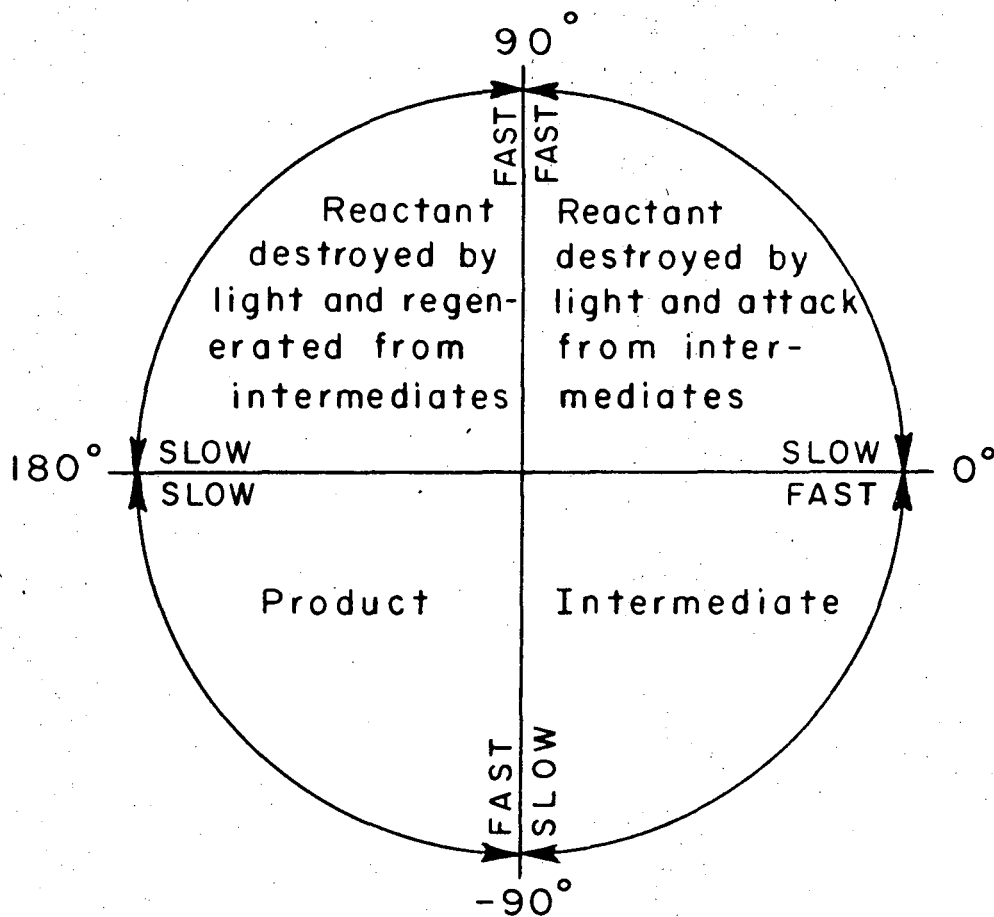
$N_2O_5-O_3$ system, NO_3 behaves like a such a reactant (Fig. 1e) with approximately a $+90^\circ$ phase shift. The photolysis of NO_3 and the reaction of NO_3 or N_2O_5 with oxygen atom, a fast intermediate, are indistinguishable processes in this system at low flashing frequencies. The expected phase shifts for various kinds of reaction species are summarized in Fig. 2.

Reactions A and B, which maintain the N_2O_5 equilibrium with NO_2 and NO_3 , are very fast compared to the modulation frequency. When NO_2 is formed by NO_3 photolysis (either directly or via the very fast $NO-O_3$ reaction), it reacts quickly with another molecule of NO_3 to form N_2O_5 and thus maintains the equilibrium. This is the physical origin of the factor of two found in Eq. (48). The N_2O_5 profile is that of a fast product (Fig. 1c) with a phase shift of -90° , and approximately one molecule of N_2O_5 is formed when two molecules of NO_3 are destroyed.

The concentration modulation of a reaction species is measured by an absorption spectroscopy technique. For absorbers that follow the Beer-Lambert law, the ratio of the monitoring light transmitted by the chemical system to that transmitted by the empty cell is related to the absorption cross section σ , the optical path length L , and the concentration c of the absorber:

$$\frac{I}{I_0} = e^{-\sigma Lc} \quad (49)$$

Small concentration changes caused by the modulation can be written as



XBL6812-7446

Fig. 2. Phase shifts of modulated reaction species.

$$\frac{I + \Delta I}{I_0} = e^{-\sigma L(c - \Delta c)} \quad (50)$$

Dividing Eq. (50) by Eq. (49) gives

$$\frac{I + \Delta I}{I} = e^{\sigma L \Delta c} \quad (51)$$

Since Δc is small, the power series expansion of the exponential is approximately $(1 + \sigma L \Delta c)$. Equation (51) then leads to

$$\frac{\Delta I}{I} = \sigma L \Delta c \quad (52)$$

Lock-in amplification techniques are used to measure the sine and cosine components, a_1 and b_1 , of the first harmonic of the modulation signal as well as the intensity I of the monitoring light. The absorber's modulation amplitude and phase shift are given by

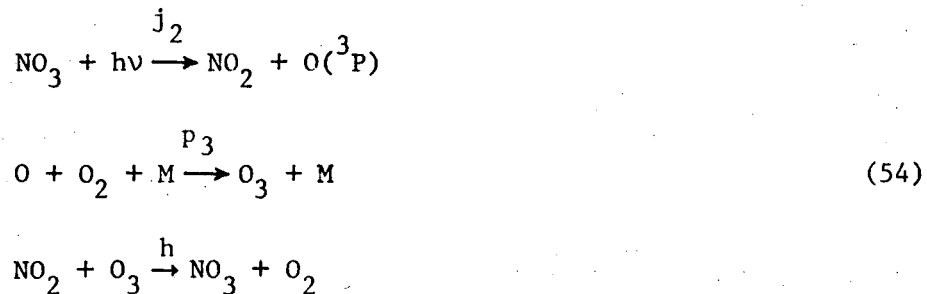
$$\Delta I = \left(a_1^2 + b_1^2 \right)^{1/2} \quad \text{and} \quad \delta_1 = \tan^{-1}(b_1/a_1) \quad (53)$$

The concentration modulation, Δc , can then be calculated from Eq. (52).

The amplitude of the NO_3 concentration modulation is the fourth experimentally measured quantity. Since Δc is the same as $[\text{NO}_3]_{\text{AC}}$ in Eq. (48), the primary quantum yield for NO_3 photolysis (contained in j_1 or j_2) can be calculated. Oxygen is used as the carrier gas to suppress contributions to the modulation amplitude from the oxygen atom reactions m and n . The quantum yields for several broad bands of visible light can be determined in this way by using photolysis lamps of different colors. After the primary quantum yields for NO_3 photolysis have been established, nitrogen can be used as the carrier gas and any changes in modulation signal will be due to oxygen atom

reactions. A known amount of oxygen is included in the system so that the oxygen atom concentration will be determined mostly by reaction p_3 . The effects due to the $O-NO_3$ reaction and the $O-N_2O_5$ reaction can be separated by varying the ratio of NO_3 to N_2O_5 . If reaction m gives O_2 and N_2O_4 (which quickly decomposes to $NO_2 + NO_2$), the NO_3 concentration modulation amplitude will be increased. The amplitude will decrease if the products of reaction m are $NO_3 + NO_3$. If both sets of products are formed, only the net amplitude change will be observed.

The products of NO_3 photolysis can be identified by observing the N_2O_5 catalyzed decomposition of ozone in an illuminated reaction cell. Oxygen is used as the M gas to suppress oxygen atom reactions. If the photolysis products are NO_2 and oxygen atom, the following reaction sequence can take place:



net: zero

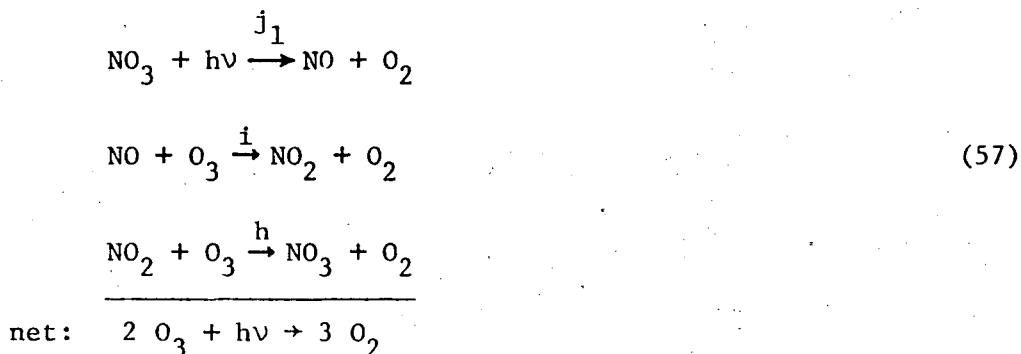
The O_3 decay will appear to be slower because the steady state NO_3 concentration has been reduced. Since photolysis is a first order process, Eq. (31) for the NO_3 steady state concentration becomes:

$$[\text{NO}_3]_i = \left(\frac{K_h}{2g}\right)^{1/3} [\text{O}_3]^{1/3} [\text{N}_2\text{O}_5]^{1/3} \left(1 - \frac{\gamma_e}{h} \frac{[\text{NO}_3]_{i-1}}{[\text{O}_3]} - \frac{w}{K_h} \frac{[\text{NO}_3]_{i-1}^2}{[\text{O}_3][\text{N}_2\text{O}_5]} - \frac{(j_1 + j_2)}{K_h} \frac{[\text{NO}_3]_{i-1}^2}{[\text{O}_3][\text{N}_2\text{O}_5]}\right)^{1/3} \quad (55)$$

where

$$\gamma = \alpha + \frac{f[\text{NO}_3] j_1 [\text{NO}_3]}{K_e [\text{N}_2\text{O}_5] (f[\text{NO}_3] + i[\text{O}_3])} \quad (56)$$

The NO_3 correction term in Eq. (35) for $1/2(K_h)^{2/3}(2g)^{1/3}$ must be similarly modified. Since oxygen is the M gas in these closed cell experiments, ozone molecules that are photolyzed are quickly reformed by reaction p_3 . If NO_3 is photolyzed to give oxygen atom, additional ozone is formed and a correction for this amount must appear in the numerator of Eq. (35) in order to obtain the correct dark value for $1/2(K_h)^{2/3}(2g)^{1/3}$. If nitric oxide is formed by NO_3 photolysis, the following ozone destroying reaction sequence can take place:



The NO_3 steady state concentration will be reduced, and a correction must also be made to Eq. (35) for the portion of the NO that reacts with ozone. (The other portion of the NO reacts with NO_3 .) The expanded form of Eq. (35) is:

$$1/2(Kh)^{2/3}(2g)^{1/3} = \frac{-1/2 \left(\frac{d[O_3]}{dt} - j_2[NO_3] + j_1(2 - \alpha)[NO_3] \right)}{[O_3]^{2/3}[N_2O_5]^{2/3}} \quad (58)$$

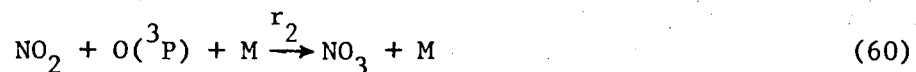
$$\left(1 - \frac{e\gamma}{h} \frac{[NO_3]}{[O_3]} - \frac{w}{Kh} \frac{[NO_3]^2}{[O_3][N_2O_5]} - \frac{(j_1 + j_2)}{Kh} \frac{[NO_3]^2}{[O_3][N_2O_5]} \right)^{1/3}$$

where $(j_2 + j_1\alpha)$ = total observed j -value for NO_3 photolysis. The values of j_1 and j_2 can be varied in Eq. (58) to give the dark value for $1/2(Kh)^{2/3}(2g)^{1/3}$. Band shapes for the photochemically active parts of the NO_3 spectrum can be roughly approximated from the overall quantum yields and the distributions of products for red, green and gold lamps. For purposes of atmospheric modeling, the wavelength integrated product (j -value) of quantum yield, absorption cross section, and solar light intensity is needed. Since the light flux in the green to red regions of the solar spectrum changes slowly with wavelength,¹ the j -values for NO_3 in the lower atmosphere have little dependence on the exact shapes of the absorption bands giving the different products.

The fifth experimental quantity, the absorption cross section for NO_3 , is used throughout this study. Equation (52) indicates that the modulation amplitude for a given reaction species is directly proportional to its absorption cross section. The concentration modulation of N_2O_5 was previously shown to be directly proportional to that of NO_3 . Therefore, the absorption cross section of N_2O_5 can be combined with the ratio of the modulation amplitudes of NO_3 and N_2O_5 to calculate the absorption cross section of NO_3 .

These five measured parameters are all necessary to describe the behavior of the N_2O_5 - O_3 system under visible illumination. The

rate constant for the $\text{NO}_2\text{-O}_3$ reaction was measured at 10°K intervals over the temperature range 231 to 298°K . The other four quantities were measured at 298, 313 and 329°K . The temperature dependence of the rate constants (A/B), g, h and w are thus well characterized. The experimentally determined rate constants can be combined with literature values for Ke, Kf, A and i to obtain a complete set of rate constants. These rate constants can then be put into a computer program using the very accurate Gear⁵⁶ method of solving coupled ordinary differential equations in order to simulate the chemical system. The rate constants⁵⁰ for the reactions

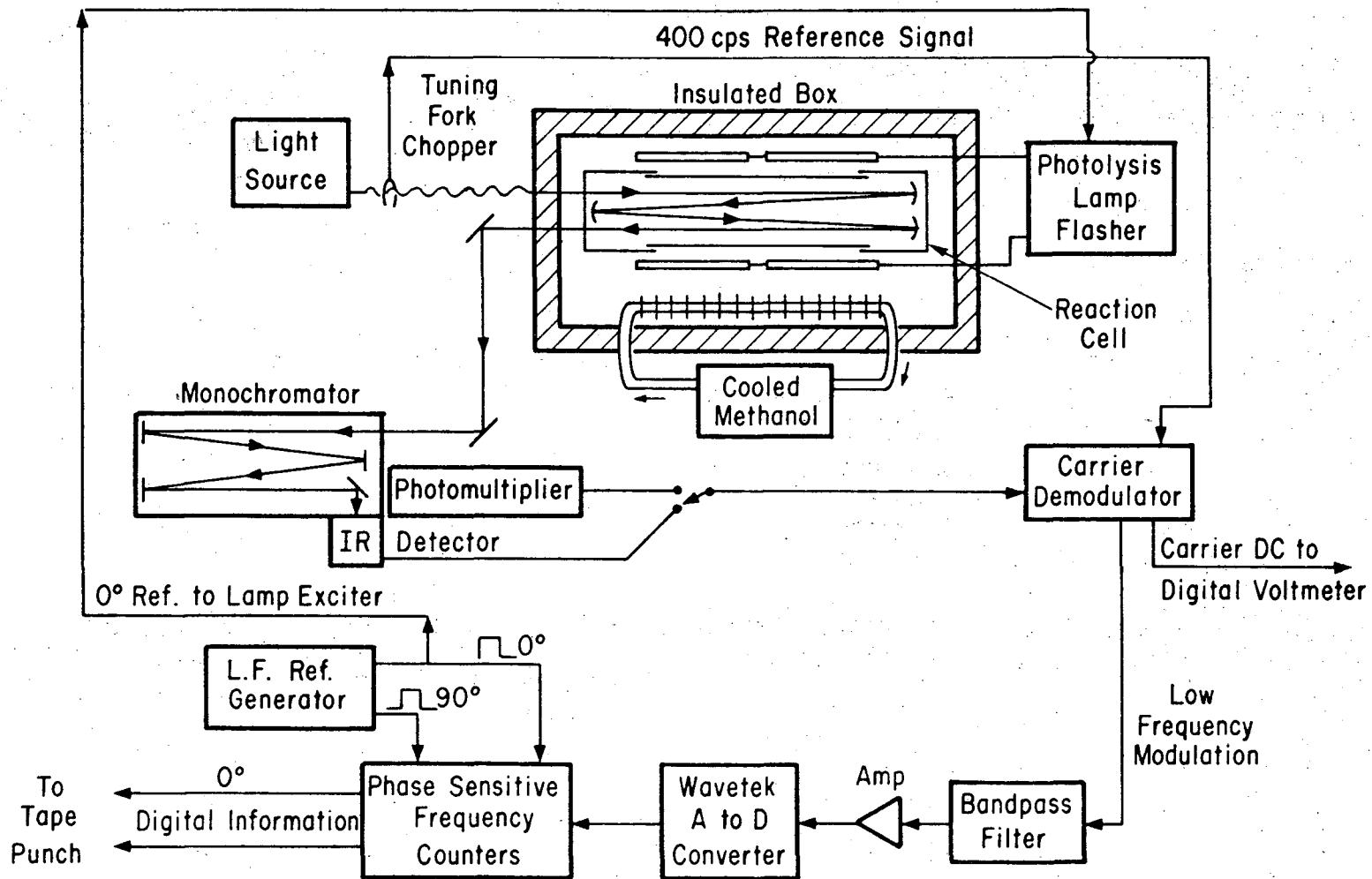


were included in all calculations, but their effects on the results were usually negligible. The phase shifts for NO_3 modulation at different flashing frequencies provide a measure of the time response of the set of reactions that determine its concentration. Computations of the expected phase shifts for the NO_3 modulation can be compared to experimental measurements to determine how well the system is described.

B. Apparatus

1. Reaction Cells and Temperature Control

A diagram of the experimental apparatus is presented in Fig. 3. The reaction cell is a cylindrical quartz tube, 15 cm in diameter and 178 cm long. The quartz tube is O-ring sealed to two nickel-plated



-31-

00004400190

XBL 759-7273

Fig. 3. Schematic diagram of experimental apparatus.

stainless steel end caps. The end caps are 18 cm and 24 cm long and are mounted in a rigid steel frame. Three 8.6 cm diameter mirrors are mounted in the end caps to give multiple reflections; optical paths of 861, 1717, 2573 and 3429 cm can be selected by an external adjustment screw. The aluminum-coated mirrors are overcoated with magnesium fluoride to maximize the ultraviolet reflectivity. The two O-ring mounted calcium fluoride windows transmit radiation from the far-ultraviolet to approximately 9.5 microns in the infrared. All O-rings were made of silicone rubber since Viton O-rings failed at temperatures below about 253°K. The reaction cell can be evacuated to less than 10^{-3} Torr by a liquid nitrogen trapped oil diffusion pump. The volume of the cell is 45.3 liters and the surface to volume ratio, including mirror mounts, is 2.52 cm^{-1} . The gas cell and optical train are mounted on a Newport Research Corporation vibration isolation table.

The cell is enclosed in an insulated box with walls of 6 in. urethane boards faced with 2 in. of coated fiberglass boards. The light beam enters through evacuated glass tubes sealed with calcium fluoride windows. Cooled methanol from a Neslab LT-9 low temperature circulator is pumped into an elevated 22 liter surge tank. The methanol then flows through a finned gravity coil mounted on top of the reaction cell frame. For work at higher temperatures, chilled water is used as fluid for the heat-exchange coil. A blower mounted inside the insulated box circulates air around the coil. The temperature of the cell is controlled by a heating wire wrapped around the cooling coil and operated by a contact thermometer and relay. Six iron-constantan

thermocouples are mounted around the cell, and one thermocouple is inside a stainless steel thermowell that extends 6 in. into the cell. The temperatures determined from these thermocouples agreed with each other to $\pm 0.2^\circ\text{K}$.

A similar reaction cell was also used for monitoring the decay of ozone in the presence of nitrogen pentoxide and for modulation experiments. This cell was constructed by Alan Harker for infrared spectroscopy.⁵⁷ Gold-coated multiple reflection mirrors are mounted in nickel-plated stainless steel end caps. A quartz tube 29 cm in diameter and 91 cm long is O-ring sealed to the end caps to give a total volume of 67.0 liters and a surface to volume ratio of 1.80 cm^{-1} . Optical path lengths between 4 and 32 meters can be obtained. A Nernst glower is the infrared source and KBr windows are used. The temperature control system for this cell was built by a co-worker, Peter Connell, and is practically identical to the one described above. The electronics, detectors, monochromator, and gas handling system used with this IR system are identical with the ones that will be described for the primary reaction cell. This secondary system will be referred to as the "IR cell", and the main reaction vessel used throughout this study will be called the "UV cell" when differentiation is necessary.

2. Spectroscopic Signals

Three light sources are used with the main reaction cell. A Sylvania DE450A deuterium arc lamp powered by a current regulated DC power supply is used for work at wavelengths below 400 nm. A tungsten

lamp powered by a Ro Associates Model 105 voltage regulated power supply is used in the visible region. Either lamp can be mounted next to a American Time Products 400 cps tuning fork chopper. The light from a 2 mm by 12 mm Nernst glower with its own 400 cps tuning fork can be used as the source beam by turning one mirror. The source beam passes through the reaction cell and then to a McPherson model 2051 one meter grating monochromator. This monochromator is used with a 150 line/mm grating blazed at 8 microns and order sorting filters for infrared spectroscopy. A 1200 line/mm grating blazed at 300 nm is used with colored glass filters for visible and ultraviolet work. A McPherson model 218 0.3 meter scanning monochromator with a 2400 line/mm grating blazed at 150 nm was used in early work for measuring absorption cross sections for HNO_3 and NO_2 .

The infrared detector is a Santa Barbara Research Center copper doped germanium photoconductor cooled to liquid helium temperature (4°K). The field of view of this detector is reduced to 40° by a liquid nitrogen cooled shield. The major source of electrical noise in the system is the detector; this noise is due to Johnson noise, shot noise, and background radiation. An EMI 9526B photomultiplier is used for ultraviolet spectroscopy, and a RCA 4832 photomultiplier is used for visible work. Both of the photomultipliers are biased by a Fluke Model 408B high voltage power supply. The infrared detector and one of the photomultipliers are mounted on the two exit slits of the one meter monochromator; turning one mirror diverts the monochromator's output from one detector to the other.

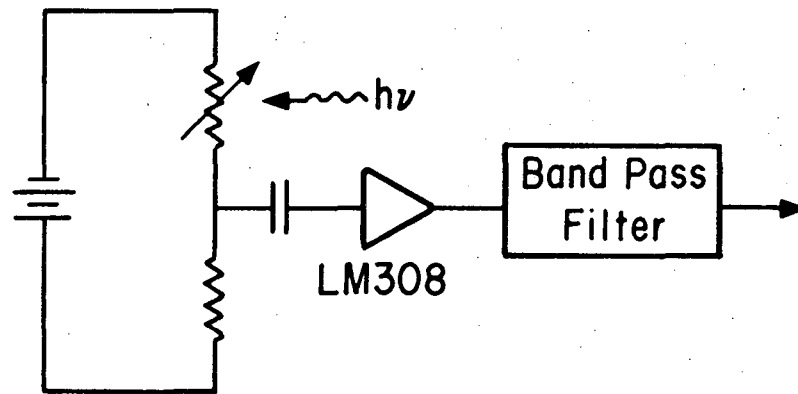
3. Electronics

a. Preamplifiers. The infrared detector circuit is depicted in Fig. 4. The resistance of the cooled photoconductor is balanced by a metal film resistor of equal value, and the circuit is biased at 135 volts to give the optimum signal to noise ratio. The signal is AC coupled to a LM308 operational amplifier set at a gain of 500. The signal is then filtered to pass frequencies from 200 to 1000 cps.

The EMI photomultiplier has a FET preamplifier with a gain of 1. The RCA photomultiplier has a LH0042 preamplifier set for a gain of 40.

b. Carrier Signal. The source beam from each of the light sources is chopped by a 400 cps tuning fork in order to have the signal information carried at a frequency above the region of electronic $1/f$ noise. The concentrations of the reaction species in the gas cell are being modulated at the flashing frequency f of the photolysis lamps. As the source beam passes through the cell, it is amplitude modulated at wavelengths where the reaction species absorb radiation. The signal produced at the detector for these wavelengths consists of the 400 cps carrier, the modulation information at the sideband frequencies $400 \pm f$ cps, and the low frequency signal at f cps which is rejected by band pass filters.

The lock-in amplifier amplifies the signal and multiplies it by a 400 cps reference signal supplied by the tuning fork driver. The output of the lock-in amplifier is the rectified 400 cps carrier signal. The $400 \pm f$ cps sidebands containing the modulation information are converted into a f cps ripple on the rectified signal. The mathematics of this process has been examined by Paukert.⁵⁸ The



XBL 759-7269

Fig. 4. Photoconductor circuitry.

signal is then split into two parts; one part is smoothed by filters and measured by a digital voltmeter. This DC voltage is directly proportional to the spectroscopic light intensity.




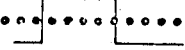
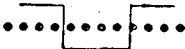

c. Dual Phase Demodulator. The other part of the signal from the 400 cps lock-in amplifier passes through a set of low frequency band pass filters that are selected for the particular flashing frequency. The resulting low frequency AC signal is amplified and drives a Wavetek model 11 voltage controlled oscillator which serves as an analog-to-digital converter. The center frequency of the Wavetek's output is set at 5000 cps, and this signal is frequency modulated by the low frequency AC modulation signal. The Wavetek square-wave output is sent to two up-down frequency counters that function as digital lock-in amplifiers.

The two digital frequency counters are controlled by references which are phase shifted 90° from each other. Table IV diagrams this counting method. The counter used for the "in phase" or sine component of the signal adds counts for the first half cycle and subtracts counts for the second half of the cycle. The "quadrature" counter provides the cosine component of the signal by counting down for the first quarter of the cycle, counting up for the second and third quarters, and counting down for the last quarter of the cycle. By counting up and down for equal periods of time, zero counts are produced due to the 5000 cps carrier signal and random noise in the signal can be averaged out to a very low level. A signal with frequency components at the switching frequency will give a net signal with a phase shift between $+180^\circ$ and -180° . (In Table IV the "-90" signal

Table IV. Examples of up-down counting for various signals.

A = counter with in phase reference

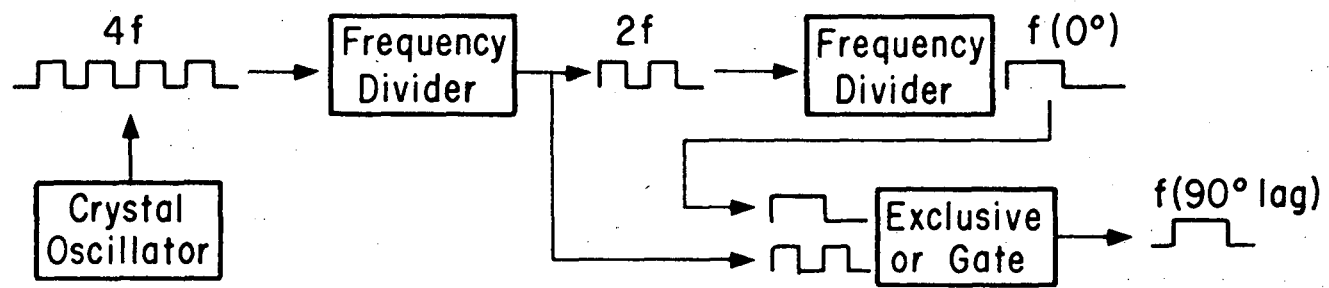
B = counter with quadrature reference (90° lag)

		1st 1/4 cycle	2nd 1/4 cycle	3rd 1/4 cycle	4th 1/4 cycle	
	A	+	+	-	-	
	B	-	+	+	-	
<u>Voltage Signal to Wavetek:</u>						<u>Result</u>
No signal	A	+100	+100	-100	-100	0
	B	-100	+100	+100	-100	0
In phase signal	A	+110	+110	-90	-90	+40
	B	-110	+110	+90	-90	0
-90° signal	A	+90	+110	-110	-90	0
	B	-90	+110	+110	-90	+40
-45° signal	A	+100	+110	-100	-90	+20
	B	-100	+110	+100	-90	+20
+90° signal	A	+110	+90	-90	-110	0
	B	-110	+90	+90	-110	-40
+90° signal	A	+105	+95	-95	-105	0
	B	-105	+95	+95	-105	-20

(a 90° lag) results in positive counts in the B counter and thus a calculated phase shift of $+90^\circ$. Since a 90° lag is arbitrarily defined as a negative phase shift in the present system, the reference signals to the counters in the laboratory are inverted so that the B counter will give negative counts for this case. Inverting the reference signals is similarly necessary for other phase shifted signals to yield answers that follow the chosen convention.)

The switching references for the counters must be very exact to prevent the carrier frequency from contributing to the net signal. The low frequency reference signals are generated from a crystal oscillator. The oscillator frequency is divided down to give a square wave signal at multiples of 0.306 cps. To produce a signal phase shifted by exactly 90° , a signal of frequency $4f$ is divided down in two steps as diagrammed in Fig. 5. This f cps signal is called the "in phase" signal and is used to drive the lamp flasher. The square waves at frequencies f and $2f$ are used in an exclusive OR circuit to generate the 90° phase shifted signal. The lamp flashing frequencies referred to in the text are nominal; the actual frequencies are 1.22 times higher⁵⁹ (e.g., 1 cps refers to 1.22 cps). The switching mechanism for the reversible counters was designed by E. D. Morris, Jr.,⁶⁰ a former graduate student of this laboratory.

The output of the in phase counter is proportional to the amplitude of the sine component of the modulation signal. The output of the quadrature counter is proportional to the amplitude of the cosine component. The amplitude and phase shift of the signal is given by



XBL 759-7270

Fig. 5. Low frequency reference generator.

$$\Delta I/I = \left(a_1^2 + b_1^2 \right)^{1/2} / V \quad \text{and} \quad \delta = \tan^{-1}(b_1/a_1) \quad (61)$$

where a_1 = number of counts from in phase counter

b_1 = number of counts from quadrature counter

V = number of counts equivalent to the DC voltage of the background light intensity.

The output of the two counters is punched on paper tape in a BCD format and is later analyzed by computer.

d. Filtering. The purpose of filtering the signal is to remove noise and the higher harmonics of the modulation signal. The higher harmonics contain kinetic information, but their amplitudes are much smaller than that of the first harmonic due to the square wave shape of the excitation and of the demodulation switching. Using only the fundamental or first harmonic of the modulation frequency simplifies the interpretation of the data and reduces signal averaging time since much of the low frequency noise is also removed by the filters.

The even harmonics of the modulation signal are cancelled out in the lock-in mixer, and the odd harmonics are multiplied by $1/n$, where n is the number of the odd harmonic. The third harmonic is reduced a factor of six by a triple section low pass filter,⁵⁹ and a factor of three by the lock-in mixer. In the square wave excitation, the third harmonic is a factor of three smaller than the fundamental; the ratio of the resulting chemical signals usually has a similar ratio. The combination of these factors makes the third harmonic approximately $1/54$ of the fundamental. This makes the higher harmonics almost negligible since modulation signals usually contain at least a 5% uncertainty. The uncertainties in some of the NO_3 signals in the

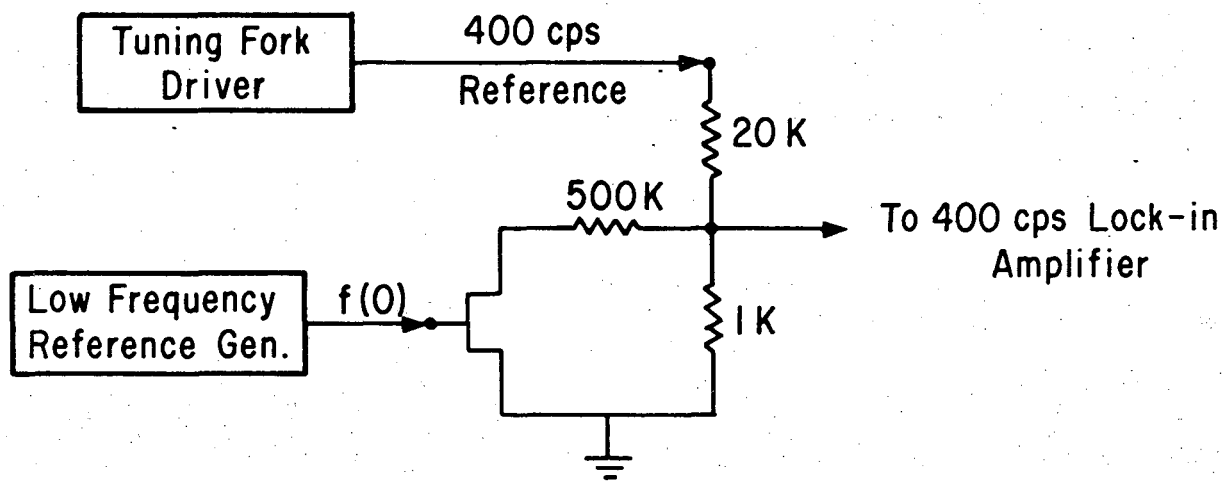
present study are smaller than this, but the triangular wave shape of these signals (Eq. (48)) discriminates against higher harmonics by another factor of $1/n$.

e. Modulation Standard. The modulation signals pass through several stages of amplification and filtering. A calibration is necessary in order to determine the effect of this signal processing on the phase of the modulation signal. The proportionality factor relating digital counts to modulation amplitude is also needed.

The circuit in Fig. 6 produces a square wave modulation with an amplitude ($\Delta I/I$) of 2×10^{-3} and a phase shift of 0° on a 400 cps carrier signal. This signal is then processed by the electronics. Since the filters extract only the first harmonic frequency of the square wave, the actual observed modulation amplitude is $4 \times 10^{-3}/\pi$. The carrier signal V in Eq. (61) is most conveniently measured in volts. At each frequency the amplitude calibration is measured as the number of counts per volt for a modulation amplitude of $4 \times 10^{-3}/\pi$. The phases measured with the modulation simulator are corrections to be subtracted from the experimentally observed quantities.

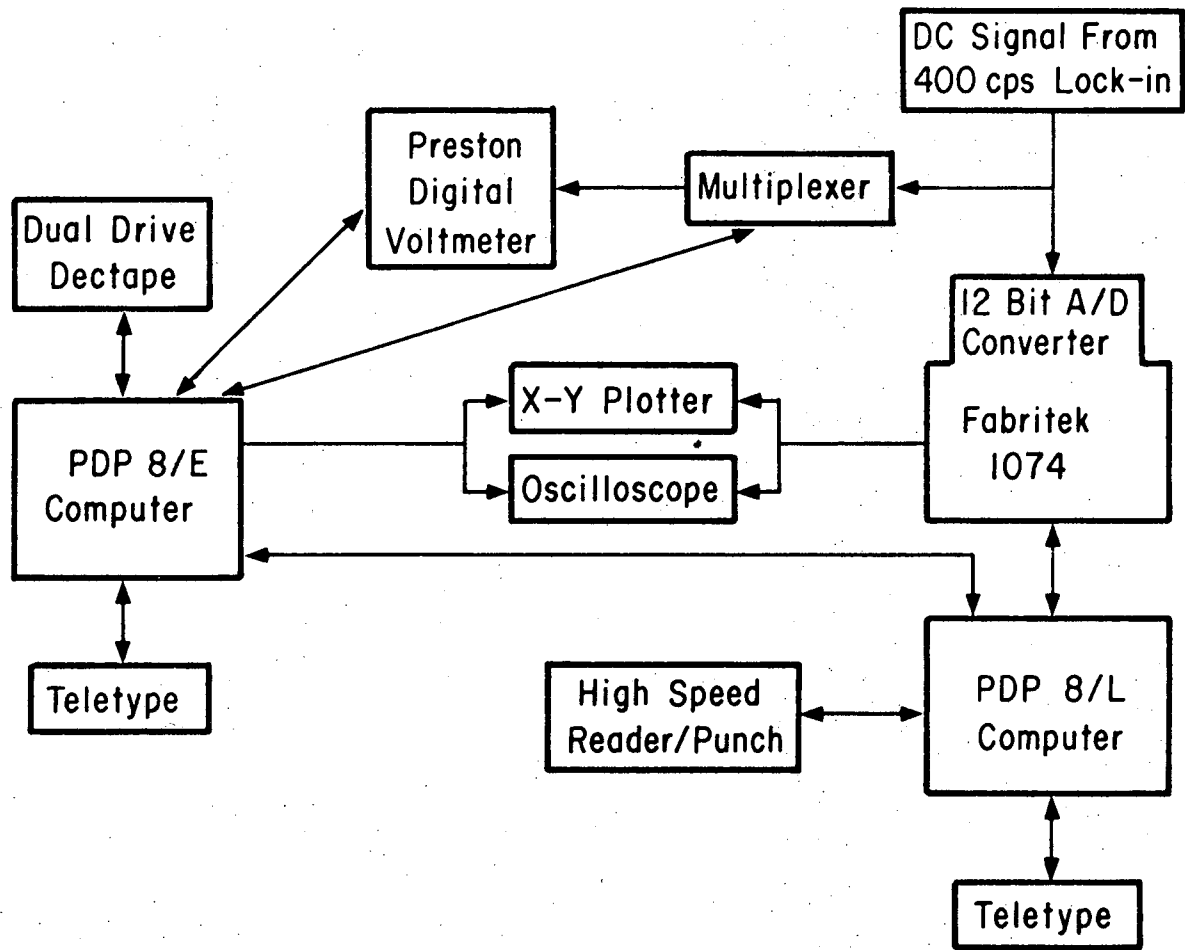
f. Computers. Two minicomputer systems were used for the acquisition and evaluation of the data in this research. A schematic diagram of the equipment configuration is provided by Fig. 7. A larger computer was used for numerical simulation of the modulation signals for the complete mechanism.

The early work on ultraviolet absorption cross sections utilized a Digital Equipment Corporation PDP 8/L minicomputer coupled to a Fabritek 1074 hard-wired signal averager. Each of these machines



XBL 759-7268

Fig. 6. Circuit for modulation standard.



XBL 759-7272

Fig. 7. Schematic diagram of laboratory computer system.

has 4096 (4K) words of memory. Spectroscopic signals are digitized by the 12-bit analog-to-digital converter of the Fabritek machine and stored in its memory. The stored spectra can be assessed by the general purpose PDP 8/L computer in order to calculate optical densities. The results can be plotted on an X-Y recorder or punched on paper tape by a high speed punch. The BCD formatted paper tape of modulation data is converted to ASCII format by this computer and punched on paper tape.

Most of this research was performed with a Digital Equipment Corporation PDP 8/E minicomputer. A computer controlled multiplexer is used to select the signal channel and amplification factor. The output of the multiplexer goes to a Preston X-Mod 723A digital voltmeter which has an accuracy of 1 part in 20,000. A programmable clock controls the sampling rate and up to 100 data points per second can be digitized and stored in the computer memory. The PDP 8/E is equipped with a dual drive Dectape unit for the storage of programs and spectra on magnetic tape. The computer is programmed⁶¹ to take spectra under interrupt control so that other calculations can be performed simultaneously. Spectra stored in the computer's memory can be displayed on an oscilloscope, plotted on an X-Y recorder, or stored on magnetic tape. An interface to the PDP 8/L computer allows the operator to utilize the high speed reader and high speed punch of that machine.

The modulation signals were simulated with a chemical kinetics program by Whitten.⁶² This program uses the Gear⁵⁶ method for solving coupled differential equations and is run on Lawrence Berkeley Laboratory's

CDC 7600 computer. A smaller version of this program was converted to Fortran II and was run on the laboratory PDP 8/E computer with its 20K of memory. A listing is provided in Appendix A.

4. Photolysis Lamps

The photolytic light for these experiments is provided by 30 watt General Electric F30T8 fluorescent lamps. Sets of red, gold and green lamps are used with four lamps per set. Two of the 36 in. lamps are placed along each side of the cell about 1 in. from the quartz. The cell is surrounded on three sides by Alzac high reflectance aluminum sheeting to increase the light intensity in the cell and make it more uniform. The electrodes on the ends of the lamps are heated to a red glow by six volt transformers to insure rapid firing of the lamps.

The lamps are powered by a 700 volt regulated power supply. The power supply switches the lamps on and off electronically in response to the in phase square wave generated by the low frequency reference generator. The light intensity is monitored by a phototransistor, mounted beneath the front end cap and pointed at the center of the cell. The output from this phototransistor reveals that the lamp output is a square wave with an initial spike. The area under the spike is less than 0.01% of the total area at one cycle per second and is, therefore, ignored. The phototransistor can be used to measure changes in the lamp output due to aging or temperature change.

C. Gases and Flow System

The carrier gases for the flow experiments were provided by Lawrence Berkeley Laboratory. High dry grade nitrogen was passed through a Matheson particulate filter and through a column containing P_2O_5 -coated glass beads in order to remove moisture. High dry oxygen was flowed through a silica tube containing copper turnings at $900^\circ K$ to convert hydrocarbons to CO_2 and water. The oxygen then passed through ascarite and P_2O_5 columns to remove the CO_2 and H_2O . Extra pure helium was used without further purification. The supplier provided the following specifications (impurities are maximums):

	<u>High Dry Nitrogen</u>	<u>High Dry Oxygen</u>	<u>Extra Pure Helium</u>
N_2	99.999% min	500 ppm	1.0 ppm
O_2	1.5 ppm	99.5% min	0.2 ppm
He	---	---	99.998% min
H_2O	1.5 ppm	1.5 ppm	0.3 ppm
CO_2	---	10 ppm	0.1 ppm
Ar	5 ppm	4000 ppm	0.1 ppm
Ne	---		14 ppm

Nitric oxide of 99.0% purity from Matheson Company was collected in a glass bulb surrounded by a dewar containing liquid nitrogen. The liquid nitrogen was poured off and the dewar was quickly replaced. The nitric oxide slowly sublimed, passed through a glass wool packed trap immersed in an isopentane slush ($113^\circ K$), and condensed in a liquid nitrogen cooled trap. Two of these vacuum distillations were performed, and the first and last portions were discarded each time.

Spectroscopic examination revealed that the pale blue solid product contained less than 1 ppm NO_2 .

Nitrogen dioxide gas of 99.5% purity from Matheson Company was liquified and stored for 2 days at 273°K with one atmosphere of oxygen. The NO_2 was then frozen at dry ice temperature, and the oxygen was pumped off. The solid was transferred twice and pumped on to remove any trapped oxygen. The white product was stored at dry ice temperature.

Nitric acid was prepared from a mixture of sodium nitrate and 96% sulfuric acid. The distilling bulb was filled at 273°K ; it was then evacuated and the temperature was raised to 313°K . The nitric acid was collected at 233°K with the first and last portions of the distillate being discarded. The white product was stored at dry ice temperature.

The above gases were prepared in a glass manifold with stainless steel Cajon Ultra-Torr fittings. Westef and Kontes high vacuum greaseless Teflon stopcocks with Viton O-rings were used. The manifold was evacuated by a liquid nitrogen trapped oil diffusion pump. An oil manometer was used for measuring gas pressures when the absorption cross sections for NO_2 and HNO_3 were measured. A Texas Instruments Model 145 quartz spiral manometer was used in subsequent work.

Ozone was prepared from the same grade of oxygen as that used for a carrier gas. The oxygen was purified by passing through a silica tube with copper turnings at 900°K , through a column containing pellets of 5% palladium on alumina at 620°K , and then through columns

of ascarite and P_2O_5 -coated glass beads. A silent electric discharge converted approximately 5% of the oxygen to ozone. The gas stream was used in the flow system or was passed through a trap containing 6 to 12 mesh silica gel at dry ice temperature to collect the ozone. The trapped ozone was desorbed from the saturator by a nitrogen carrier gas for use in the flow system, or was used for absorption cross section measurements.

A tank of 0.1% NO_2 in N_2 from Matheson Company was used in some of the flow experiments. The tank was analyzed by ultraviolet spectroscopy to contain 812 ± 9 ppm NO_2 and 43 ± 1 ppm NO . A tank of 0.65% NO_2 in N_2 was also prepared in this laboratory for use in flow experiments.

The flow rates of the gases into the reaction cell were measured with Manostat Predictability flowmeters or Hastings mass flowmeters. These flowmeters were calibrated for the gases used by an American Meter Company wet test flowmeter. Tank gases passed through a two-stage high pressure regulator, a low pressure line regulator, any purification processes applicable, a metering valve, and then the appropriate flowmeters. The gases were mixed and jetted into the reaction cell through a glass disperser tube. This tube lay in the bottom of, and ran the length of the reaction cell. The disperser tube had holes spaced an inch apart and sized to give approximately equal throughput at the typical operating condition of 4000 cm^3 per minute. The gases left the cell through a similar tube located at the top of the cell. The pressure drop through the cell at one atmosphere flow conditions was approximately 4 Torr.

III. EXPERIMENTAL PROCEDURE AND DATA

A. Absorption Cross Sections

The experimental apparatus described in the previous section was used as a single beam spectrometer for the measurement of absorption cross sections in the visible and infrared spectral regions using a tungsten lamp and a Nernst glower. The output of the ultraviolet source lamp, a deuterium arc, changed much more rapidly with time than the other light sources. For the measurement of ultraviolet cross sections, a pair of mirrors was mounted on the front of the UV gas cell. A part of the source beam was deflected by these mirrors to serve as a reference beam that could be scanned by the monochromator and used to correct for background drift. In the visible and infrared regions, adjustments of the backgrounds were made to give a zero optical density where no species absorb. These methods resulted in an average uncertainty in the optical density (base e) of 0.005 in the ultraviolet and of 0.002 in the visible and infrared regions for a single spectrum. A low pressure mercury lamp and the 486.0 nm deuterium line were used for wavelength calibration. Absorptions in the various spectral regions could be easily compared since the movement of two mirrors and the changing of the grating quickly converted the ultraviolet-visible spectrometer into an infrared instrument. The spectra were taken at 298°K unless otherwise specified. The absorption cross section σ at the average wavelength λ is defined by

$$\ln_e \left(\frac{I_o(\lambda)}{I(\lambda)} \right) = \sigma(\lambda) cL \quad (62)$$

where c is the concentration in molecules cm^{-3} , L is the optical path length in cm, I_0 is the incident beam, and I is the transmitted beam.

1. Ultraviolet Region

Nitric acid vapor samples were collected in an 80.2 cm^3 or a 2964 cm^3 bulb at 298°K , and the pressure was measured with an oil manometer. Fifteen gas samples were used and gave cell concentrations between 8×10^{13} and 6×10^{16} molecules cm^{-3} . Optical path lengths of 861 cm and 1717 cm were used with a resolution (full width at half maximum) of 0.67 nm. Nitrogen dioxide was discovered as a 0.1 to 0.2% impurity in the spectra, and its concentration was determined from its spectrum between 330 and 370 nm. The absorption due to this source was subtracted from the HNO_3 spectra. The composite spectrum of HNO_3 is presented in Fig. 8. Table V contains the HNO_3 cross sections with a standard deviation of 3% from 190 to 220 nm, 1% from 221 to 290 nm, and 5% above 290 nm. No deviations from the Beer-Lambert law were observed, and no pressure dependence was noted when one atmosphere of N_2 was added.

Nitrous acid vapor was prepared from mixtures of NO , NO_2 and H_2O . The concentration of HNO_2 was calculated from thermochemical data^{63,64} for the equilibrium



All gas pressures were measured with a Texas Instruments quartz spiral manometer. The pressure of NO_2 in a 80.2 cm^3 bulb was measured, and the NO_2 was expanded into the evacuated cell. Water vapor was added to the cell and the total pressure was measured. A large concentration

Table V. Ultraviolet absorption cross sections for NO₂, N₂O₅, HNO₃, and HNO₂ at 298 K. (N₂O₅ results of Jones and Wulf²³ are in brackets.)

λ (nm)	NO ₂	N ₂ O ₅	HNO ₃	HNO ₂
	————— cm ² molecule ⁻¹ , base e —————			
190	6.12 × 10 ⁻¹⁹		1.32 × 10 ⁻¹⁷	
191	5.63		1.24	
192	4.82		1.15	
193	4.13		1.08	
194	3.88		9.9 × 10 ⁻¹⁸	
195	3.64		9.1	
196	3.16		8.4	
197	3.22		7.7	
198	3.27		7.0	
199	3.08		6.3	
200	3.19		5.5	
201	3.57		4.86	
202	3.54		4.23	
203	3.43		3.62	
204	3.87		3.06	
205	4.27	6.9 × 10 ⁻¹⁸	2.55	
206	4.01	6.6	2.13	
207	3.97	6.3	1.77	
208	4.53	5.9	1.45	
209	4.89	5.6	1.18	
210	4.52	5.2	9.7 × 10 ⁻¹⁹	
211	4.44	4.8	7.7	
212	5.03	4.4	6.3	
213	5.44	4.0	5.1	
214	4.98	3.7	4.1	
215	4.65	3.3	3.28	
216	5.05	3.0	2.75	
217	5.65	2.76	2.26	
218	5.23	2.48	1.87	
219	4.60	2.26	1.64	

contd.

Table V, contd.

220	4.38×10^{-19}	2.06×10^{-18}	1.44×10^{-19}
221	5.09	1.89	1.27
222	5.26	1.71	1.13
223	4.41	1.55	1.01
224	3.84	1.41	9.29×10^{-20}
225	3.71	1.31	8.51
226	4.29	1.23	7.78
227	4.41	1.15	7.18
228	3.30	1.06	6.63
229	2.89	9.9×10^{-19}	6.12
230	2.52	9.3	5.63
231	3.00	9.0	5.16
232	2.99	8.4	4.77
233	2.63	8.0	4.39
234	1.62	7.5	4.05
235	1.36	7.2	3.74
236	1.73	6.9	3.45
237	1.59	6.6	3.18
238	1.59	6.3	2.97
239	1.02	6.0	2.78
240	0.90	5.7	2.60
241	0.47	5.5	2.45
242	0.61	5.3	2.33
243	1.00	5.1	2.24
244	0.505	4.7	2.17
245	0.393	4.5	2.10
246	0.353	4.3	2.05
247	0.268	4.1	2.01
248	0.165	3.8	1.99
249	0.212	3.6	1.97
250	0.345	3.5	1.95
251	0.190	3.3	1.94
252	0.150	3.0	1.94
253	0.149	2.83	1.94
254	0.149	2.72	1.94

contd.

Table V, contd.

255	0.155×10^{-19}	2.63×10^{-19}	1.94×10^{-20}
256	0.159	2.55	1.93
257	0.161	2.45	1.93
258	0.166	2.33	1.92
259	0.186	2.26	1.91
260	0.184	2.12	1.90
261	0.184	2.04	1.89
262	0.200	1.97	1.86
263	0.208	1.94	1.85
264	0.225	1.86	1.83
265	0.243	1.77	1.80
266	0.249	1.70	1.77
267	0.244	1.67	1.74
268	0.265	1.64	1.70
269	0.312	1.59	1.66
270	0.332	1.52	1.63
271	0.325	1.46	1.58
272	0.326	1.42	1.54
273	0.369	1.38	1.49
274	0.407	1.31	1.45
275	0.420	1.25	1.40
276	0.417	1.20	1.35
277	0.439	1.18	1.30
278	0.467	1.15	1.25
279	0.514	1.11	1.19
280	0.570	1.07	1.14
281	0.578	1.02	1.08
282	0.600	9.9×10^{-20}	1.03
283	0.592	9.3	9.86×10^{-21}
284	0.66	8.9	9.25
285	0.72	8.3	8.77
286	0.77	7.8	8.26
287	0.77	7.5	7.78
288	0.77	7.1	7.27

contd.

Table V, contd.

289	0.81×10^{-19}	6.7×10^{-20}	6.77×10^{-21}	
290	0.88	6.3[4.2]	6.34	
291	0.95	5.9	5.89	
292	1.02	5.7	5.51	
293	1.04	5.2	5.08	
294	0.99	4.9	4.67	
295	1.07	4.6	4.26	
296	1.07	4.4	3.97	
297	1.23	4.2	3.67	
298	1.36	3.8	3.32	
299	1.31	3.4	3.02	
300	1.33	3.2[2.45]	2.76	0.68×10^{-20}
301	1.31	2.9	2.50	0.67
302	1.40	2.7	2.26	0.59
303	1.55	2.6	2.04	0.65
304	1.63	2.4	1.86	0.70
305	1.65	2.2	1.68	0.84
306	1.64	2.1	1.52	0.87
307	1.72	1.9	1.37	0.73
308	1.77	1.8	1.21	0.83
309	1.84	1.7	1.07	0.95
310	1.97	1.5[1.3]	9.5×10^{-22}	0.91
311	1.98		8.4	0.96
312	2.09		7.3	1.10
313	2.18		6.4	1.07
314	2.12		5.5	1.25
315	2.24		4.7	1.10
316	2.29		4.0	0.74
317	2.34		3.4	0.87
318	2.57		2.7	1.34
319	2.55		2.2	1.29
320	2.61	$[7.5 \times 10^{-21}]$	1.8	1.60
321	2.70		1.4	2.15
322	2.69		1.0	1.77
323	2.84		0.7	1.75

contd.

Table V, contd.

324	2.86×10^{-19}	0.4×10^{-22}	2.03×10^{-20}
325	2.94	0.2	1.66
326	3.12		1.24
327	3.13		1.88
328	3.20		2.80
329	3.21		2.10
330	3.38	$[4.0 \times 10^{-21}]$	2.85
331	3.33		4.08
332	3.39		2.75
333	3.78		2.17
334	3.68		2.56
335	3.61		2.55
336	3.72		2.03
337	3.79		1.66
338	3.70		2.59
339	4.17		4.19
340	4.17	$[2.7 \times 10^{-21}]$	3.09
341	4.28		4.23
342	4.39		7.75
343	3.98		4.71
344	4.12		2.84
345	4.30		2.87
346	4.47		3.05
347	4.72		2.82
348	4.79		2.31
349	5.15		2.38
350	4.48	$[1.8 \times 10^{-21}]$	3.50
351	4.71		4.72
352	4.73		4.26
353	4.55		6.44
354	4.87		10.09
355	5.53		9.98
356	5.00		4.88
357	5.40		3.26

contd.

Table V, contd.

358	5.64×10^{-19}		3.22×10^{-20}
359	5.10		2.95
360	4.96	$[1.0 \times 10^{-21}]$	2.54
361	5.39		2.25
362	5.45		2.17
363	5.45		2.46
364	5.37		3.37
365	5.84		4.03
366	6.04		4.56
367	5.51		6.54
368	5.79		10.79
369	5.66		10.56
370	5.70	$[4.7 \times 10^{-22}]$	6.06
371	5.56		3.59
372	6.09		2.73
373	6.20		2.30
374	5.81		1.81
375	5.74		1.45
376	6.40		1.28
377	6.48		1.39
378	5.73		1.52
379	5.82		1.82
380	6.52	$[1.3 \times 10^{-22}]$	2.20
381	6.45		2.76
382	6.18		3.61
383	5.92		4.86
384	6.18		5.80
385	6.45		5.35
386	6.27		3.90
387	6.11		2.57
388	6.39		1.72
389	6.41		1.17
390	6.51		0.84
391	6.44		0.60

contd.

Table V, contd.

392	6.71×10^{-19}	0.60×10^{-20}
393	6.31	0.49
394	5.95	0.36
395	6.08	0.29
396	6.58	0.28
397	6.03	0.23
398	6.49	0.17
399	6.61	0.18
400	6.68	0.12
401	6.96	
402	6.42	
403	5.84	
404	6.15	
405	6.52	
406	6.22	
407	5.50	
408	6.13	
409	6.91	
410	6.59	
411	6.61	
412	5.76	
413	6.55	
414	6.92	
415	6.03	
416	5.38	
417	5.37	
418	5.80	
419	5.96	
420	6.24	

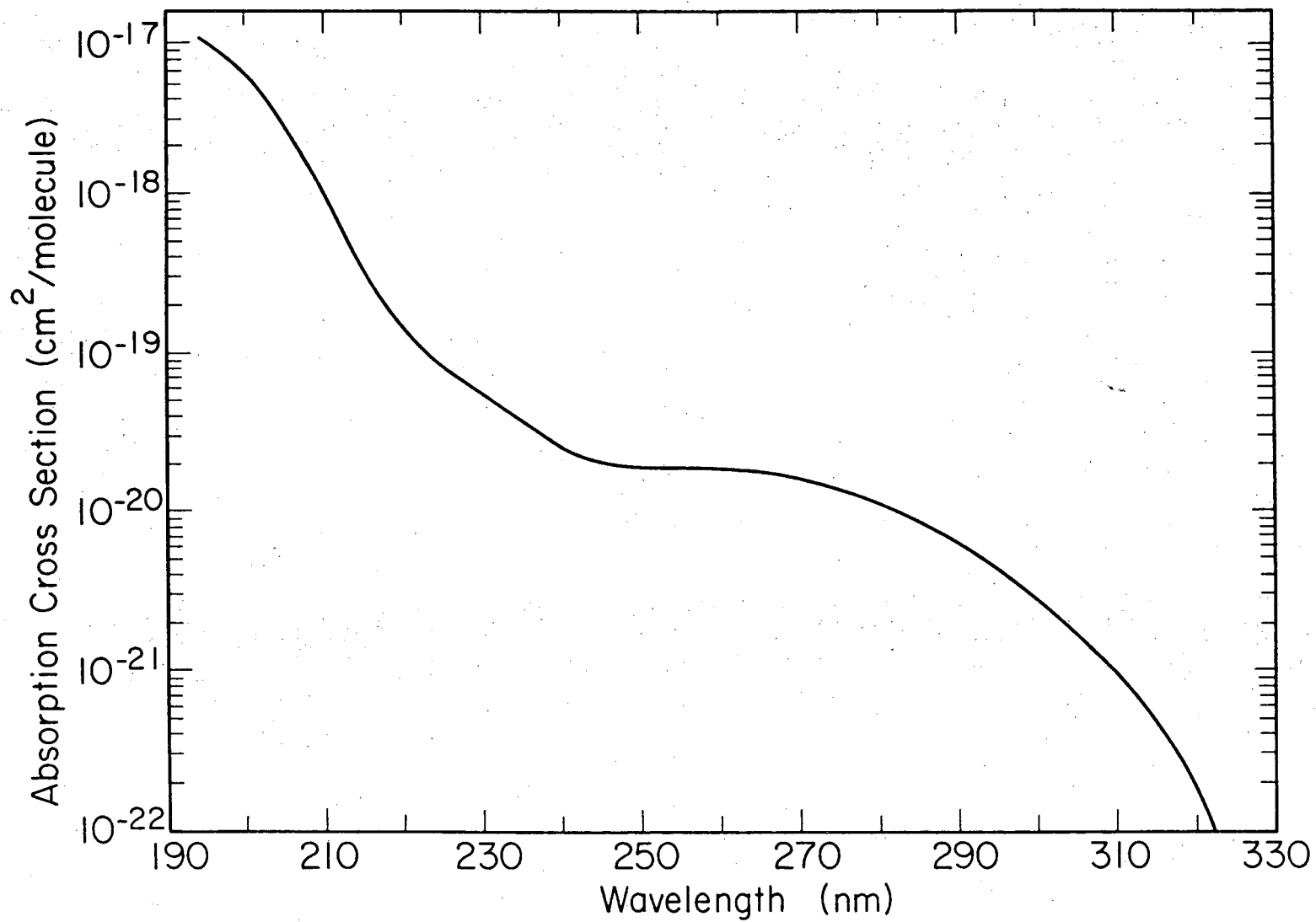


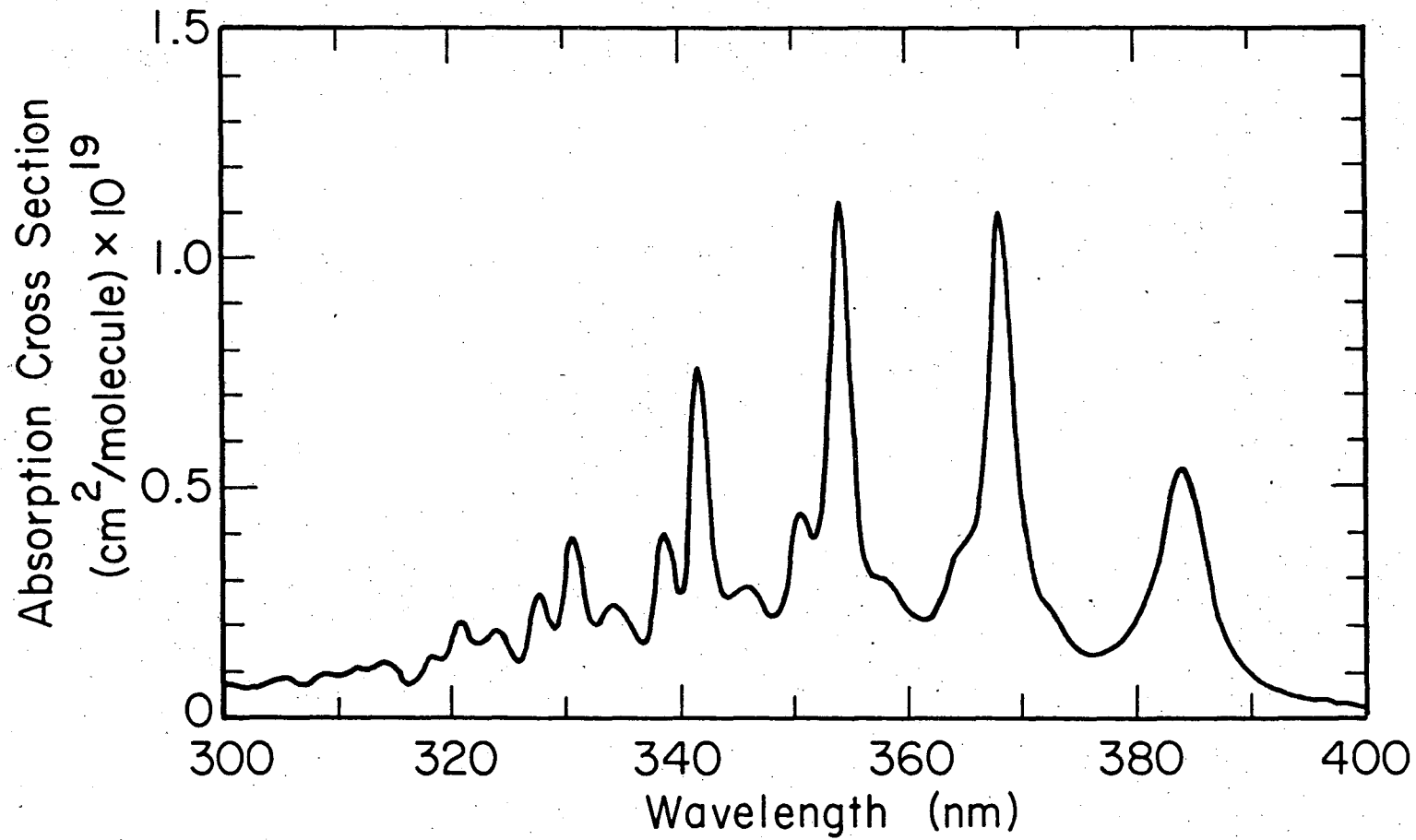
Fig. 8. Nitric acid (HNO₃) ultraviolet spectrum at 298°K.

XBL 759-7281

of NO was added, and the total pressure was measured again. The residual concentration of NO₂ was determined from its absorption spectrum above 400 nm. The NO and H₂O concentrations were determined from the initial pressure measurements with a small correction for the HNO₂ formed. Corrections for the intense structureless spectrum of N₂O₃ were made by obtaining its spectrum in separate experiments. The N₂O₃ concentration was calculated from the data of Verhoek and Daniels.⁶⁵ The corrections to the HNO₂ spectrum between 300 and 400 nm due to NO₂ and N₂O₃ were much larger than the actual HNO₂ absorption. Other complications were uncertainties in the N₂O₃ corrections and possible mixing problems. Since this introduced considerable uncertainty in regions of low HNO₂ cross section, the best run was selected for presentation of Table V and Fig. 9. The uncertainty in the absolute value of the cross section is estimated to be ±20%. The conditions for the chosen run were 298°K, 861 cm path, 0.83 nm resolution, and

	Molecules cm ⁻³
NO	2.97×10 ¹⁹
NO ₂	1.09×10 ¹⁵
H ₂ O	6.5×10 ¹⁶
N ₂ O ₃	1.3×10 ¹⁵ (calc.)
HNO ₂	1.43×10 ¹⁶ (calc.)

In other experiments several aliquots of He and H₂O were added to a similar mixture of gases. Beer's law was obeyed within the above experimental uncertainty over the HNO₂ concentration range of (2-8)×10¹⁵ molecules cm⁻³.



-61-

00004400205

XBL 759-7278

Fig. 9. Nitrous acid (HNO₂) near ultraviolet spectrum at 298°K.

Nitrogen dioxide gas samples were collected in a 80.2 cm^3 bulb immersed in a 298.0°K water bath, and the pressure was measured by an oil manometer. Corrections for N_2O_4 were made using the equilibrium constant data of Verhoek and Daniels.⁶⁵ The samples were then expanded into the evacuated cell. The absorption spectrum is calculated from gas samples with $(1-10)\times 10^{14}$ molecules cm^{-3} . The maximum amount of N_2O_4 present, as calculated from thermodynamic data,⁵² was always less than 0.1% of the NO_2 concentration. Optical pathlengths of 861 or 1717 cm were used. The spectra from 190 to 420 nm were taken with the 0.3 meter monochromator using 0.5 mm slits for a resolution of 0.67 nm. Table V contains the NO_2 cross sections averaged over each nm with an uncertainty of approximately 3% between 240 and 290 nm and 1% elsewhere. The NO_2 spectrum is presented in Fig. 10. The Beer-Lambert absorption law was obeyed and no pressure dependence was observed between 50 millitorr and one atmosphere total pressure. The manner in which the buffer gas was added, however, could cause long term fluctuations of up to 10% in the cross section due to poor mixing.

Nitrogen pentoxide was prepared from O_3 and NO_2 in a one atmosphere flow system. The concentrations of N_2O_5 , HNO_3 and O_3 , all of which absorb in the ultraviolet region, were determined from their infrared absorptions. The nitric acid was apparently formed by a heterogeneous reaction of the N_2O_5 with ppm concentrations of H_2O in the carrier gas. According to Morris and Niki,⁶⁶ the reaction of water with N_2O_5 to give HNO_3 has a gas phase reaction rate of less than 1.3×10^{-20} at 298°K . The fast heterogeneous rate they observed for this process is probably the cause of nitric acid formation in the present system. For

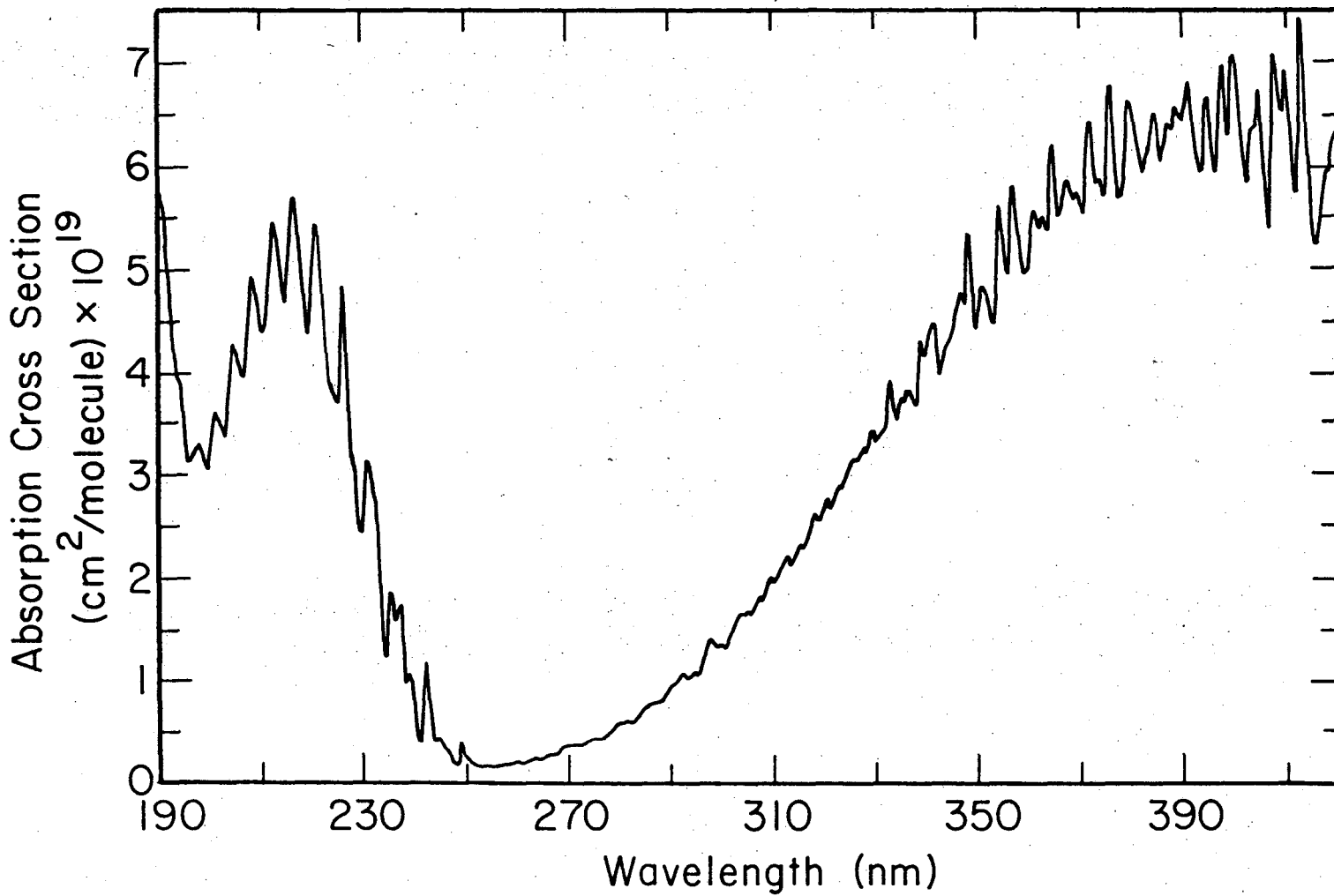


Fig. 10. Nitrogen dioxide (NO₂) ultraviolet spectrum at 298°K.

XBL 759-7279

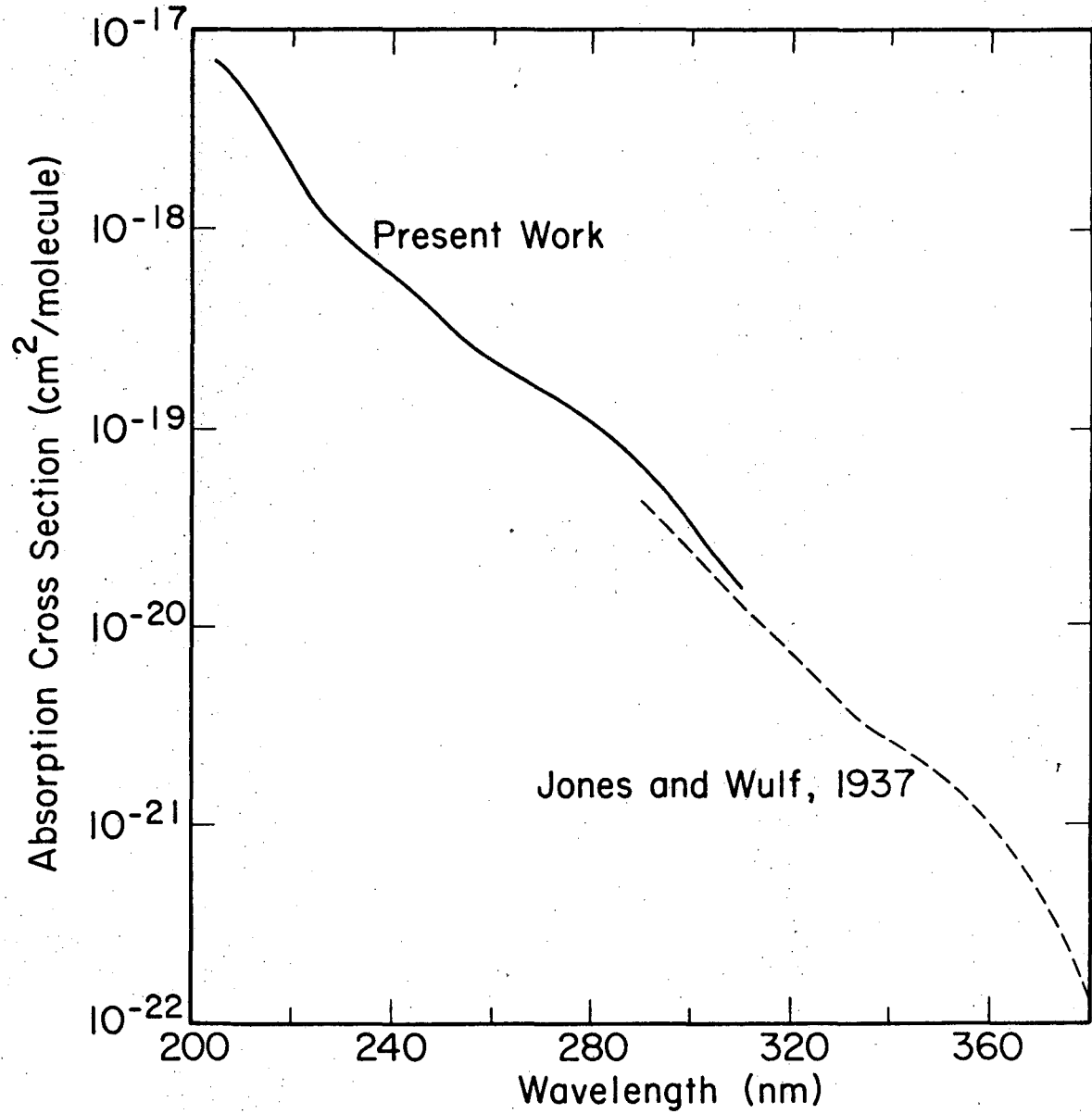
00004400206

conditions of very low ozone concentration, an appreciable amount of NO_2 is also present. The NO_2 concentration can be determined from its near ultraviolet spectrum. Six spectra with 0.83 nm resolution were taken with N_2O_5 concentrations of $(3-10) \times 10^{14}$ molecules cm^{-3} . The absorptions due to O_3 , HNO_3 and NO_2 were subtracted from the spectra, and the average N_2O_5 cross sections are presented in Table V. The average uncertainty is approximately 10% for wavelengths from 205 to 260 nm, and the main source of error is the determination of the ozone concentration. The N_2O_5 cross sections for higher wavelengths are estimated to be $\pm 20\%$. In Fig. 11 the results of this study are indicated by a solid line, and the results of Jones and Wulf¹⁶ are represented by a dashed line.

2. Visible Region

Spectra in the visible region were always taken at 0.83 nm resolution (1 mm slits) with a 0.3 second time constant. The monochromator scanned at $500\text{\AA}/\text{min}$ and data points were taken at 0.2 sec intervals. A 3-71 Corning color filter was used when needed to exclude light diffracted in second order. Concentration determinations in this spectral region were made by scanning.

The reaction cell and gas handling manifold were evacuated and then aged with 1 to 2 torr of ozone for several days. After this treatment, pure ozone in the 298°K cell had a decay rate of approximately 1% per hr; ozone mixed with one atmosphere of oxygen decayed at 0.2% per hr. Liquid ozone is very dangerous due to its unstable nature,⁶⁷ and work with this material was performed behind a 1/4-in. Plexiglas shield. The vacuum pumps were protected from ozone by a



XBL 759-7287

Fig. 11. Nitrogen pentoxide (N_2O_5) ultraviolet spectrum at 298°K.

cold trap lined with silver foil (a very good catalyst for ozone destruction), and no safety problems were experienced. Ozone from a dry ice temperature silica gel trap was liquified at liquid nitrogen temperature and pumped on to remove oxygen. The ozone was allowed to vaporize slowly into the evacuated gas cell, and the final cell pressure of 2 to 3 torr was measured with the TI gage. Using the visible cross sections of Griggs⁶⁸ as a standard, the ozone decomposition during transfer to the gas cell was determined to be 1%. The spectrum is presented in Fig. 12. The visible ozone cross sections obeyed Beer's law and were independent of pressure. Measurements at 298°K and 329°K gave identical results. Concentrations of ozone in later experiments were measured by averaging three data points at each of the two absorption maxima and using the following cross sections ($\text{cm}^2 \text{ molecule}^{-1}$):

$$\begin{aligned}\sigma(574.7 \text{ nm}) &= 4.78 \times 10^{-21} \\ \sigma(602.5 \text{ nm}) &= 5.17 \times 10^{-21}\end{aligned}\tag{64}$$

The absorption spectrum of NO_3 is presented in Fig. 13, and Table VI contains the cross sections averaged over each nm. The spectrum was taken in a $\text{N}_2\text{O}_5\text{-O}_3$ flow system, and the absorption due to ozone to be subtracted was determined by an infrared absorption measurement. The absolute values of the NO_3 cross sections were determined from the ratio of the NO_3 modulation measured at 627.0 nm to the N_2O_5 modulation measured in the infrared (see Section III-E-2). The NO_3 cross sections at 627.0 nm determined by this method were

Table VI. Absorption cross sections ($\text{cm}^2/\text{molecule}$, base e) for the nitrogen trioxide (NO_3) free radical averaged over each nm.

λ	$10^{19}\sigma$	λ	$10^{19}\sigma$	λ	$10^{19}\sigma$	λ	$10^{19}\sigma$	λ	$10^{19}\sigma$	λ	$10^{19}\sigma$
400	0.0	431	1.5	461	3.6	491	9.2	521	15.8	551	21.4
401	0.1	432	1.4	462	3.5	492	8.9	522	17.2	552	21.6
402	0.1	433	1.5	463	3.8	493	8.9	523	16.6	553	22.2
403	0.3	434	1.7	464	4.1	494	8.8	524	15.0	554	24.5
404	0.2	435	2.1	465	4.5	495	9.1	525	13.8	555	27.8
405	0.5	436	2.1	466	4.5	496	10.4	526	13.7	556	29.5
406	0.3	437	1.8	467	4.8	497	11.2	527	15.1	557	30.0
407	0.1	438	1.8	468	5.0	498	10.8	528	17.9	558	31.7
408	0.3	439	2.1	469	5.2	499	10.3	529	21.0	559	34.3
409	0.5	440	1.9	470	4.9	500	9.8	530	20.9	560	32.3
410	0.6	441	1.9	471	5.0	501	9.4	531	19.1	561	28.5
411	0.5	442	2.0	472	5.4	502	9.1	532	18.1	562	26.8
412	0.3	443	1.9	473	5.5	503	9.5	533	17.3	563	25.9
413	0.7	444	2.1	474	5.6	504	10.5	534	17.7	564	24.8
414	0.7	445	2.3	475	5.9	505	11.6	535	20.2	565	24.7
415	0.6	446	2.3	476	6.4	506	11.9	536	23.2	566	25.8
416	0.3	447	2.5	477	6.8	507	11.4	537	23.8	567	25.5
417	0.4	448	2.8	478	6.6	508	10.6	538	21.1	568	25.7
418	0.6	449	2.8	479	6.4	509	11.2	539	18.8	569	26.3
419	0.9	450	2.7	480	6.4	510	13.0	540	18.1	570	25.3
420	0.9	451	2.8	481	6.5	511	15.1	541	16.8	571	25.1
421	0.9	452	3.1	482	6.3	512	16.1	542	16.8	572	24.8
422	0.8	453	3.2	483	6.1	513	15.1	543	14.3	573	24.7
423	1.0	454	3.4	484	6.2	514	14.1	544	13.9	574	25.5
424	1.2	455	3.5	485	6.6	515	14.0	545	16.2	575	27.0
425	1.3	456	3.2	486	7.4	516	14.0	546	20.4	576	29.2
426	0.9	457	3.4	487	8.0	517	13.0	547	25.6	577	30.5
427	0.8	458	3.7	488	8.0	518	12.1	548	27.5	578	30.3
428	1.2	459	3.9	489	8.6	519	12.8	549	24.9	579	29.4
429	1.2	460	3.9	490	9.3	520	14.4	550	22.4	580	29.9
430	1.2										

contd.

Table VI, contd.

λ	$10^{19}\sigma$	λ	$10^{19}\sigma$	λ	$10^{19}\sigma$	λ	$10^{19}\sigma$	λ	$10^{19}\sigma$
581	32.0	611	14.3	641	7.8	671	6.0	701	0.2
582	31.0	612	16.9	642	6.8	672	5.7	702	0.2
583	26.8	613	21.7	643	6.9	673	4.7	703	0.1
584	24.7	614	22.4	644	7.1	674	3.6	704	0.0
585	24.6	615	19.9	645	6.7	675	3.0		
586	27.5	616	17.4	646	5.6	676	3.1		
587	34.8	617	16.7	647	4.9	677	4.0		
588	44.8	618	18.3	648	4.3	678	5.5		
589	55.2	619	20.2	649	3.7	679	5.9		
590	56.7	620	24.7	650	3.2	680	4.9		
591	51.9	621	39.8	651	3.3	681	3.5		
592	48.3	622	76.1	652	3.9	682	2.5		
593	43.2	623	120.4	653	4.7	683	1.6		
594	39.2	624	116.6	654	5.7	684	0.9		
595	39.1	625	86.5	655	6.9	685	0.5		
596	41.6	626	70.0	656	8.9	686	0.3		
597	40.9	627	69.0	657	11.8	687	0.2		
598	35.4	628	68.9	658	16.8	688	0.4		
599	28.9	629	67.0	659	27.6	689	0.2		
600	24.5	630	64.1	660	51.2	690	0.1		
601	24.5	631	50.2	661	101.5	691	0.0		
602	28.4	632	32.7	662	170.8	692	0.0		
603	33.9	633	19.9	663	170.4	693	0.1		
604	40.0	634	13.2	664	115.4	694	0.1		
605	41.8	635	10.6	665	73.5	695	0.2		
606	33.8	636	12.3	666	48.6	696	0.4		
607	23.2	637	16.4	667	29.7	697	0.4		
608	15.9	638	17.6	668	17.5	698	0.4		
609	13.3	639	13.4	669	10.7	699	0.4		
610	13.5	640	9.8	670	7.5	700	0.3		

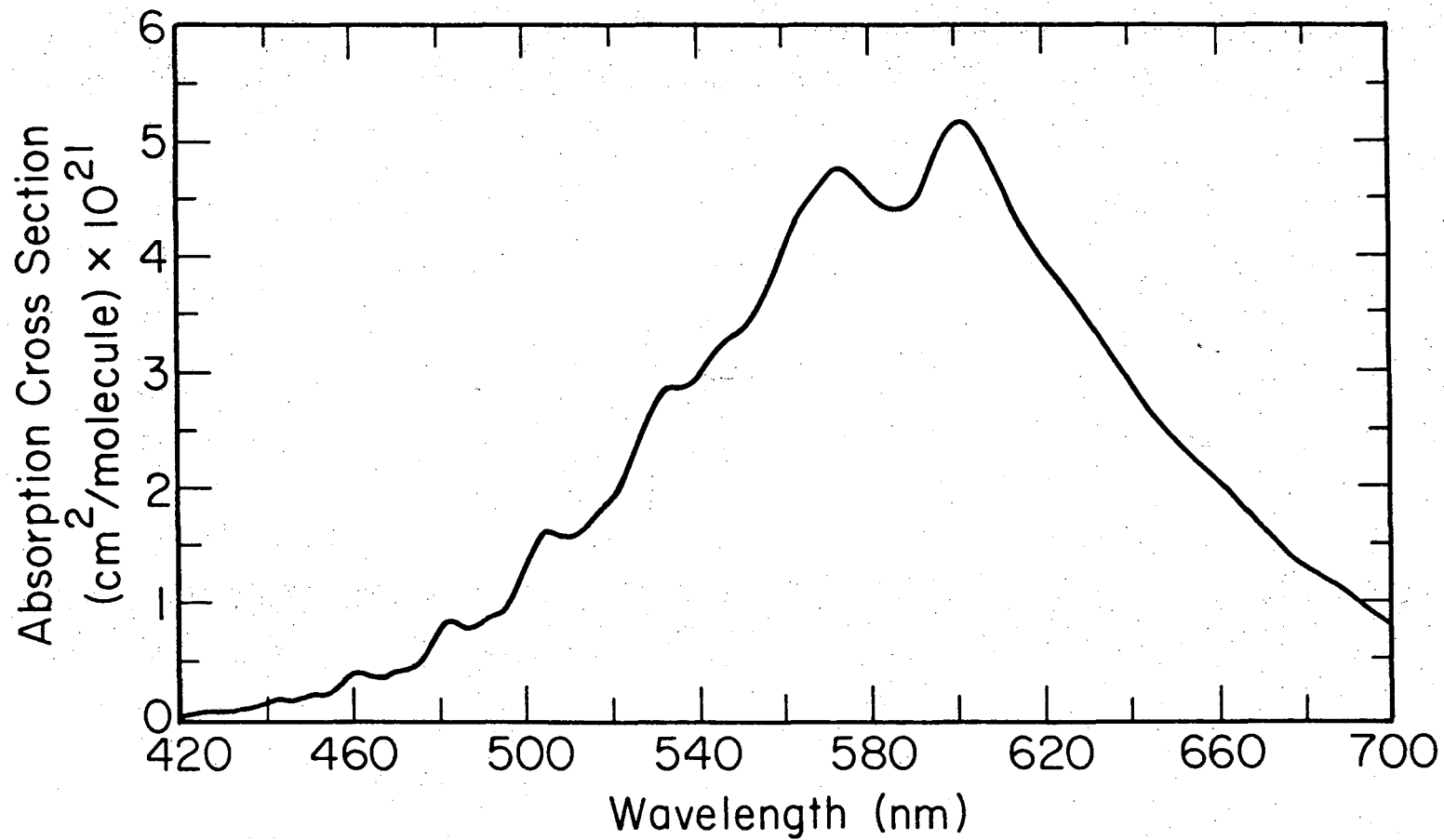
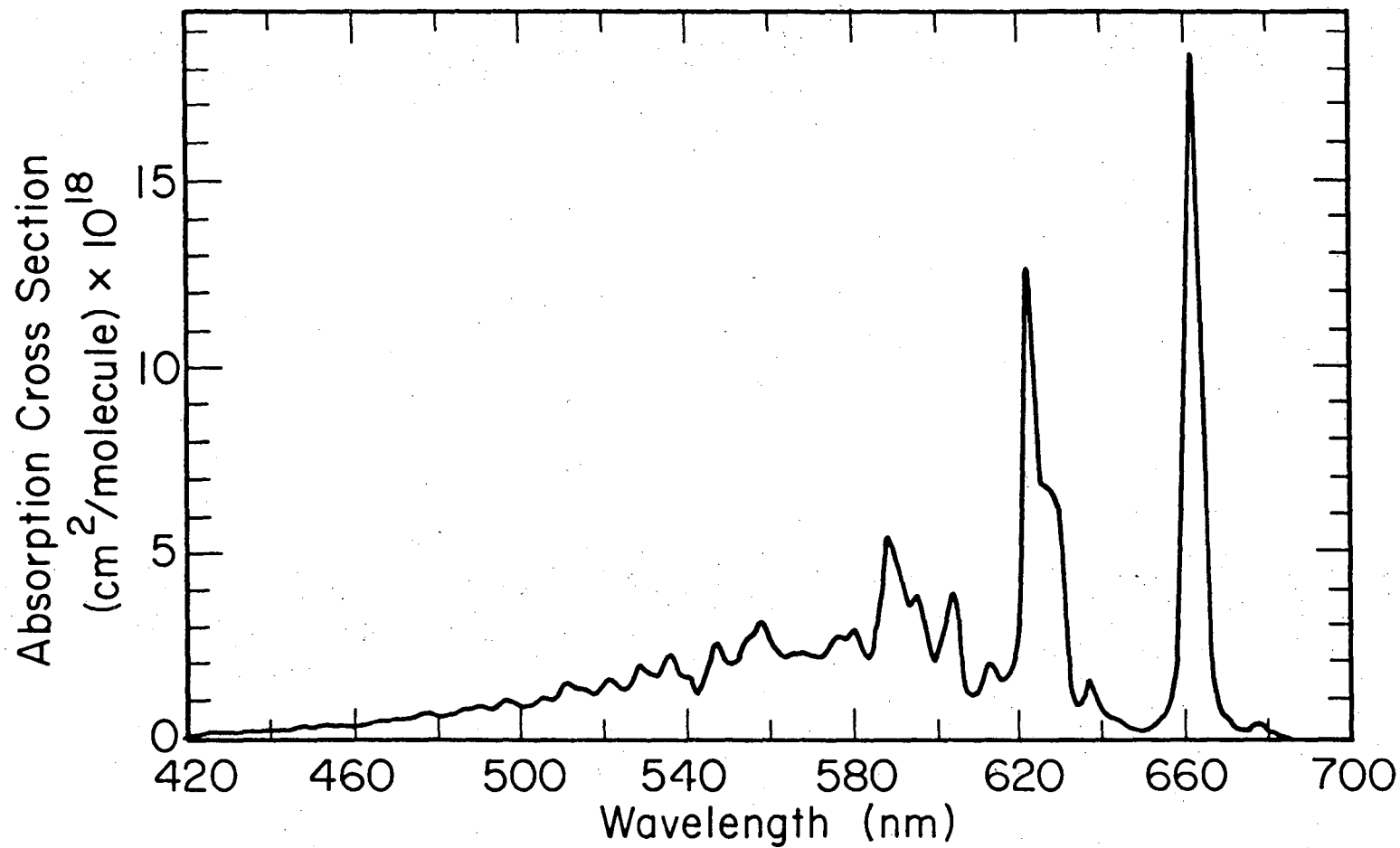


Fig. 12. Ozone (O₃) visible spectrum at 298°K.

XBL 759-7284



-70-

Fig. 13. Nitrogen trioxide (NO₃) visible spectrum at 298°K.

XBL 759-7280

-71-

$$\begin{aligned}
 \sigma_{627}(298^\circ\text{K}) &= (7.03 \pm 0.18) \times 10^{-18} \text{ cm}^2 \text{ molecule}^{-1} \\
 \sigma_{627}(313^\circ\text{K}) &= (7.01 \pm 0.13) \times 10^{-18} \text{ cm}^2 \text{ molecule}^{-1} \\
 \sigma_{627}(329^\circ\text{K}) &= (7.04 \pm 0.13) \times 10^{-18} \text{ cm}^2 \text{ molecule}^{-1}
 \end{aligned}
 \tag{65}$$

The uncertainties quoted for NO_3 cross sections are the standard deviations of the mean and include contributions from the N_2O_5 cross section and the ratio of modulation amplitudes. Concentration determinations in later experiments were made by averaging the three optical density data points at the NO_3 absorption peak at 662.2 nm and subtracting one half of the average of three data points at 650.5 nm and at 674.7 nm. The NO_3 concentration was then calculated from

$$[\text{NO}_3] = A/L \sigma_o (1 - 0.7212 \times 10^{-3} A - 0.4678 \times 10^{-2} A^2) \tag{66}$$

for $A \leq 3.0$

where L = optical path and A = optical density as measured above.

$$\begin{aligned}
 \sigma_o &= \text{cross section in cm}^2 \text{ molecule}^{-1} \text{ at 662.2 nm for } \lim A \rightarrow 0 \\
 \sigma_o(298^\circ\text{K}) &= (1.860 \pm 0.048) \times 10^{-17} \\
 \sigma_o(313^\circ\text{K}) &= (1.830 \pm 0.035) \times 10^{-17} \\
 \sigma_o(329^\circ\text{K}) &= (1.816 \pm 0.035) \times 10^{-17}
 \end{aligned}$$

The σ_o 's at 662.2 nm were obtained from the 627.0 nm values by computing the ratio of the optical density at 627.0 nm to that at 662.2 nm (divided by its apparent Beer's law deviation) for 92 spectra. Some spectral resolution was sacrificed by using a 0.3 sec time constant. A shorter time constant would give a cross section about 3% higher. A resolution of 0.42 nm would give another increase of 3% in cross section at the 662 nm peak, and going to 0.21 nm resolution seems to

give an additional 1% increase. The change of cross section with optical density could be determined very sensitively by changing optical path lengths.

3. Infrared Region

Spectra in the infrared region were always taken at 0.013 μ resolution (2 mm slits) with a 1.0 sec time constant. The monochromator scanned at 0.4 μ /min and data points were taken at 0.2 sec intervals. Some degradation of peak height is possible due to the high time constant and fast scanning conditions, but a high signal-to-noise ratio and fast data acquisition were overriding considerations. The infrared concentration determinations were made by scanning the appropriate regions. All spectra were taken at one atmosphere total pressure.

The ozone cross sections at 4.715 and 4.773 μ were based on concentrations determined from the ozone spectrum in the visible region. The infrared spectra were adjusted to give a zero optical density from 4.636 to 4.663 μ . Three optical density data points were averaged on each peak and applied to the following equations:

$$4.715\mu: [O_3] = A_1/L\sigma_1$$

where

$$\begin{aligned}\sigma_1(298^\circ\text{K}) &= (3.575 - 0.1742A_1 - 0.03164A_1^2) \times 10^{-20} \\ \sigma_1(313^\circ\text{K}) &= (3.483 - 0.1723A_1 - 0.02863A_1^2) \times 10^{-20} \\ \sigma_1(329^\circ\text{K}) &= (3.430 - 0.2096A_1 - 0.01602A_1^2) \times 10^{-20}\end{aligned}\tag{67}$$

for $0.2 \leq A \leq 2.2$.

$$4.773\mu:[O_3] = A_2/L\sigma_2$$

where

$$\sigma_2(298^\circ\text{K}) = (2.252 - 0.09625A_2 + 0.005596A_2^2) \times 10^{-20}$$

$$\sigma_2(313^\circ\text{K}) = (2.205 - 0.1039A_2 + 0.002941A_2^2) \times 10^{-20}$$

$$\sigma_2(329^\circ\text{K}) = (2.190 - 0.1697A_2 + 0.04274A_2^2) \times 10^{-20}$$

for $0.15 \leq A_2 \leq 1.5$. The ozone concentration was taken as the average of these two values. The absolute uncertainty in $[O_3]$ arises mainly from the visible absorption cross sections and is estimated to be about 1%. A representative ozone spectrum is shown in Fig. 14.

The determination of infrared nitrogen pentoxide cross sections was complicated by the presence of a nitric acid impurity due to the moisture in the carrier gases. A steady state flow system was established using NO_2 from a tank of N_2 - NO_2 mixed gases, a small amount of O_2 flowing through a nonoperating ozonizer, and a nitrogen carrier gas. The NO_2 concentration was determined from its visible absorption spectrum, and the concentration of NO was calculated from the previously determined ratio of NO to NO_2 in the tank of mixed gases. The ozonizer was turned on and the 7.0 to 8.365 μ region was scanned after the system came to equilibrium. The visible NO_3 absorption was also measured. A water saturator was placed in the gas line after the ozonizer and the same infrared and visible regions were again scanned for the new steady state concentration conditions. The ozonizer was then turned off and the water saturator removed. After the system returned to its original condition, the final NO_2 concentration was measured optically. From this type of experiment, the cross sections

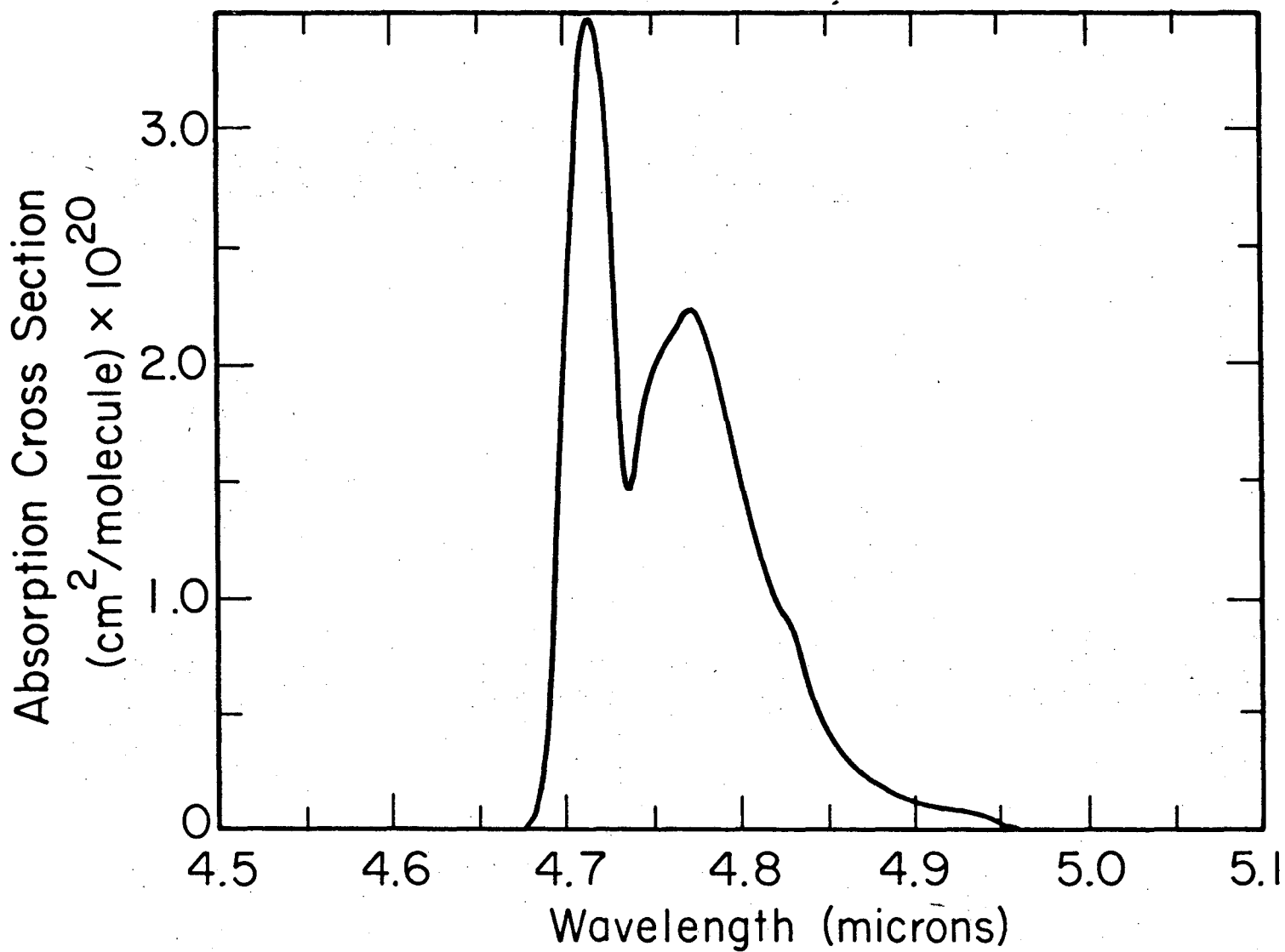


Fig. 14. Representative ozone (O₃) infrared spectrum at 298°K.

XBL 759-7274

of HNO_3 and N_2O_5 can be determined from the NO_x mass balance. Since the N_2O_5 to HNO_3 ratio was changed when water vapor was added to the system, two linear equations for the different ratios can be solved simultaneously:

$$[\text{NO}_x]_{\text{total},i} = [\text{NO}_3]_i + [\text{HNO}_3]_i + 2[\text{N}_2\text{O}_5]_i \quad (69)$$

where

$$[\text{HNO}_3]_i = A_{\text{HNO}_3,i} / L\sigma_{\text{HNO}_3}$$

$$[\text{N}_2\text{O}_5]_i = A_{\text{N}_2\text{O}_5,i} / L\sigma_{\text{N}_2\text{O}_5}$$

The N_2O_5 cross section was measured as the average of three data points at its peak absorption, 8.028 μ . The N_2O_5 spectrum for 298°K is presented in Fig. 15, and the measured cross sections ($\text{cm}^2 \text{molecule}^{-1}$) were

$$\begin{aligned} \sigma(298^\circ\text{K}) &= (1.75 \pm 0.01) \times 10^{-18} \\ \sigma(313^\circ\text{K}) &= (1.68 \pm 0.02) \times 10^{-18} \\ \sigma(329^\circ\text{K}) &= (1.56 \pm 0.03) \times 10^{-18} \end{aligned} \quad (70)$$

(Uncertainties are the standard deviations of the mean.) The HNO_3 cross section was measured as the average of 20 data points between 7.689 and 7.716 μ . The HNO_3 spectrum at 298°K and one atmosphere is presented in Fig. 16. The absorption cross sections were ($\text{cm}^2 \text{molecule}^{-1}$):

$$\begin{aligned} \sigma(298^\circ\text{K}) &= (5.43 \pm 0.04) \times 10^{-19} \\ \sigma(313^\circ\text{K}) &= (5.44 \pm 0.08) \times 10^{-19} \\ \sigma(329^\circ\text{K}) &= (5.71 \pm 0.10) \times 10^{-19} \end{aligned} \quad (71)$$

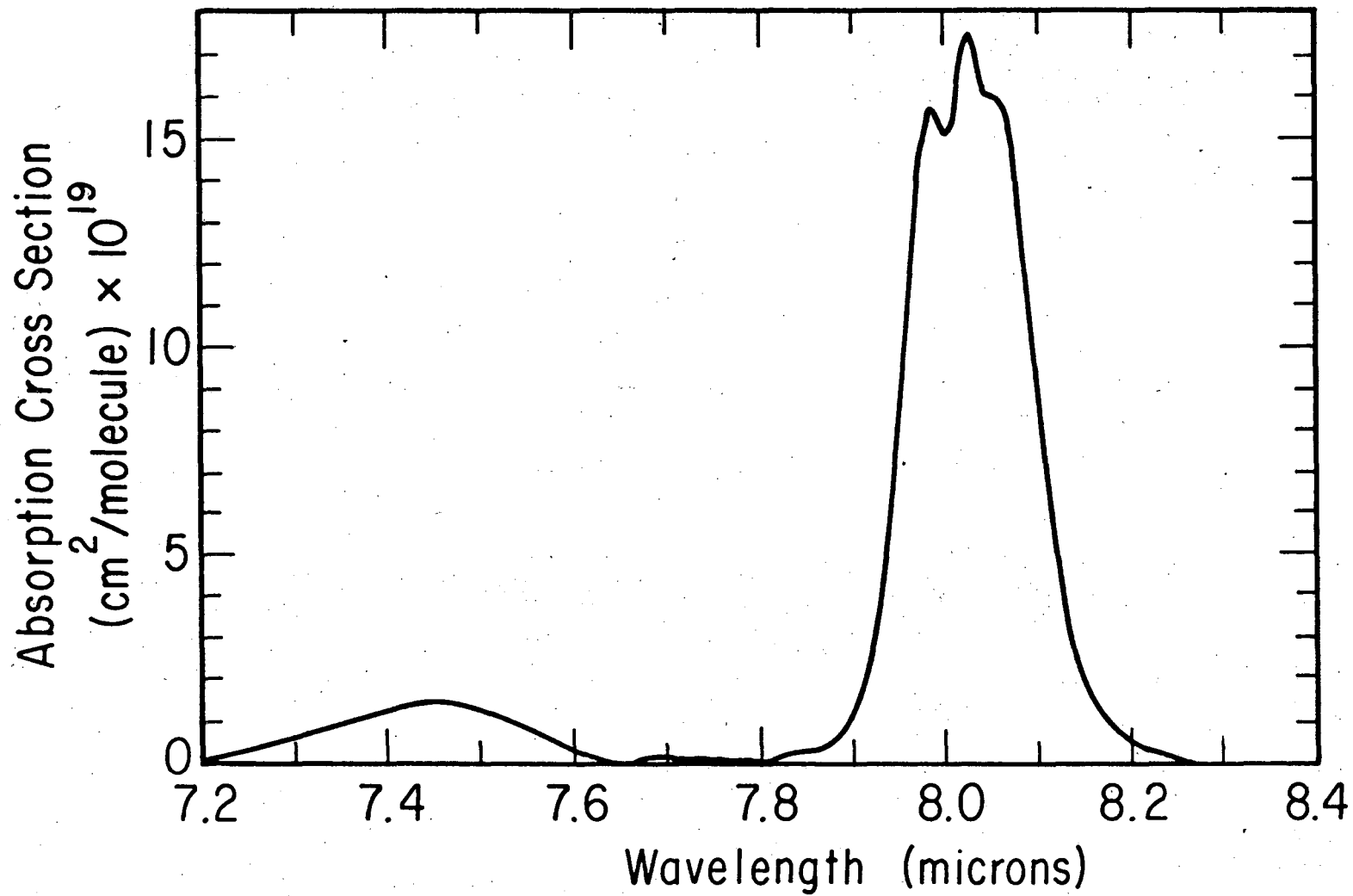


Fig. 15. Nitrogen pentoxide (N₂O₅) infrared spectrum at 298°K.

XBL 759-7276

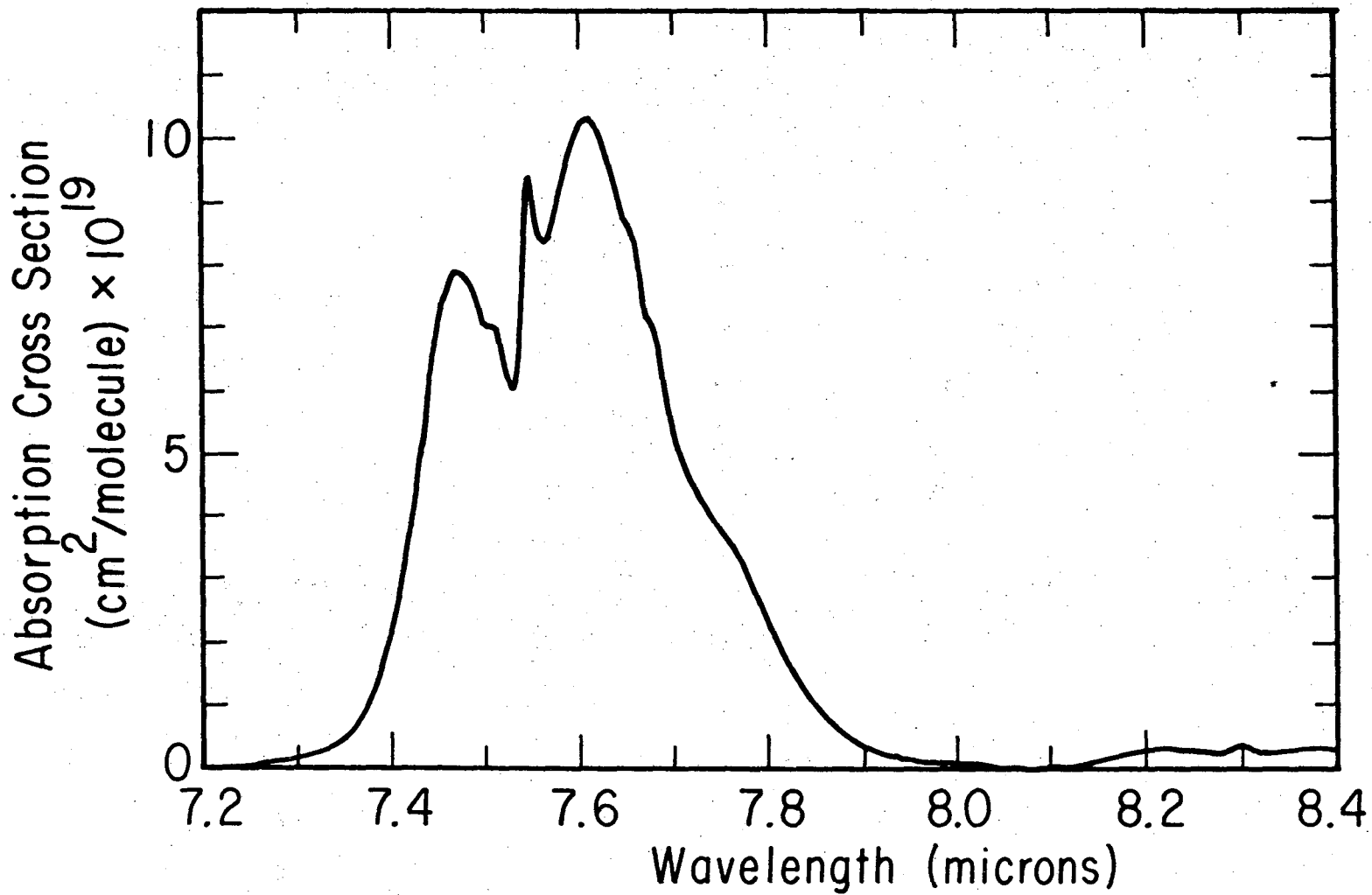


Fig. 16. Nitric acid (HNO₃) infrared spectrum at 298°K.

XBL 759-7275

When the backgrounds for the 7.0 to 8.365 μ scans are adjusted to zero optical density at 8.284 μ , a small correction must be made due to a HNO_3 absorption at that wavelength. The correction is approximately 3.5, 3.0 and 2.5% (for 298, 313 and 329°K) of the optical density of HNO_3 measured by the above technique. Absorption by water in this region must also be taken into account for both HNO_3 and N_2O_5 . When corrections are made for these factors, the selected HNO_3 and N_2O_5 absorption obey Beer's law for optical densities ≤ 2.5 .

Infrared cross sections for HNO_3 were also measured by expanding a known amount of the pure gas into the evacuated cell and adding one atmosphere of nitrogen. This technique gave results that were 2 to 4% lower than those observed by the first technique. The difference can probably be attributed to nitric acid coating out on the walls. The shape of the HNO_3 absorption changed slightly in the temperature range studied, and a slight spread was observed for the N_2O_5 band with increasing temperature. Two experiments were run to measure the ratio of the HNO_3 cross sections at 298 and 329°K. A steady state flow system was established at 298°K with part of the nitrogen carrier gas passing through a temperature-controlled saturator of pure liquid nitric acid. After the HNO_3 spectrum was scanned several times, the gas cell temperature was raised to 329°K. Another set of spectra was then taken, and the cell temperature was returned to 298°K for the final spectra. The ratio of nitric acid optical densities, corrected for the ratio of atmospheric gas densities at the two temperatures, agreed to within 1% with the ratio of the cross sections reported in Eq. (71).

The values for the NO_3 cross sections at 627 nm are directly proportional to the N_2O_5 cross sections. These visible cross sections varied by less than 2% (the experimental uncertainty) over the 298 to 329°K temperature range while the N_2O_5 infrared cross sections varied by 12%. This result gives additional support to the N_2O_5 cross sections since electronic spectra usually have a smaller temperature dependence than infrared spectra.

B. Static Cell Decays

1. NO_2 - O_3 Reaction

The UV reaction cell was conditioned with ozone before use, and either ozone or nitrogen dioxide alone in the cell was stable for the time of a kinetic experiment. The destruction of O_3 due to the source lamp was calculated to be less than 10^{11} molecules cm^{-3} during a run; this quantity was below the detection sensitivity of the experiment.

The NO_2 pressure was measured in a calibrated volume by the TI gage before being admitted to the evacuated cell. Concentration corrections due to N_2O_4 ^{52,65} were made, and the NO_2 absorption cross section was measured at 390 nm for a 0.83 nm resolution. The cross section was 6.6×10^{-19} cm^2 molecule⁻¹ over the temperature range of 231 to 298°K. Initial ozone concentrations were determined from the O_3 absorption cross sections at 290, 295 and 300 nm, and ozone decay was monitored at 255 nm. (The absorption due to the NO_2 cross section at 255 nm was negligible since the ozone cross section is over 600 times higher for this wavelength. The absorption cross section of N_2O_5 is only 40 times smaller than that of ozone, and reactions were stopped

long before the ozone was totally consumed to avoid this interference.) These wavelengths were calibrated for O_3 absorption at different temperatures by adding excess nitric oxide and measuring the NO_2 formed. The O_3 cross section was constant for 255 nm, but increased with temperature by about 10% for the other wavelengths:

$$\begin{aligned}\sigma(255) &= 1.11 \times 10^{-17} \text{ cm}^2 \text{ molecule}^{-1} \\ \sigma(290) &= (9.561 + 0.001625T) \times 10^{-19} \\ \sigma(295) &= (4.616 + 0.001079T) \times 10^{-19} \\ \sigma(300) &= (2.079 + 0.0006283T) \times 10^{-19}\end{aligned}\tag{72}$$

where $231^\circ\text{K} \leq T \leq 298^\circ\text{K}$. Since the monochromator had up to 2\AA of slippage, cross section determinations for NO_2 and O_3 were made throughout the series of experiments. The estimated overall uncertainty in the cross sections is $\pm 2\%$.

Ozone was always admitted to the evacuated cell first, and its concentration was measured optically. The monochromator was then set to either 390 nm to follow NO_2 disappearance or 255 nm to follow O_3 disappearance. The initial NO_2 concentration was measured by its pressure in a calibrated volume and was then mixed with enough nitrogen to give a final cell pressure of 0.2 Torr. The mixture was flushed into the reaction cell through a disperser tube. Blank runs with nitrogen in the cell instead of O_3 were used to measure the profile of NO_2 buildup; more than 99% of the final NO_2 concentration was in the cell after 40 sec. These profiles were then used in calculating rate constants from the decay of the reactants. Kinetic experiments were run at 10°K intervals between 298 and 231°K . The concentrations of NO_2 and O_3 were varied from 10^{14} to 10^{15} molecules cm^{-3} ,

and the ratio of initial concentrations, $[\text{NO}_2]_0/[\text{O}_3]_0$, ranged from 0.3 to 5.2. Reaction times were from 200 to 1000 sec, and 1000 data points were taken per experiment. A typical NO_2 concentration profile is shown in Fig. 17. The differential rate of reaction was calculated point by point and averaged for the region from approximately 20% to 60% of reaction completion. Corrections were made for the small amount of N_2O_4 present. After the reaction was about 80% complete, the reaction stoichiometry was measured by going from 390 nm where NO_2 is measured, to 255 nm to measure O_3 , and then back to 390 nm.

The evaluation of the rate data for the $\text{NO}_2\text{-O}_3$ reaction depends on the stoichiometry ($\Delta\text{NO}_2/\Delta\text{O}_3$) of the reaction. Since the concentration of only one reactant is usually monitored during a kinetic run, the concentration of the other reactant in the differential rate expression must be calculated from a knowledge of this stoichiometry and the initial concentrations. Figure 18 shows a plot of the calculated rate constant vs time for the NO_2 concentration profile of Fig. 17 both for a stoichiometry of 2.00 and for the average measured stoichiometry of 1.89. This provides another test of the stoichiometry since the calculated rate constant must be the same throughout the experiment. This effect is easily observable only when one of the reactants, in this case the ozone, has almost disappeared.

The results of the kinetic runs and the stoichiometry measurements are presented in Table VII. The 22 stoichiometry measurements are plotted in Fig. 19 vs the ratio of initial reactant concentrations. The solid line in the figure is the average value of 1.89 ± 0.08 (standard deviation), and no dependence on temperature or initial concentrations

Table VII. Rate constants for the NO₂ + O₃ reaction.

T (K)	[O ₃] ₀ (units of 10 ¹⁴ molecules cm ⁻³)	[NO ₂] ₀ (molecules cm ⁻³)	Stoich. (ΔNO ₂ /ΔO ₃)	h _{2.00} (units of 10 ⁻¹⁷ cm ³ molecule ⁻¹)	h _{1.89} (units of 10 ⁻¹⁷ cm ³ molecule ⁻¹)
298.0	4.00	12.59	1.87	2.36	3.87
	2.65	3.63	2.02	3.06	3.49
	1.99	6.05		2.78	3.33
	1.64	7.88		2.46	3.30
	*1.60	3.35		3.76	3.55
	*2.25	2.94		4.16	3.93
	*1.75	3.17		3.50	3.35
	*2.83	7.64		3.61	3.38
	*2.51	4.45		3.57	3.33
	*1.55	8.10		3.57	3.37
288.0	4.40	3.93	1.90	2.35	2.62
	3.14	2.52	1.94	2.40	2.65
	4.61	7.19	1.89	2.17	2.49
	4.80	11.97	1.83	1.87	2.29
	4.88	2.19		2.26	2.48
278.0	3.78	12.67	1.80	1.46	1.80
	4.42	10.89	1.80	1.37	1.70
	4.80	12.30	1.77	1.44	1.74
	9.83	9.12	1.85	1.70	1.92
	5.70	10.33	1.87	1.59	1.86
	8.75	3.96		1.62	1.78
	11.87	3.79		1.63	1.79
	4.65	3.08		1.68	1.85
268.0	13.1	6.20		1.25	1.38
	4.3	14.9		1.08	1.13
	5.7	8.02		1.40	1.58
	3.53	12.2		1.01	1.18
	7.35	4.33		1.26	1.38

contd.

Table VII, contd.

268.0 contd.					
	4.7	11.2		1.22	1.42
	6.37	7.95		1.24	1.40
	1.37	4.42		1.29	1.51
	4.86	8.65		1.25	1.47
	*2.49	2.45		1.37	1.27
	*2.05	8.12		1.38	1.32
	*1.57	2.22		1.58	1.51
258.0					
	2.54	9.68	1.86	0.690	0.800
	2.06	4.94	1.95	0.814	0.922
	3.40	8.76	1.84	0.705	0.808
	3.40	6.27	1.79	0.762	0.858
	5.87	8.89	1.89	0.811	0.931
	9.19	7.33		0.874	0.974
	5.26	11.60		0.868	1.015
	12.0	3.92		0.836	0.925
	6.71	9.80		0.912	1.044
	*2.48	9.76	1.91	0.952	0.919
	*2.65	3.91		0.829	0.791
	*3.83	4.79	1.90	0.959	0.872
	*1.78	5.10		0.942	0.911
248.0					
	6.3	3.57		0.536	0.590
	8.7	4.63		0.587	0.645
	3.33	10.58		0.505	0.573
	3.43	8.29		0.540	0.616
	2.40	7.51		0.472	0.587
	*2.30	5.01	1.81	0.736	0.673
	*1.90	7.33	1.89	0.630	0.617
	*2.70	2.51		0.796	0.702
	†2.30	3.42	1.92	0.572	0.674
	†2.30	3.42	1.92	0.860	0.683
	†1.25	6.20	1.85	0.429	0.522
	†1.25	6.20	1.85	0.587	0.575

Table VII, oontd.

238.0	4.04	15.25	0.357	0.460
	5.00	7.87	0.410	0.473
	3.53	14.72	0.388	0.511
	8.8	14.75	0.375	0.450
	9.0	7.97	0.385	0.445
	3.13	10.39	0.362	0.439
	4.40	13.08	0.350	0.460
	5.00	6.37	0.369	0.415
	7.4	3.21	0.370	0.387
	8.6	14.28	0.366	0.437
	2.52	6.48	0.326	0.372
	*1.42	5.58	0.429	0.421
	*2.12	4.98	0.429	0.413
	*2.09	2.18	0.443	0.423
	*2.50	6.77	0.413	0.404
	*2.55	6.68	0.429	0.411
231.2	4.21	10.98	0.268	0.312
	5.60	7.37	0.281	0.315
	5.70	4.31	0.281	0.311
	7.12	10.05	0.280	0.315
	4.00	12.32	0.241	0.281
	3.83	3.35	0.314	0.351

* Runs in which [O₃] was monitored.

† Runs in which both [O₃] and [NO₂] were monitored.

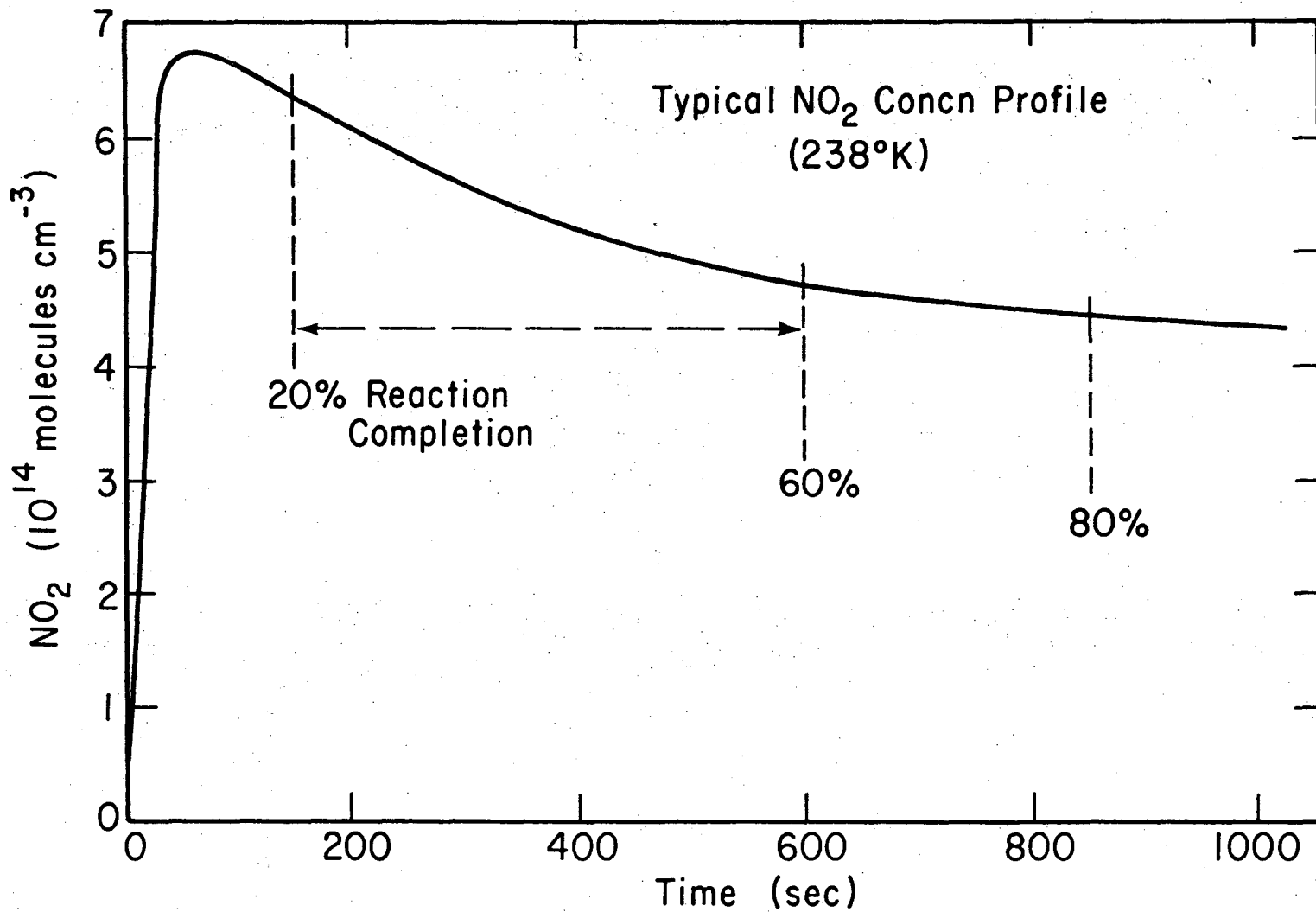
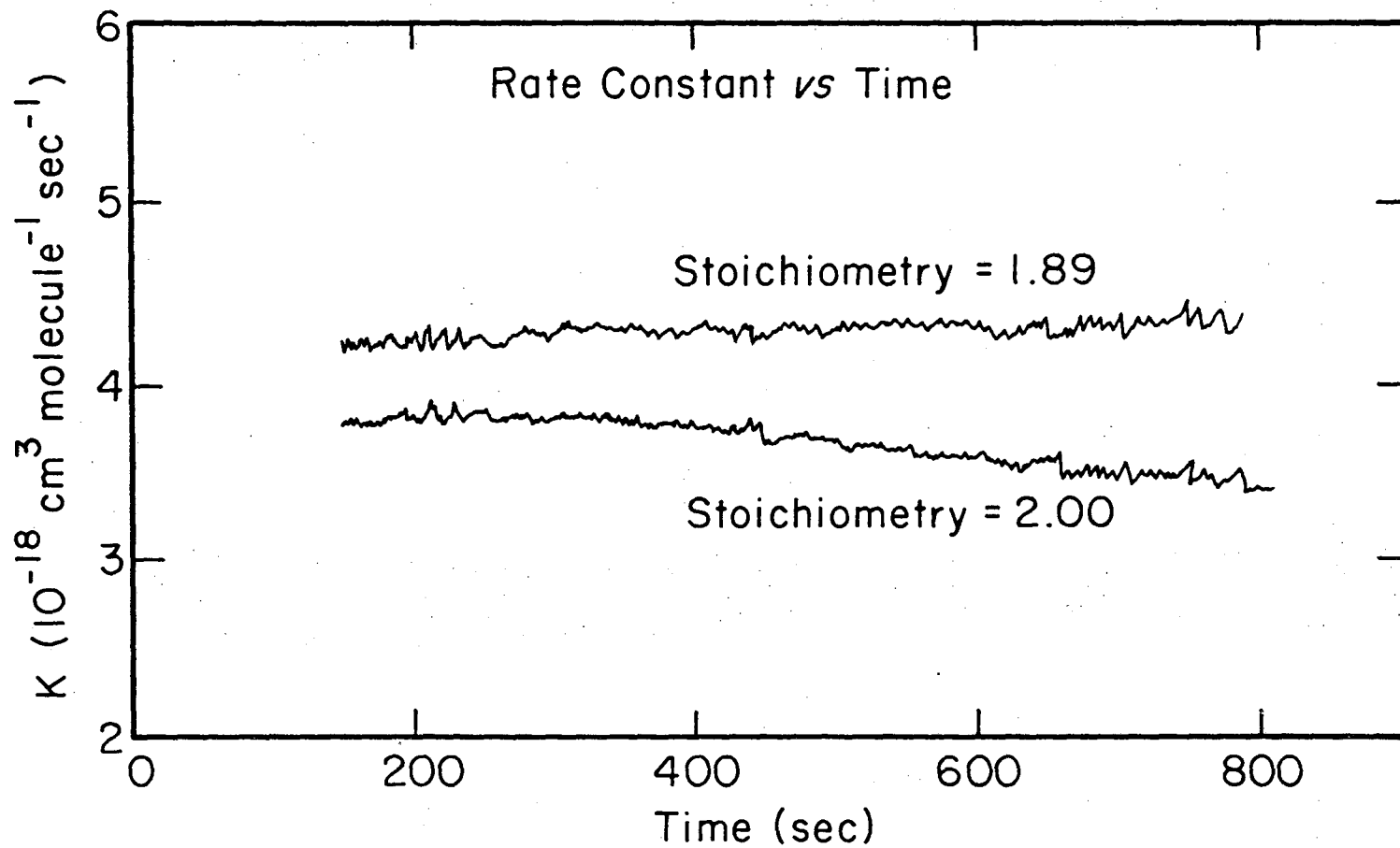


Fig. 17. [NO₂] vs time for a NO₂-O₃ kinetic experiment.

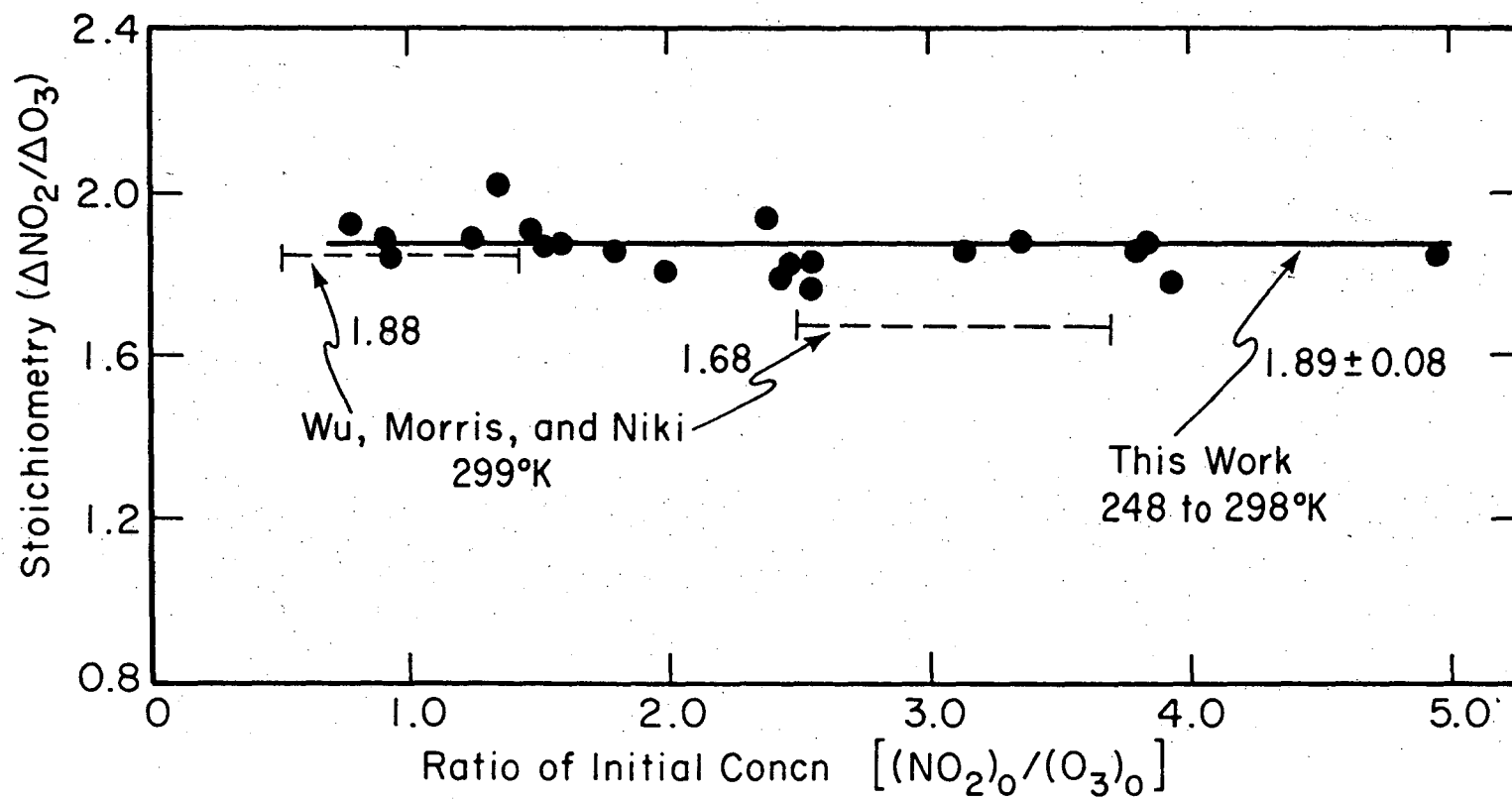
XBL 743-5736



-98-

Fig. 18. Results of rate constant calculation for an NO₂-O₃ experiment.

XBL 743-5735



-87-

Fig. 19. Plot of measured stoichiometries vs initial reactant ratio for $\text{NO}_2\text{-O}_3$ experiments.

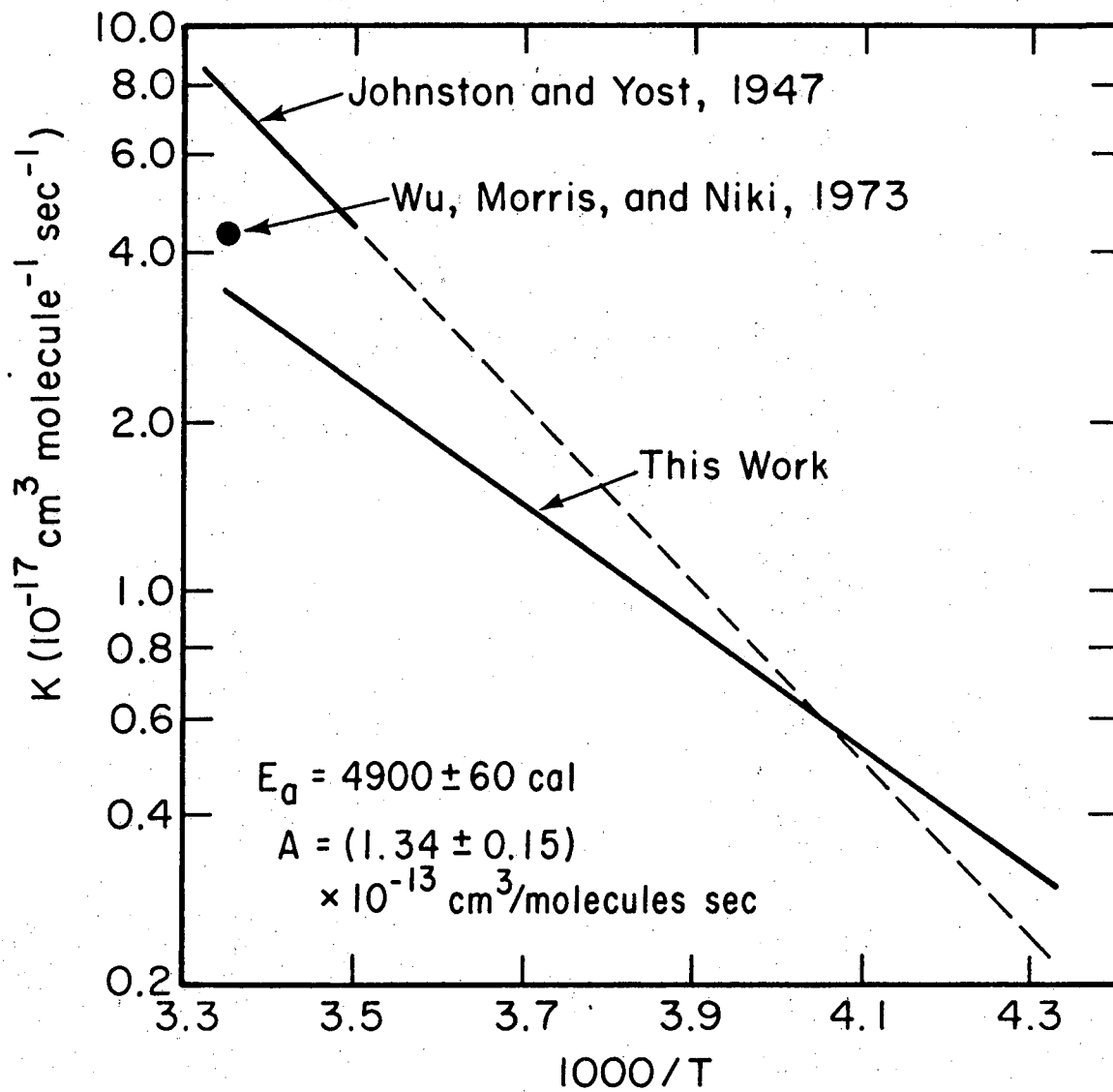
XBL 743-5738

could be detected. The average stoichiometries measured by Wu et al.³³ at 299°K are plotted as dashed lines. Their average uncertainty was 0.15 for both the case of excess O₃ and the case of excess NO₂. Two reactions were run at 248°K in which data points for both O₃ and NO₂ were recorded. This was done by going back and forth between the wavelengths for following the separate species (255 nm and 390 nm). The data points for each wavelength were then fitted by a least-squares treatment to a polynomial. Evaluation of the polynomial curves showed that the stoichiometry was approximately constant throughout the reaction.

The rate constants in Table VII calculated using the experimental stoichiometry have much less scatter than those calculated from an assumed value of 2.00. This gives support to the contention that the experimental stoichiometry best describes the system and should be used to evaluate the data. An Arrhenius plot of the rate constants calculated using the measured stoichiometry is presented in Fig. 20. The results of Johnston and Yost²⁷ are given by the upper solid line which indicates the temperature range of their experiments; the dashed line is an extrapolation of their data. The room temperature result of Wu, Morris and Niki is also plotted. The other solid line indicates the temperature range of the present results and is calculated from 82 kinetic runs. A linear least squares fit of the data in Table VII to Arrhenius parameters gives:

$$h = (1.34 \pm 0.11) \times 10^{-13} e^{-(4900 \pm 60)/RT} \text{ cm}^3 \text{ molecule}^{-1} \text{ sec}^{-1} \quad (73)$$

(uncertainties are standard deviations).



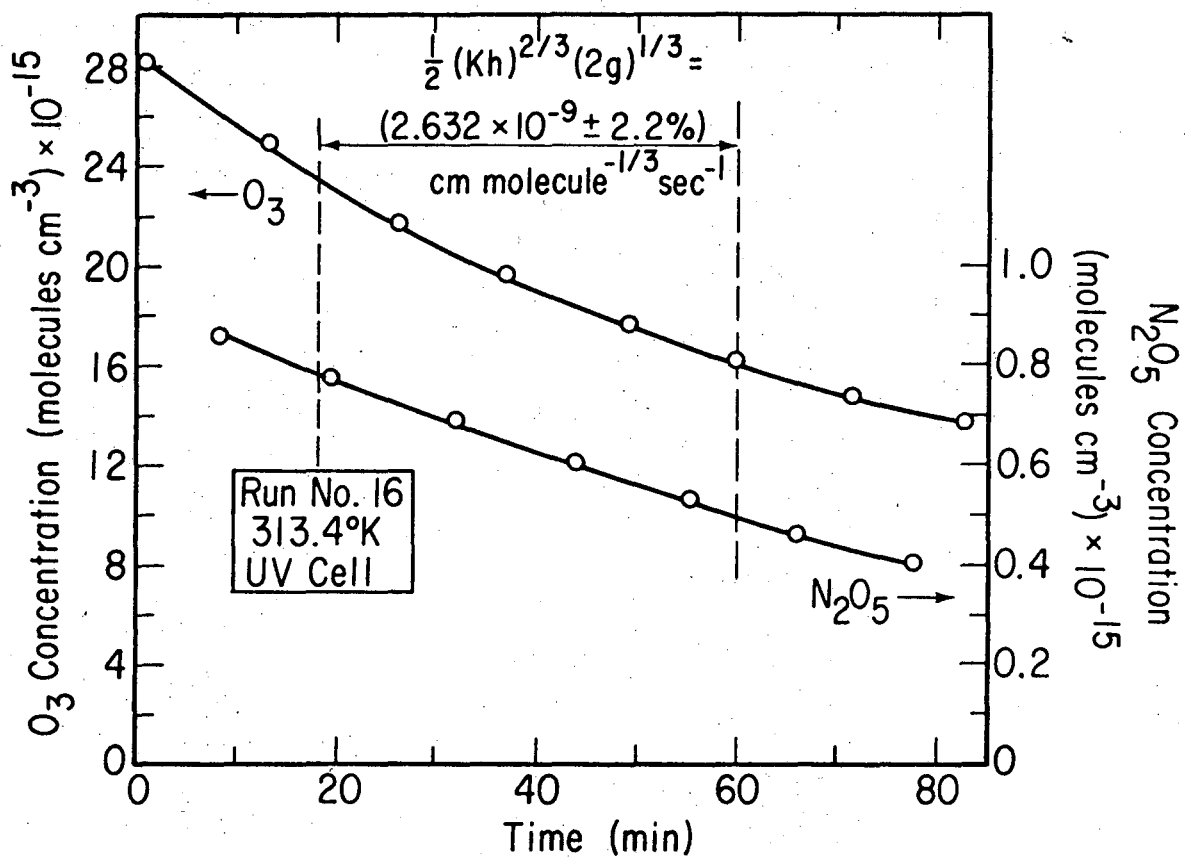
XBL743-5737

Fig. 20. Arrhenius plot for the $\text{NO}_2\text{-O}_3$ reaction.

2. N₂O₅-O₃ Reaction

Measurements of the N₂O₅ catalyzed decomposition of ozone were carried out using infrared scanning techniques for monitoring O₃, N₂O₅ and HNO₃. The reaction cell was conditioned with N₂O₅ and O₃ in a flow system at one atmosphere total pressure. The relative amount of N₂O₅ being converted to HNO₃ on the walls decreased slowly with time, but was always greater than 10%. When the flows were stopped, the N₂O₅ would be completely converted to nitric acid in 2 to 4 hr.

The reaction cell was closed off from the flow system at the start of an experiment. Ozone was measured by scanning the 4.4 to 5.765 μ region. Nitric acid and nitrogen pentoxide were then measured by scanning the 7.0 to 8.365 μ region. A set of measurements of all three species took 10 to 11 min. The starting time for each scan was recorded from a Precision Scientific Company timer, and allowance was made for the time needed to reach each absorption band of interest. From 5 to 10 determinations of the concentrations of the three species were made over the course of an experiment by repeating the pair of scans as quickly as possible. The data points for each reactant were least-squares fitted to a third-order polynomial to give its concentration profile as a function of time. The decays of O₃ and N₂O₅ are typified by the concentration vs time profiles presented in Fig. 21 for run number 16. The polynomial curves for [O₃] and [N₂O₅] usually fit the data points with a standard deviation smaller than 0.2%. The coefficients for the polynomials can be found in Appendix B. The differential rate of change of ozone is calculated from the



XBL 759-7288

Fig. 21. Concentration profiles for N_2O_5 - O_3 static cell decay.

concentration profile polynomials and used in Eq. (35). The rate constants from the central portions of the curves were averaged and are presented in Table VIII. The total percent standard deviation combines the standard deviation of the rate constants for a single experiment with uncertainties in the reactant cross sections. The data was weighted by the total standard deviation and least squares fitted to Arrhenius parameters. The results for the two cells differed by 10 calories in the activation energy. The combined data gives

$$1/2(Kh)^{2/3} (2g)^{1/3} = \quad (74)$$

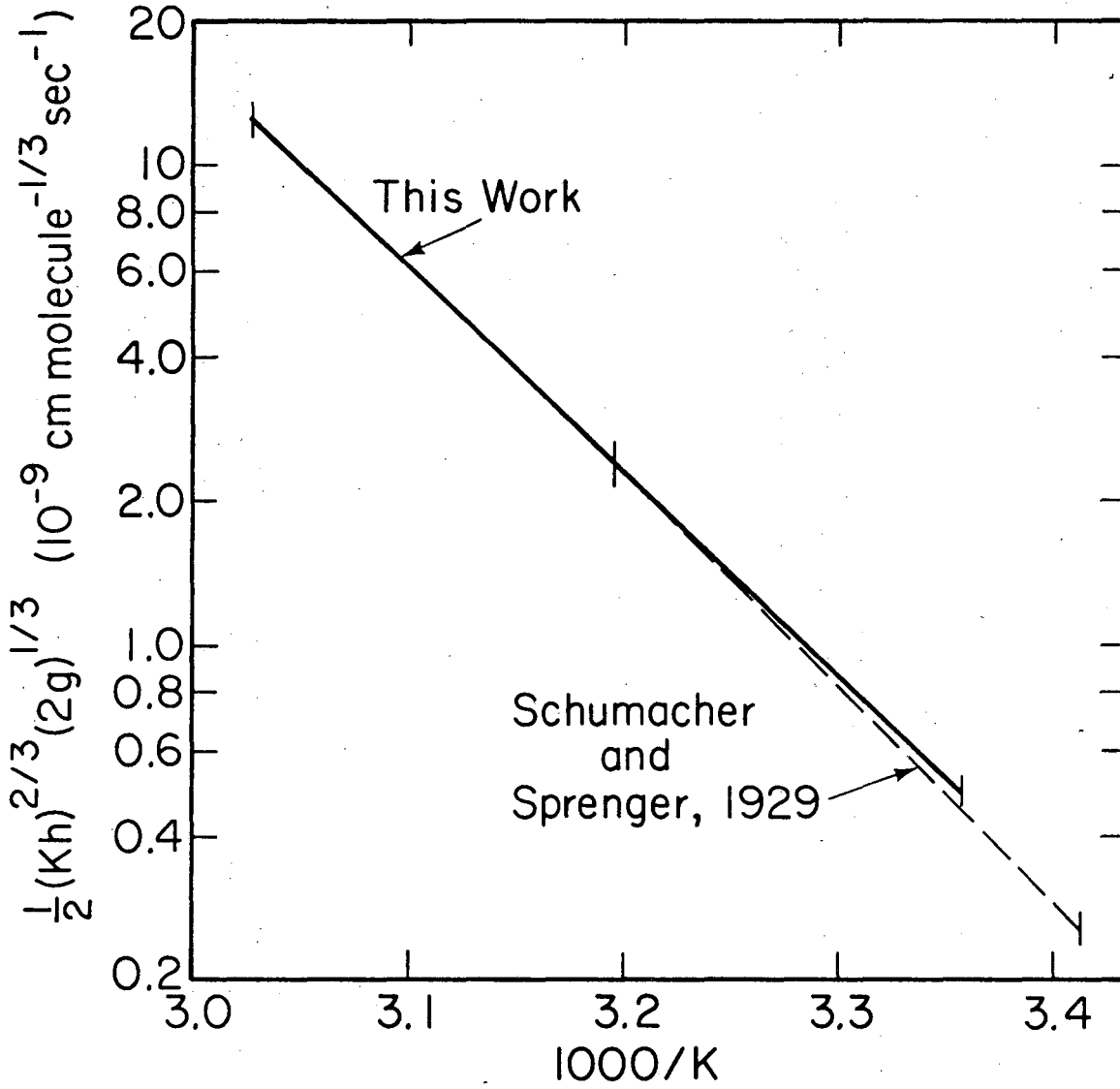
$$(1.39 \pm 0.19) \times 10^5 e^{-(19700 \pm 80)/RT} \text{ cm molecules}^{-1/3} \text{ sec}^{-1}$$

An Arrhenius plot is shown in Fig. 22 with the solid line giving the present results. The results of Schumacher and Sprenger are shown by a dashed line.

Experiments of this type were also carried out with photolysis lamps flashing at 8 cps. Oxygen was used as the carrier gas to keep the steady state concentration of oxygen atoms low. The normal ozone decay will then be affected only by reactions j_1 and j_2 for NO_3 photolysis. Table IX contains the results from experiments in the UV cell using red, green and gold lamps. The data was evaluated using Eq. (35), and no corrections were made to the rate constants to take into account the effects of reactions j_1 and j_2 . When the temperature of the system rose due to heating by the lamps, the rate constants were extrapolated back to 297.8°K by Eq. (74). Most of the dark runs included in Table IX are within the experimental uncertainty

Table VIII. N_2O_5 catalyzed decomposition of ozone.

Run No.	Temp. (K)	$[\text{O}_3]_0$ (10^{15} molecules/cm ³)	$[\text{N}_2\text{O}_5]_0$ (10^{-9} cm molecules ⁻¹ sec ⁻¹)	$\frac{1}{2}(\text{Kh})^{\frac{2}{3}}(2g)^{\frac{1}{3}}$ (10^{-9} cm molecules ⁻¹ sec ⁻¹)	Total % Stand.Dev.
(Surface/Volume = 0.180 cm^{-1})					
1	298.8	29.0	2.03	0.547	1.6
2	298.8	72.6	1.40	0.561	1.7
3	298.8	63.7	1.09	0.547	0.8
4	314.4	55.3	0.96	2.972	2.3
5	314.4	43.8	1.23	2.891	1.1
6	314.4	38.7	1.71	2.808	1.5
7	330.2	21.9	0.42	12.41	5.4
8	330.2	9.31	0.31	12.31	4.1
(Surface/Volume = 0.252 cm^{-1})					
9	297.8	53.3	0.58	0.488	1.9
10	297.8	58.8	1.07	0.482	1.2
11	297.8	67.4	1.38	0.462	1.5
12	297.8	31.7	1.28	0.504	2.6
13	297.9	85.1	1.10	0.499	2.2
14	297.9	40.4	0.56	0.479	1.8
15	313.4	30.1	0.67	2.558	3.5
16	313.4	23.6	0.79	2.632	2.2
17	313.4	31.2	0.76	2.597	1.9
18	329.0	39.0	0.25	10.99	2.7
19	329.0	29.2	0.45	10.82	4.4
20	329.0	31.4	0.83	11.09	4.1



XBL 759-7282

Fig. 22. Arrhenius plot for $\frac{1}{2}(Kh)^{2/3}(2g)^{1/3}$.

Table IX. Apparent rate constants for the N_2O_5 catalyzed decomposition of ozone in the illuminated UV cell.

Run No.	Lamps	Temp. (K)	$[O_3]_0$ (10^{15} molecules/cm ³)	$[N_2O_5]_0$ (10^{-9} molecules/cm ³)	$\frac{1}{2}(Kh)^{\frac{2}{3}}(2g)^{\frac{1}{3}}$ (10^{-9} cm molecules ^{-1/3} sec ⁻¹)	Total % Stand.Dev.
21	Red	298.4 (297.8)	81.6	0.968	0.546 (0.511)	1.0
22	(dark)	297.8	74.5	1.049	0.484	2.5
23	Red	297.9 (297.8)	70.8	0.919	0.494 (0.488)	2.4
24	Green	298.1 (297.8)	81.3	0.824	0.436 (0.422)	1.2
25	(dark)	297.8	79.1	0.866	0.494	2.3
26	Green	297.9 (297.8)	79.9	0.950	0.445 (0.441)	2.0
27	Gold	297.8	80.1	1.422	0.478	1.6
28	(dark)	297.8	76.5	1.800	0.487	1.9
29	Gold	297.8	71.5	1.433	0.472	2.6
30	Gold	297.8	83.1	1.357	0.468	1.5
31	(dark)	297.8	72.8	1.715	0.484	0.9

of the average $1/2(Kh)^{2/3}(2g)^{1/3}$ dark value of $(0.484 \pm 0.012) \times 10^{-9}$ cm molecule $^{-1/3}$ sec $^{-1}$ for 297.8°K in Table VIII.

The effects of the NO₃ photolysis reactions will be evaluated later (Section IV-B).

3. Effects of Reactant Self-Heating

The enthalpy changes of chemical reactions can cause nonuniform temperature distributions in isolated reaction cells. Since the N₂O₅-O₃ and NO₂-O₃ reactions are both quite exothermic (34.1 kcal/mole and 47.3 kcal/mole, respectively), the effects of reactant self-heating on the measured reaction rates must be considered.

Analytical solutions for temperature profiles in exothermic reaction systems have been summarized by Boddington and Gray.⁶⁹ Their equations for the case of an infinite cylinder will be used to predict self-heating effects on the present results. The Frank-Kamenetskii parameter, δ , is a dimensionless rate of heat release:

$$\delta = \left(qdAe^{-E/RT_0} \right) \frac{a^2 E}{\lambda RT_0^2} \quad (75)$$

where q = reactant exothermicity

d = density of reactant mixture

A = Arrhenius pre-exponential factor

E = Arrhenius activation energy

R = universal gas constant

a = radius of reaction vessel

T_0 = ambient temperature of surroundings or thermostat

λ = thermal conductivity of the reactant system

The dimensionless temperature excess, Θ , is given by

$$\Theta = (T - T_o) \frac{E}{RT_o^2} \quad (76)$$

and the temperature profile is

$$\Theta(\rho) = \ln \frac{8C}{\delta(1 + C\rho^2)^2} \quad (77)$$

where $\rho = \frac{r}{a}$, the dimensionless distance from the center of the cell

C = the lower solution of the equation

$$\delta = \frac{8C}{(1 + C)^2} \quad (78)$$

These equations are used for the sample calculations for the $N_2O_5-O_3$ reaction summarized in Table X. The worst cases for each reaction cell are used in the calculations. A similar calculation for the NO_2-O_3 reaction gives a δ of 0.034 and a maximum temperature rise of $0.15^\circ K$, a quantity insignificant for a reaction with only a 4.9 kilocalorie activation energy. The $N_2O_5-O_3$ reaction, however, has an activation energy of 19.7 kilocalories and this results in an increase in the reaction rate of 1% per $0.1^\circ K$.

The above calculations are based on the assumption that conduction is the only mode of heat transfer. The contribution of natural convection to the heat transfer rate has been observed to depend on the Rayleigh number.⁷⁰ (The Rayleigh (Ra) number can be calculated by⁷¹

$$Ra = Aa^3 \Delta T \quad (79)$$

where A = a property of the fluid called the convection modulus

a = radius of vessel

Table X. Reaction cell temperature profile calculations for the $N_2O_5-O_3$ reaction.

UV Cell		ρ	$\Theta(\rho)$	$\Delta T(K)$
a	= 7.5 cm	0	0.024	0.26
T_0	= 329.0 K	0.2	0.023	0.25
O_3	= 31.4×10^{15} molecules cm^{-3}	0.4	0.019	0.22
N_2O_5	= 0.83×10^{15} molecules cm^{-3}	0.6	0.015	0.17
δ	= 0.0883	0.8	0.009	0.10
C	= 0.0113	1.0	0.001	0.01
IR Cell		ρ	$\Theta(\rho)$	$\Delta T(K)$
a	= 15 cm	0	0.049	0.54
T_0	= 330.2 K	0.2	0.047	0.51
O_3	= 21.9×10^{15} molecules cm^{-3}	0.4	0.041	0.45
N_2O_5	= 0.42×10^{15} molecules cm^{-3}	0.6	0.031	0.34
δ	= 0.195	0.8	0.016	0.18
C	= 0.0256	1.0	0	0

The convection modulus A is approximately $65 \text{ cm}^{-3} \cdot \text{K}^{-1}$ for air at 328°K .) Ashmore, Tyler and Wesley⁷⁰ found that for spherical vessels the ratio of temperature rise calculated to temperature rise observed varies linearly with the logarithm of the Rayleigh number for $Ra > 600$. The Rayleigh numbers for the $\text{N}_2\text{O}_5\text{-O}_3$ reactions presented in Table X are 7.1×10^3 and 1.2×10^5 for the UV cell and IR cell, respectively. Applying these numbers to their graph, the maximum expected temperature rise becomes 0.12°K for both cells. The reaction cells' thermowells were located at about $\rho = 0.4$, and the thermocouple signals measured at these points were used for determining the temperatures of the static cell experiments. No temperature rise due to the presence of reactants was detected.

C. NO_3 Steady State Concentrations

Nitrogen trioxide is a free radical intermediate in the $\text{N}_2\text{O}_5\text{-O}_3$ system, and its concentration depends on those of O_3 and N_2O_5 and on the rate constants relating the three species. The concentrations of NO_3 , O_3 and N_2O_5 were measured under steady state flow conditions in the UV cell. The NO_3 visible spectrum was scanned, and after a quick conversion of the system to infrared use, the N_2O_5 and O_3 spectra in the infrared were scanned. When several sets of data were taken at one flow condition, the concentrations of N_2O_5 and O_3 at the time of an NO_3 scan were obtained by interpolation. The cross sections used for the reactants have been described in earlier sections.

The steady state concentration data is summarized in Table XI. The quantity β refers to the left side of Eq. (37), and the values listed in the table are the ones calculated after the iteration process

Table XI. NO₃ steady state concentrations and data for equation (37).

	[NO ₃]x10 ⁻¹³	[O ₃]x10 ⁻¹⁶	[N ₂ O ₅]x10 ⁻¹⁴	$\frac{(\text{NO}_3)^2}{(\text{O}_3)(\text{N}_2\text{O}_5)} \times 10^{-4}$	B (molec cm ⁻³)
297.8°K	3.844	2.509	8.630	0.682	2.714
	3.880	2.511	8.630	0.695	2.787
	2.672	2.859	2.619	0.954	2.599
	2.697	2.869	2.619	0.968	2.662
	3.074	2.048	5.510	0.837	2.663
	3.098	2.062	5.510	0.845	2.706
	1.241	1.055	0.834	1.750	2.239
	1.244	1.055	0.829	1.769	2.269
	1.038	1.064	0.505	2.005	2.135
	1.043	1.064	0.502	2.037	2.178
	1.558	1.875	0.835	1.550	2.468
	1.844	1.957	1.349	1.288	2.427
	1.860	1.972	1.372	1.279	2.430
	1.764	1.177	2.103	1.257	2.306
	1.792	1.182	2.103	1.292	2.405
	1.800	1.199	2.171	1.245	2.329
	4.285	5.037	5.860	0.622	2.711
	4.340	5.030	5.860	0.639	2.820
	3.239	1.603	3.290	0.789	2.662
	3.253	1.606	3.360	0.788	2.639
	1.197	0.579	1.608	1.539	1.970
	1.197	0.582	1.608	1.531	1.960
	2.699	0.973	3.830	2.348	2.466
	2.722	0.973	3.910	0.855	2.505
	0.988	0.664	0.807	1.822	1.838
	1.012	0.663	0.807	1.914	2.028
	2.694	0.990	8.160	0.898	2.594
	2.706	0.985	8.160	0.911	2.641
	4.701	3.347	11.29	0.585	2.832
	4.725	3.394	11.39	0.573	2.810
	4.777	3.463	11.48	0.574	2.823
	4.831	3.544	11.56	0.570	2.831
	3.224	3.198	3.893	0.835	2.748
	3.228	3.195	3.894	0.838	2.760
	3.220	3.188	3.908	0.832	2.736
	3.217	3.177	3.907	0.834	2.738
	4.206	3.159	8.540	0.656	2.835
	4.221	3.212	8.570	0.647	2.808
	4.251	3.284	8.590	0.641	2.798
	4.298	3.364	8.550	0.642	2.834
	3.682	1.606	12.33	0.685	2.664
	3.682	1.572	12.43	0.694	2.702
	3.649	1.542	12.54	0.689	2.661
	3.622	1.515	12.59	0.632	2.641
	3.787	4.864	4.160	0.706	2.714
	3.824	5.044	4.154	0.698	2.709
	3.861	5.157	4.146	0.697	2.731
	3.882	5.238	4.137	0.695	2.739
	5.534	5.563	10.79	0.510	2.879
	5.542	5.511	10.79	0.517	2.918
	5.522	5.483	10.83	0.514	2.891
	5.538	5.458	10.86	0.517	2.922
	5.328	8.905	5.953	0.535	2.883
	5.345	9.063	5.932	0.531	2.870
	5.385	9.230	5.907	0.532	2.893
	6.975	8.400	14.31	0.405	2.868

Table XI. (Cont.)

	$[\text{NO}_3] \times 10^{-13}$ (molecules cm^{-3})	$[\text{O}_3] \times 10^{-16}$ (molecules cm^{-3})	$[\text{N}_2\text{O}_5] \times 10^{-14}$ ()	$\frac{(\text{NO}_3)^2}{(\text{O}_3)(\text{N}_2\text{O}_5)} \times 10^{-4}$	$\frac{\delta}{(\text{molec cm}^{-3})}$
<u>297.8°K</u>	7.187	9.140	14.38	0.393	2.866
	7.396	9.930	14.44	0.381	2.861
	7.609	10.84	14.41	0.371	2.857
	4.719	6.648	5.843	0.573	2.742
	4.745	6.739	5.847	0.571	2.748
	4.766	6.804	5.852	0.570	2.755
	4.776	6.805	5.860	0.572	2.768
<u>313.4°K</u>	1.975	0.535	0.890	8.192	17.44
	1.978	0.538	0.890	8.171	17.42
	1.483	0.228	1.151	8.399	14.78
	1.504	0.224	1.151	8.758	15.57
	3.818	0.605	6.450	3.736	16.51
	3.873	0.605	6.510	3.809	17.03
	5.283	1.221	7.140	3.201	18.41
	5.324	1.221	7.220	3.215	18.63
	7.350	3.090	6.960	2.512	19.24
	7.360	3.108	6.960	2.504	19.20
	4.800	3.412	1.880	3.592	17.67
	4.823	3.411	1.880	3.627	17.92
	3.567	3.493	0.710	5.130	18.59
	3.555	3.506	0.710	5.077	18.34
	5.774	2.343	4.860	2.928	17.71
	5.858	2.346	4.860	3.010	18.45
	12.76	7.490	14.37	1.513	19.83
	12.87	7.520	14.68	1.500	19.84
	12.96	7.550	14.92	1.491	19.86
	13.03	7.570	15.13	1.482	19.85
	10.19	6.820	8.000	1.903	19.85
	10.24	6.930	8.040	1.882	19.72
	10.37	7.120	8.060	1.874	19.87
	10.44	7.300	8.070	1.850	19.75
	11.36	5.816	13.34	1.663	19.51
	11.39	5.731	13.78	1.643	19.34
	11.37	5.625	13.99	1.643	19.32
	11.32	5.516	14.11	1.646	19.29
	7.960	5.075	5.200	2.401	19.59
	7.920	5.008	5.200	2.409	19.56
	7.930	4.982	5.210	2.423	19.70
	7.910	4.996	5.220	2.399	19.46
	7.950	5.019	5.250	2.399	19.56
	3.506	1.565	1.619	4.851	17.73
	3.530	1.558	1.636	4.839	17.99
	3.545	1.571	1.651	4.845	17.90
	3.590	1.599	1.677	4.806	17.98
	2.146	0.811	0.756	7.511	16.99
	2.167	0.809	0.759	7.648	17.46
	2.183	0.817	0.762	7.655	17.59
	2.199	0.829	0.766	7.615	17.62

Table XI. (Cont.)

	$[\text{NO}_3] \times 10^{-13}$	$[\text{O}_3] \times 10^{-16}$	$[\text{N}_2\text{O}_5] \times 10^{-14}$	$\frac{(\text{NO}_3)^2}{(\text{O}_3)(\text{N}_2\text{O}_5)} \times 10^{-4}$	β (molec cm^{-3})
	(molecules cm^{-3})		
<u>329.0°K</u>	13.25	4.940	4.850	7.328	101.0
	13.50	4.940	4.930	7.483	105.0
	9.820	2.329	4.340	9.540	100.2
	9.930	2.330	4.340	9.751	103.4
	11.26	2.716	5.380	8.677	104.1
	11.24	2.722	5.380	8.627	103.3
	14.93	6.748	4.911	6.726	103.6
	14.92	6.678	4.930	6.762	104.1
	14.89	6.615	4.953	6.767	104.0
	14.86	6.546	5.003	6.743	103.5
	11.70	6.125	2.550	8.764	105.2
	11.61	5.944	2.595	8.739	104.2
	11.66	5.799	2.632	8.908	106.7
	11.56	5.647	2.635	8.931	106.7
	15.80	5.609	6.980	6.376	104.9
	15.93	5.684	7.040	6.342	105.2
	16.01	5.710	7.090	6.331	105.5
	16.02	5.695	7.170	6.285	104.8
	10.74	5.174	2.471	9.022	99.84
	10.63	5.005	2.472	9.133	100.1
	10.53	4.881	2.474	9.182	99.76
	10.47	4.756	2.503	9.209	99.56
	5.952	1.613	1.452	15.13	95.66
	5.971	1.574	1.437	15.23	96.76
	5.992	1.569	1.522	15.04	95.94
	6.005	1.561	1.537	15.03	96.15
	7.359	1.787	2.492	12.16	95.85
	7.343	1.720	2.531	12.39	97.56
	7.389	1.742	2.578	12.16	96.39
	9.006	3.272	2.390	10.37	97.46
	8.968	3.257	2.410	10.25	95.94
	8.986	3.210	2.446	10.28	96.55
	8.987	3.217	2.474	10.15	95.32

(Four significant figures were generated by the computer printout, but the precision for all quantities is \approx .1%.)

has converged to a final value for $(Kh/2g)$. At each temperature a linear least squares fit of β vs $[NO_3]^2/[O_3][N_2O_5]$ was made with the quantities weighted by the standard deviations of the cross sections. The results were:

T (°K)	$\frac{Kh}{2g}$ (molecules cm^{-3})	$\frac{w}{2g}$ (molecules cm^{-3})	
297.8	$(3.127 \pm 0.059) \times 10^9$	$(0.573 \pm 0.056) \times 10^{13}$	
313.4	$(2.018 \pm 0.034) \times 10^{10}$	$(0.454 \pm 0.071) \times 10^{13}$	(80)
329.0	$(1.116 \pm 0.039) \times 10^{11}$	$(1.12 \pm 0.39) \times 10^{13}$	

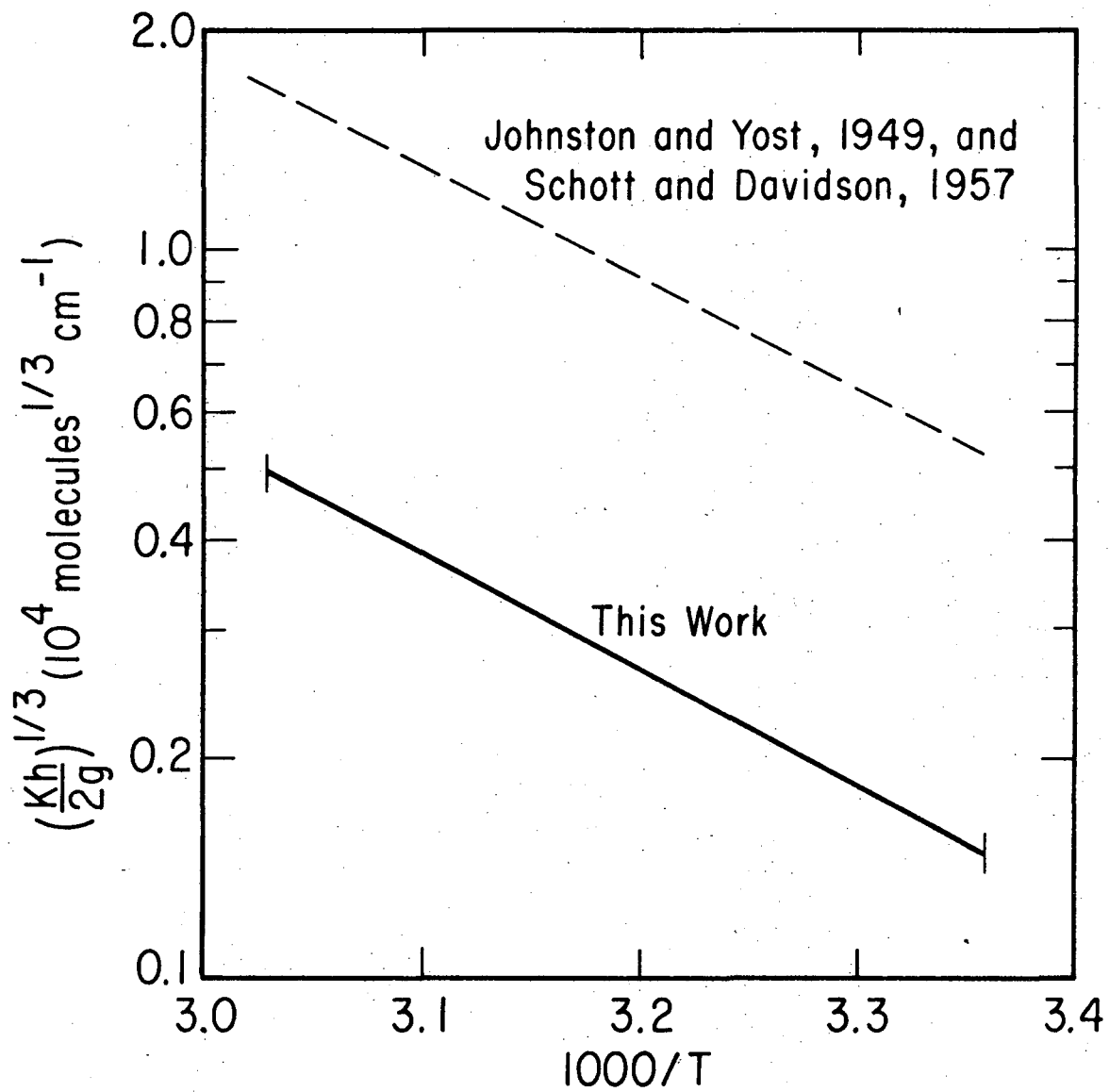
The values for $(Kh/2g)^{1/3}$, weighted by their standard deviations, were then least squares fitted to Arrhenius parameters to give:

$$\left(\frac{Kh}{2g}\right)^{1/3} = (4.04 \pm 0.47) \times 10^8 e^{-(7413 \pm 74)/RT} \text{ molecules}^{1/3} \text{ cm}^{-1} \quad (81)$$

The solid curve in Fig. 23 gives the present results and the dashed line gives the results predicted in Table III from the work of Johnston and Yost²⁷ and Schott and Dvaidson.¹⁸

D. Photolysis Lamp Calibration

The photolysis lamps used in this research produced broad bands of low intensity visible light. Both the spectral distribution of the lamps' output and the total photon flux in the reaction cell were needed to determine the NO_3 quantum yields from the modulation data. This information was also necessary to interpret the effects of illumination on static cell $N_2O_5-O_3$ reactions.



XBL 759-7286

Fig. 23. Arrhenius plot for $(\frac{Kh}{2g})^{1/3}$.

1. Spectral Distribution

In order to obtain the true spectra of the photolysis lamps, the spectral response of the UV cell's optical system was calibrated with a General Electric 30A/T24/17 tungsten ribbon lamp. This lamp was mounted behind the tuning fork chopper normally used with the deuterium arc lamp. The output of the lamp was stabilized by a feedback circuit using a photodiode to monitor the light intensity. The photodiode was covered by a blue Corning No. 5030 glass filter to make it more sensitive to temperature changes.

The light intensity I of a true black body is given by the Planck distribution law:

$$I_{\lambda, T} d\lambda = \frac{2\pi c}{\lambda^4} \frac{d\lambda}{(e^{hc/\lambda kT} - 1)} \quad (82)$$

where I = photons/cm² sec unit wavelength

λ = wavelength in cm

c = speed of light

h = Planck's constant

k = Boltzmann's constant

The emissivity of a substance, $E(\lambda, T)$, is the ratio of its radiative emission to that of a black body at the same temperature and wavelength. Using the emissivities for a tungsten ribbon determined by De Vos,⁷² the intensity distribution of the tungsten ribbon lamp can be determined from

$$I_{\lambda, T} d\lambda = \frac{2\pi c}{\lambda^4} \frac{E(\lambda, T) d\lambda}{(e^{hc/\lambda kT} - 1)} \quad (83)$$

The temperature used in Eq. (83) must be the true temperature of the tungsten ribbon. The brightness temperature S of the tungsten ribbon was measured with a Leeds and Northrup Model 8622-C optical pyrometer which was calibrated at the Lawrence Berkeley Laboratory. The true temperature T can then be calculated by⁷³

$$\frac{1}{T} - \frac{1}{S} = \frac{\lambda}{C_2} \ln[0.92E(\lambda, T)] \quad (84)$$

where $C_2 = 1.438$ cm degrees

$\lambda = 6500$ Angstroms

0.92 = transmission factor for the window

The spectrum of the tungsten ribbon lamp was scanned from 280 to 900 nm, and glass filters were used when necessary to eliminate light diffracted in second order. A RCA C31025J photomultiplier with a sapphire window was used for detection. Lamp spectra were taken at brightness temperatures of $2100 \pm 1^\circ\text{K}$ and $2173 \pm 1^\circ\text{K}$ (true temperatures of 2300°K and 2388°K). Correction curves for the optical system were obtained by dividing the observed lamp spectra by the spectra calculated from Eq. (83). When normalized at one point, the two correction curves agreed within a 1% average uncertainty. The average correction curve, normalized to one at 470 nm, is presented in Fig. 24.

Photolysis lamps of various colors were powered by the lamp flasher power supply and mounted behind the tuning fork chopper. Their spectra were taken with the same filters used with the tungsten ribbon lamp. The corrected photolysis lamp spectra are presented in Fig. 25. The ratios of the total light fluxes for the green, gold and red lamps

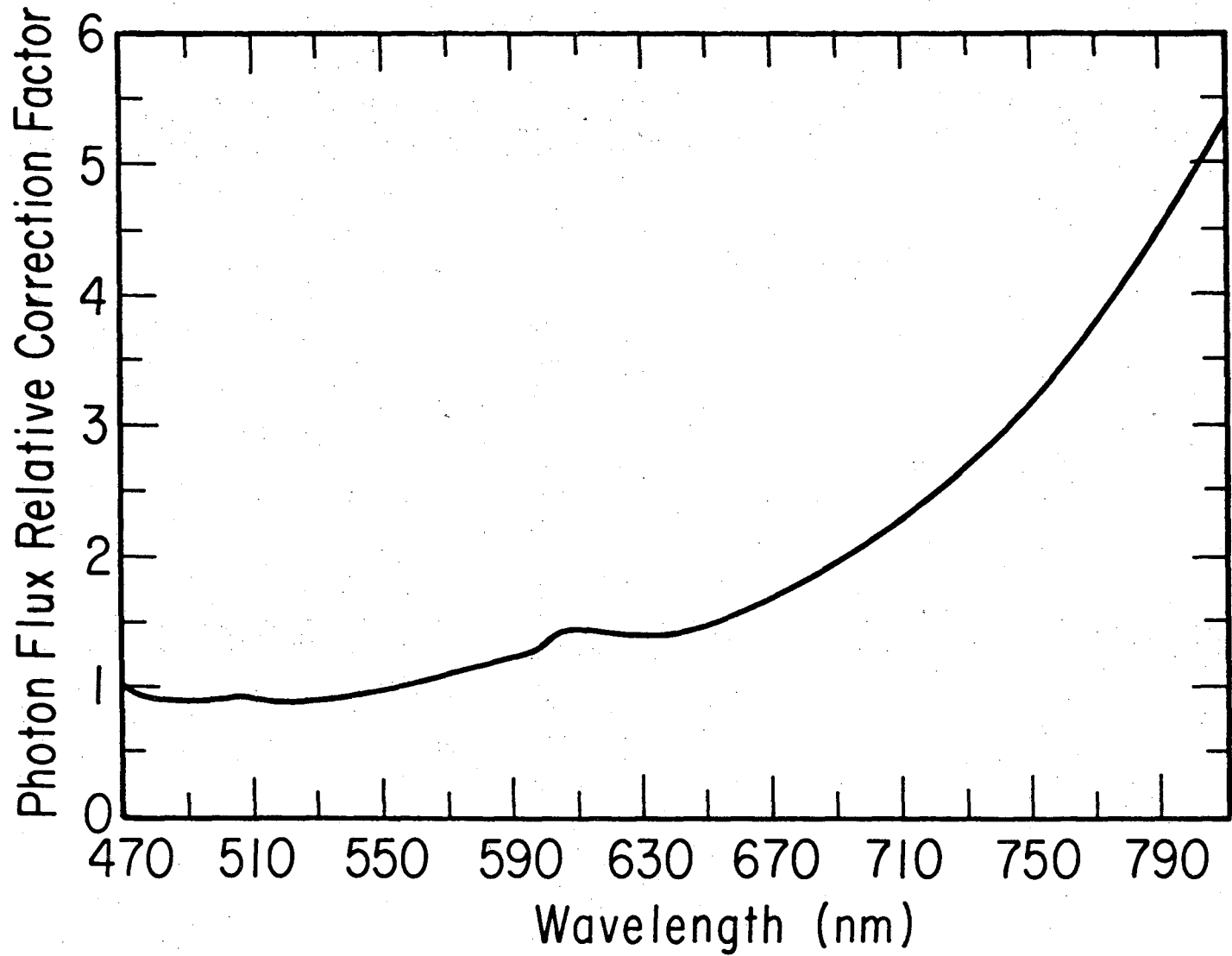
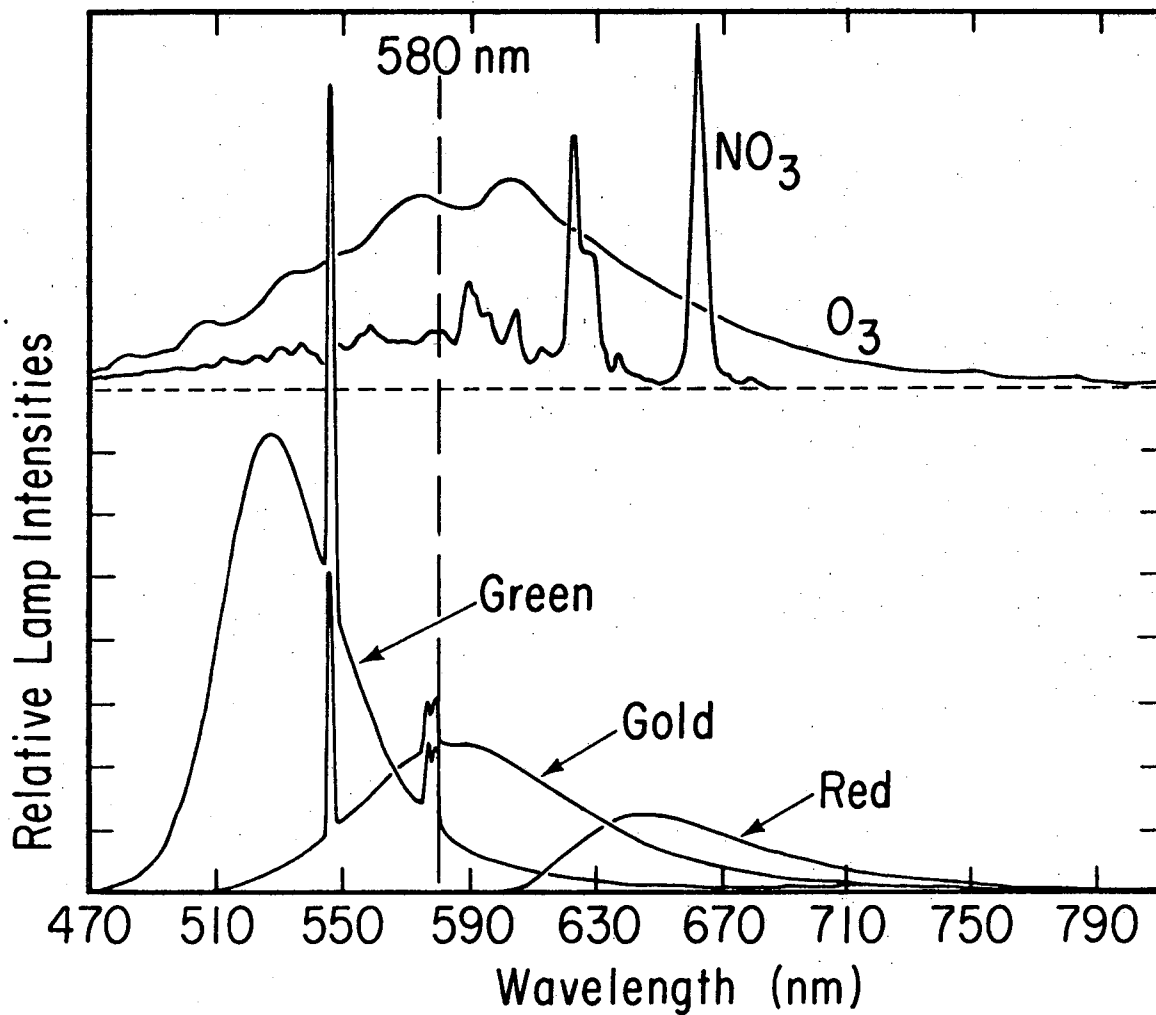


Fig. 24. Photon flux correction curve for UV reaction cell. XBL 759-7277



XBL 759-7285

Fig. 25. Relative intensities of photolysis lamps at 298°K.

were 1.0:0.56:0.23, respectively. The visible spectra of NO_3 and O_3 are included in Fig. 25 to show the degree of overlap with the various lamps.

The average cross section for NO_3 absorption for each lamp spectrum is the wavelength integrated product of cross section (σ_λ) and lamp intensity (L_λ):

$$\sigma_{\text{avg}}(\text{NO}_3) = \frac{\int \sigma_\lambda(\text{NO}_3) L_\lambda d\lambda}{\int L_\lambda d\lambda} \quad (85)$$

Since nitrogen dioxide and oxygen atom are energetically possible products only for wavelengths less than 580 nm, the average NO_3 cross section is computed both for the region above and the region below this wavelength. Table XII contains the average NO_3 cross sections and the fraction of the light in each wavelength region. The average ozone cross section for each lamp is also included in the table.

2. Light Flux Calibration

The products of ozone photolysis by light in the 570 to 630 nm region are ground state oxygen atom and oxygen, and no energy chains that destroy ozone have been observed.^{54,55} Since the rate constants for oxygen atom reacting with O_2 and O_3 are well known,⁵⁰ ozone can be used for actinometry with the photolysis lamps.

Ozone from a dry ice temperature silica gel trap was liquified at liquid nitrogen temperature and pumped on to remove oxygen. The ozone was then allowed to vaporize slowly into the evacuated cell until the pressure reached 2 to 3 Torr. Concentration determinations were made from ozone's visible absorption spectrum. The ozone

Table XII. Wavelength averaged cross sections ($\text{cm}^2 \text{ molecule}^{-1}$) of NO_3 and O_3 for different photolysis lamps.

Lamp	σ_{NO_3}	% Light	σ_{NO_3}	% Light	σ_{O_3}
	($\lambda \leq 580 \text{ nm}$)		($\lambda > 580 \text{ nm}$)		
<u>298 K</u>					
Green	1.88×10^{-18}	93	2.99×10^{-18}	7	2.76×10^{-21}
Gold	2.51×10^{-18}	37	3.11×10^{-18}	63	3.82×10^{-21}
Red	---	0	2.12×10^{-18}	100	2.13×10^{-21}
<u>329 K</u>					
Green	2.01×10^{-18}	93	3.10×10^{-18}	7	2.76×10^{-21}
Gold	2.67×10^{-18}	37	3.22×10^{-18}	63	3.82×10^{-21}
Red	---	0	2.17×10^{-18}	100	2.13×10^{-21}

-111-

concentrations were measured before and after 30 min periods of illumination by the flashing lamps. The ozone decay rate for 30 min in the dark was measured after each period of illumination. Since 30% of the cell volume was in the end caps and shielded from the lamps, the actual intensity of the lamps was a factor of $\frac{1}{0.70}$ larger than that calculated from ozone destruction. (The path lengths used for modulation calculations were multiples of 708 cm, the part of the monitoring beam's path that was illuminated by the lamps.) After a period of illumination, about 30 min were required for the ozone concentration to equalize throughout the cell. Several determinations of the ozone concentration were made during this period so that an extrapolation could be made back to the point where the lamps were turned off. Only 25% of the initial ozone was destroyed in an experiment. Under these conditions, the overall quantum yield for ozone photolysis was ≥ 1.995 .

The light intensities measured for the primary reaction cell were:

<u>Lamp</u>	<u>297.8°K</u>	<u>329.0</u>
Green	1.55±0.15	2.03±0.21
Gold	1.07±0.02	
Red	0.33±0.04	0.29±0.05

(units are 10^{16} photos/cm² sec)

Both ozone's low visible absorption cross section and the concentration fluctuations due to the end caps were responsible for the large uncertainties in the light flux measurements. The ratios of the 298°K intensities for the green, gold and red lamps were 1.0:0.69:0.21.

Since these ratios are similar to those obtained in the determination of the spectral distributions of the lamps, it appears that no energy chains are present in the photolysis of ozone by green light.

E. Modulation Experiments

The modulation experiments produced several types of kinetic information. The absorptions and roles of several major reaction species were identified by their modulation phase shifts and amplitudes. Other modulation derived information included the NO_3 visible absorption cross sections, the primary quantum yields for NO_3 photolysis, and the rate constants for oxygen atoms reacting with NO_3 and N_2O_5 . All modulation experiments were performed in a flow system at one atmosphere total pressure.

1. Identification of Reaction Species

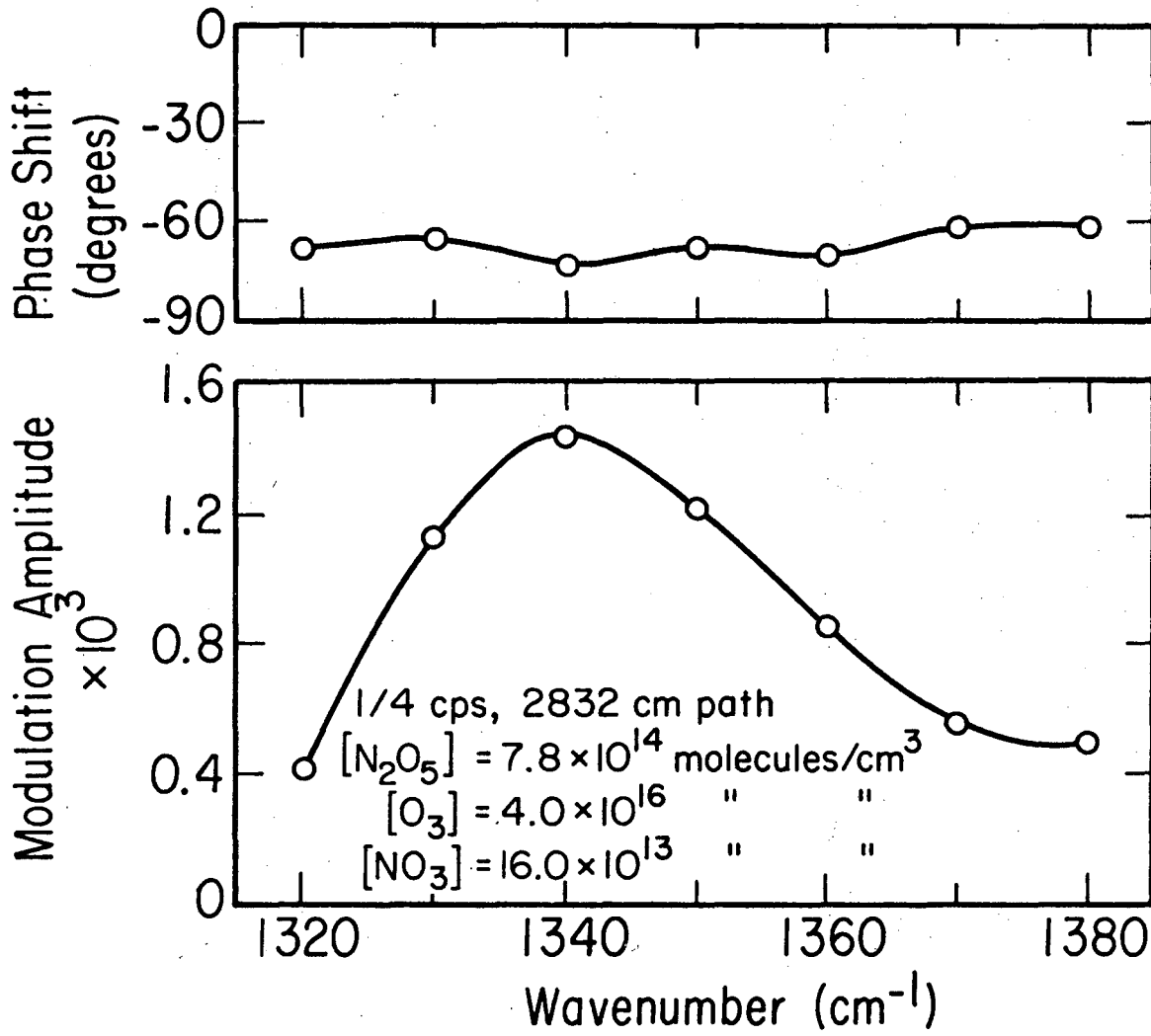
Preliminary experiments were carried out to determine the modulation behavior of the various reaction species. In the $\text{N}_2\text{O}_5\text{-O}_3$ flow system, the species present in significant concentrations were O_3 , N_2O_5 , HNO_3 and NO_3 . The NO_3 modulation was monitored by its strong visible absorption spectrum. The amplitudes for different wavelengths in this spectrum were proportional to their respective NO_3 absorption cross sections, and the phase shifts were identical throughout the region. The NO_3 phase shifts for flashing frequencies near 1 cps were approximately 90° , and this indicates that NO_3 is a reactant being destroyed by light or fast intermediates. Ozone has a weak absorption that overlaps the NO_3 spectrum, but its predicted modulation amplitude was several orders of magnitude smaller than that of NO_3 and could not be detected. The ozone concentration

modulation was also undetectable at the near ultraviolet Huggins bands and the 4.7 μ infrared absorption bands.

The infrared absorption of HNO_3 at 7.70 μ was monitored to determine if nitric acid played a role in the modulation kinetics. Since no phase coherent signal was detected, the HNO_3 concentration modulation is at least a factor of 10 smaller than that of N_2O_5 .

The N_2O_5 modulation was monitored at its 8.028 μ infrared absorption peak. The phase shift for this signal always differed from that for NO_3 by approximately 180°, and this indicates that NO_3 and N_2O_5 have a reactant-product relationship. Modulation data was taken at 10 cm^{-1} intervals in the 1325 to 1375 cm^{-1} region where an NO_3 absorption band has been reported.²⁰ The NO_3 phase shift at 627 nm was 121°, and the N_2O_5 phase shift at 8.028 μ was -62°. The amplitude and phase shift data in Fig. 26 indicates that this absorption band is due to N_2O_5 . The absorption cross sections for this band were calculated from the 8.028 μ N_2O_5 cross section and the ratio of modulation amplitudes. These cross sections are plotted in Fig. 15.

Nitrogen dioxide is a low concentration, fast intermediate in this system and attempts were made to detect this species by its strong near ultraviolet absorption spectrum. Since no modulation signal could be detected, the ratio of the NO_3 concentration modulation to that for NO_2 was greater than a factor of 10. Nitric oxide and oxygen atom modulations in this system were much too small to be detected.



XBL 759-7289

Fig. 26. Modulation amplitude and phase shifts for the 1320 to 1380 cm⁻¹ region at 329°K with green lamps.

2. NO₃ Absorption Cross Sections

Absorption cross sections for N₂O₅ were determined by an NO_x mass balance in flow experiments as described in an earlier section. The concentration of NO₃, however, was much too small to be accurately determined by the NO_x mass balance. Since the destruction of two NO₃ molecules results in the production of approximately one N₂O₅ molecule, the NO₃ absorption cross section can be calculated from the ratio of modulation signals for N₂O₅ and NO₃. Both green and gold photolysis lamps were used in these measurements. Since the only quantity of interest in this part of the study was the ratio of modulation amplitudes, accurate values for the photon fluxes were not needed. The contributions of oxygen atom reactions to the modulation amplitudes had the same ratio as that of the photolysis reactions. The N₂O₅ modulation signal was averaged for 30 to 60 min at 1/4 cps, and the much stronger NO₃ signal for 10 min. The NO₃ modulation was monitored at 627 nm, the center of a fairly broad absorption band that obeyed Beer's law, and N₂O₅ was observed at its 8.028 μ infrared absorption peak. The stoichiometric factor (S.F.) relating the NO₃ and N₂O₅ concentration modulations was obtained for each set of conditions by a complete computer simulation. The NO₃ cross section at 627 nm could then be obtained from the N₂O₅ cross sections (Eq. (70)) and the ratios of modulation amplitudes and optical path lengths:

$$\sigma_{627} = \sigma_{N_2O_5} \frac{1}{S.F.} \frac{A_{NO_3}}{A_{N_2O_5}} \frac{L_{N_2O_5}}{L_{NO_3}} \quad (87)$$

The data for Eq. (87) is summarized in Table XIII. The resulting NO_3 cross sections have been presented in Eq. (65).

3. NO_3 Quantum Yields

According to Eq. (48), the NO_3 modulation amplitude is directly proportional to its primary quantum yield. Modulation experiments were carried out to measure the quantum yield using red, green and gold lamps. Oxygen was used as the carrier gas in order to suppress possible contributions to the modulation amplitude from oxygen atom reactions with NO_3 and N_2O_5 . These experiments were performed in the UV reaction cell, and a summary of the data is presented in Table XIV. The quantum yields were calculated from a computer simulation of the reaction system for each set of conditions. The light fluxes from Eq. (86) and the absorption cross sections from Table XII were used in the calculations. The uncertainties in the quantum yields include contributions from uncertainties in the light fluxes and from complications in the $[\text{NO}_3]$ determination: the green and gold lamps reduce the steady state concentration of NO_3 by 5 to 30% in the lighted portion of the reaction cell, but the optical path for spectroscopic monitoring also passes through the end caps (29.6% of the volume) where no NO_3 is photolyzed. Convective mixing between the lighted and unlighted portions of the reaction cell adds to the uncertainty in NO_3 concentration. The correction for these effects introduces about a 2% uncertainty in the quantum yields.

The calculation of the primary quantum yield depends strongly on the NO_3 photolysis products. The rate of reaction f , $\text{NO} + \text{NO}_3$,

Table XIII. NO₃ absorption cross sections derived from modulation data.

Temp. (K)	Gas Cell and Lamps	% O ₂	$\frac{O_3}{N_2O_5}$	Stoich. Factor	$\frac{A_{NO_3}}{A_{N_2O_5}}$	$\frac{L_{N_2O_5}}{L_{NO_3}}$	% S.D. of Mean	$\sigma_{627} \times 10^{18}$
			(molecules cm ⁻³)		(cm)	(cm ² molecule ⁻¹)		
298	UV Cell Green	4	4.6×10^{16} 5.3×10^{14}	2.04	0.0228 0.000785	708 2832	8.8	6.23
298	UV Cell Green	99	9.1×10^{16} 6.3×10^{14}	2.02	0.0289 0.000887	708 2832	13.8	7.06
298	IR Cell Gold	4	3.9×10^{16} 3.4×10^{14}	2.04	0.00510	1200 800	9.1	7.67
298	IR Cell Gold	4	4.0×10^{16} 3.1×10^{14}	2.04	0.00495 0.000828	1200 800	5.5	7.69
298	UV Cell Green	.5	6.7×10^{16} 6.0×10^{14}	2.03	0.0127 0.00157	708 708	4.3	6.97
298	UV Cell Green	.5	6.7×10^{16} 6.0×10^{14}	2.03	0.0122 0.00154	708 708	5.1	6.81
313	IR Cell Gold	99	3.5×10^{16} 13.9×10^{14}	2.10	0.0164 0.000881	400 800	7.0	7.46
313	IR Cell Gold	.5	5.2×10^{16} 11.5×10^{14}	2.07	0.0242 0.00139	400 800	2.2	7.06
313	UV Cell Green	91	7.6×10^{16} 8.4×10^{14}	2.05	0.0237 0.00270	708 708	4.7	7.19
313	UV Cell Green	91	7.6×10^{16} 8.4×10^{14}	2.05	0.0239 0.00267	708 708	4.3	7.34
313	UV Cell Green	.5	6.0×10^{16} 5.4×10^{14}	2.07	0.0273 0.00328	708 708	2.3	6.76

contd.

00004400233

Table XIII, contd.

313	UV Cell Green	.5	7.5×10^{16} 5.4×10^{14}	2.07	0.0296 0.00340	708 708	2.4	7.07
329	IR Cell Gold	.5	10.5×10^{16} 10.1×10^{14}	2.07	0.0187 0.00180	400 400	5.7	7.83
329	IR Cell Gold	.5	8.6×10^{16} 10.2×10^{14}	2.07	0.0184 0.00193	400 400	5.2	7.18
329	IR Cell Gold	99	3.5×10^{16} 13.8×10^{14}	2.16	0.0217 0.00125	400 800	4.5	6.27
329	IR Cell Gold	99	3.5×10^{16} 13.8×10^{14}	2.16	0.0217 0.00117	400 800	7.3	6.70
329	UV Cell Green	99	5.1×10^{16} 1.5×10^{14}	2.07	0.0182 0.00747	2832 708	2.8	7.34
329	JV Cell Green	99	5.1×10^{16} 1.7×10^{14}	2.07	0.0196 0.00823	2832 708	2.7	7.18
329	UV Cell Green	99	6.0×10^{16} 5.2×10^{14}	2.08	0.0265 0.00565	1416 708	4.2	7.02
329	UV Cell Green	99	5.7×10^{16} 5.2×10^{14}	2.09	0.0259 0.00535	1416 708	3.0	7.24
329	UV Cell Green	99	5.1×10^{16} 2.6×10^{14}	2.08	0.0216 0.00873	2832 708	3.0	7.42
329	UV Cell Green	99	4.9×10^{16} 2.7×10^{14}	2.08	0.0211 0.00910	2832 708	3.9	6.96
329	UV Cell Green	.5	5.2×10^{16} 7.4×10^{14}	2.10	0.0411 0.00452	708 708	2.6	6.74
329	UV Cell Green	.5	4.7×10^{16} 7.6×10^{14}	2.11	0.0402 0.00428	708 708	1.7	6.96

and that of reaction i, $\text{NO} + \text{O}_3$, were about the same under most of the experimental conditions of the present study. If NO is a photolysis product of NO_3 , reaction f would increase the observed destruction of NO_3 and thus the apparent quantum yield. The quantum yields in Table XIV were calculated assuming that the products of red light photolysis were NO and O_2 and that green light gave NO_2 and oxygen atom. The 37% of the gold lamps' output below 580 nm was assumed to give NO_2 and $\text{O}(^3\text{P})$ and the residual modulation amplitude was assumed to be due to production of NO and O_2 by light of wavelengths greater than 580 nm. Refinements of these product distributions by considering the data from the illuminated N_2O_5 catalyzed destruction of ozone will be presented in Section IV-B.

4. Oxygen Atom Reactions

Ground state oxygen atoms ($\text{O}(^3\text{P})$) are generated in the $\text{N}_2\text{O}_5\text{-O}_3$ system from photolysis of both O_3 and NO_3 . Because oxygen atom is a very fast intermediate, reactions m and n would result in a NO_3 modulation with the same phase shift as the NO_3 photolysis reactions. Nitrogen was used as a carrier gas in experiments to measure the rate constants for reactions m and n. A low, known concentration of oxygen was present due to a small oxygen flow through the ozonizer. Since the rate of reaction p_3 , $\text{O} + \text{O}_2 + \text{M}$, was about 10 times that of any other oxygen atom reaction, the oxygen atom concentration was almost directly proportional to the rate constant for this reaction. The primary quantum yields for NO_3 determined from the data in the previous section were used to calculate the NO_3 modulation amplitudes due to the photolysis reactions j_1 and j_2 . The residual amplitudes observed

Table XIV. Primary quantum yields for NO₃ photolysis from 1/4 cps modulation data.

Lamps	Temp (K)	[NO ₃] × 10 ⁻¹³	[N ₂ O ₅] × 10 ⁻¹⁴ molecules cm ⁻³	[O ₃] × 10 ⁻¹⁶	L (cm)	Mod. Amp. (@627nm)	Primary Q.Y.	
Red	298	6.00	11.19	6.076	1416	0.000457	0.055	} j ₁ : 0.049±0.010
	298	2.274	3.22	1.157	2832	.000338	.050	
	298	5.33	13.62	3.364	1416	.000332	.043	
Red	329	12.04	8.38	2.045	1416	0.000668	0.043	} j ₁ : 0.044±0.09
	329	13.70	16.97	1.545	1416	.000768	.045	
Green	298	2.74	3.96	3.11	708	0.00518	1.11	} j ₂ : 1.07±0.09
	298	4.00	8.65	3.434	708	.00740	1.06	
	298	5.25	11.00	5.94	708	.01002	1.08	
	298	5.02	5.96	9.35	708	.00914	1.03	
Green	329	14.71	5.07	6.35	708	0.0267	0.80	} j ₂ : 0.80±0.14
	329	11.22	2.640	5.48	708	.0218	.86	
	329	7.35	4.15	1.120	708	.01336	.80	
	329	11.49	7.19	2.40	708	.01991	.77	
	329	17.49	14.85	3.86	708	.02800	.75	
Gold	298	5.49	11.41	6.12	1416	0.01757	0.37±0.44	} j ₁ : 0.43±0.02
	298	5.58	11.86	6.17	1416	.01775	.37±0.44	
	298	3.656	15.24	1.607	1416	.01144	.37±0.40	
	298	3.645	15.16	1.583	1416	.01154	.37±0.41	} j ₂ : 0.37 (assumed)
	298	5.71	12.66	6.27	1416	.01324	.37±0.44	
	298	5.83	13.09	6.32	1416	.01855	.37±0.44	

with the nitrogen carrier gas were attributed to reactions m and n. Computer simulations showed a linear relationship between the rate constants m and n and the calculated modulation amplitudes due to these reactions. The modulation contributions from these two reactions can thus, in principle, be separated by varying the NO_3 to N_2O_5 ratio and solving the resulting simultaneous equations for the rate constants m and n. Since the calculations are based on the conclusions drawn from the other parts of this study, analysis of the data will be deferred to Section IV-C.

IV. KINETIC RESULTS

Information from the various experimental techniques employed in this study must be combined in order to elucidate the kinetics of the $N_2O_5-O_3$ system under visible illumination. The complexity of the system increases from studies of the reactions without light, to studies employing visible illumination with oxygen as the carrier gas, and finally to studies of illuminated reactions with nitrogen as the carrier gas and with the consequent oxygen atom reactions.

A. $N_2O_5-O_3$ Kinetics

The behavior of the $N_2O_5-O_3$ system in the unilluminated reaction cell can be well described by reactions A through i and w. The only directly measured rate constant was for the NO_2-O_3 reaction (Eq. (73)). The N_2O_5 catalyzed decomposition of ozone gave $1/2(Kh)^{2/3}(2g)^{1/3}$, Eq. (74), and measurements of the steady state concentration of NO_3 as a function of N_2O_5 and O_3 led to $(Kh/2g)^{1/3}$, Eq. (81). The equilibrium constant K can be obtained by multiplying Eq. (74) by Eq. (81) and dividing by the rate constant h. Substituting K and h in Eq. (74) or Eq. (81) then gives the rate constant g. These rate constants are listed in Table XV. The uncertainties for K and g were obtained by propagation of the standard deviations of the quantities in Eqs. (73), (74) and (81).

This rather involved method of obtaining values for K and g results in calculated uncertainties about twice as large as those for the experimentally measured quantities. A consideration of the parameters involved in obtaining the quantities in Eqs. (74) and (81) will show that the above error limits are conservative. Neglecting the NO_3

Table XV. Comparison of rate constants with literature values.

Temp. Range of Data (K)	Reaction	Pre-exponential Factor ($\text{cm}^3 \text{ molecule}^{-1} \text{ sec}^{-1}$)	E_a (calories) 300°K	Reference
231-298	h	$(1.34 \pm .11) \times 10^{-13}$	4900±60	This work
298-329	K	$(8.4 \pm 1.8) \times 10^{26}$ molecules cm^{-3}	22210±200	This work
298-329	g	$(8.5 \pm 2.8) \times 10^{-13}$	4870±200	This work
286-302	h	9.8×10^{-12}	7000±600	27
450-550	K	2.0×10^{26} molecules cm^{-3}	21,000±1000	18
550-1100	g	3.2×10^{-12}	7100±1000	18
260-343	h	$(9.76 \pm .54) \times 10^{-14}$	4824±280	35
259-362	h	$(1.57 \pm .41) \times 10^{-13}$	4985±150	36

correction terms, Eqs. (35) and (37) become

$$\left(\frac{Kh}{2g}\right)^{1/3} = \frac{[\text{NO}_3]}{[\text{O}_3]^{1/3} [\text{N}_2\text{O}_5]^{1/3}} \quad (88)$$

$$1/2(Kh)^{2/3} (2g)^{1/3} = \frac{-\frac{d[\text{O}_3]}{dt}}{[\text{O}_3]^{2/3} [\text{N}_2\text{O}_5]^{2/3}} \quad (89)$$

Multiplying these two equations together and dividing by h gives

$$K = \frac{-\frac{d[\text{O}_3]}{dt} [\text{NO}_3]}{h[\text{O}_3][\text{N}_2\text{O}_5]} \quad (90)$$

The concentrations of these chemical species were determined from experimentally measured absorption cross sections. Since the NO_3 cross section is directly proportional to that of N_2O_5 , the cross sections in Eq. (90) cancel out and uncertainties due to the O_3 and N_2O_5 cross sections disappear. Approximately one third of the calculated uncertainty in K is due to these cross sections.

The results of Johnston and Yost²⁷ and Schott and Davidson¹⁸ are included in Table XV for comparison with the present study. The error limits for only the equilibrium constant K from the two studies overlap. The recent mass spectrometric results of Davis and co-workers³⁵ and Herron and Huie³⁶ give strong support to the value of h measured in the present study and are included in the table. The equilibrium constant from the present work can be combined with literature values for A, K_e and K_f (in Table II) to obtain values for B, e and f. These rate constants are listed in Table XVI. Rate constants for reaction w

Table XVI. Rate constants obtained by combining literature data with K.
(Total pressure = 1 atm.)

Temp. Range of Data (K)	Literature Reaction Quantity	Reaction	Pre-exponential Factor ($\text{cm}^3 \text{ molecule}^{-1} \text{ sec}^{-1}$)	Activation Energy (calories)	Reference
300	A	B	$(1.48 \pm .33) \times 10^{-13}$	-1710 ± 600	46,47
338-396	Ke	e	$(2.5 \pm .5) \times 10^{-14}$	2440 ± 200	40
297	Kf	f	$(1.87 \pm .41) \times 10^{-11}$	---	49

can be obtained from the data of Eq. (80):

<u>Temp. (°K)</u>	<u>w(sec⁻¹)</u>	
298	0.00259±0.00025	
313	0.0031±0.0005	(91)
329	0.0055±0.0020	

The loss of NO₃ due to reaction w was assumed to lead to NO₂ as a product in the above calculations, but the possibility of NO being the product has not been eliminated. A chemiluminescence study of the NO₂-O₃ reaction, discussed in Section V-A, indicates that no significant amount of NO is found in the gas phase of this system. This does not, however, forbid heterogeneous reactions from giving NO. Fortunately, only the rate constant for reaction w is dependent on the choice of products. If NO is the product of reaction w, a term must be added to the definition of α in Eq. (28):

$$\alpha' = \alpha + \frac{f[\text{NO}_3] w[\text{NO}_3]}{K_e[\text{N}_2\text{O}_5](f[\text{NO}_3] + i[\text{O}_3])} \quad (92)$$

The value of $1/2(Kh)^{2/3}(2g)^{1/3}$ from Eq. (35) was changed by less than 0.2% by replacing α by α' because the second order decay of NO₃ was the dominant factor in these experiments with high ozone concentrations. The slope, w/2g, obtained from Eq. (37) was reduced by using α', but the value of the intercept, (Kh/2g), was changed by less than 0.1%. (This is expected since the intercept represents conditions where NO₃ loss is due entirely to reaction g.) If NO is the reaction product, the rate constants for reaction w would be:

<u>Temp. (°K)</u>	<u>w' (sec⁻¹)</u>	
298	0.0035±0.0003	
313	0.0017±0.0006	(93)
329	0.0061±0.0041	

The temperature dependent behavior of reaction w in either Eq. (91) or Eq. (93) indicates that it is probably a heterogeneous reaction.

The enthalpy of formation of NO₃ can be obtained from the energy change of the equilibrium constant K and Eq. (38):

$$\Delta H_{f,300^{\circ}\text{K}} = 17.6 \pm 0.2 \text{ kcal/mole} \quad (94)$$

Eq. (39) and Eq. (40) then give the calculated threshold wavelength for the photolysis of NO₃ to give NO₂ and O(³P):

$$\Delta E_{300^{\circ}\text{K}} = 49.3 \pm 0.2 \text{ kcal/mole} \quad \text{and} \quad \lambda \leq 580 \pm 3 \text{ nm} \quad (95)$$

B. NO₃ Photochemistry

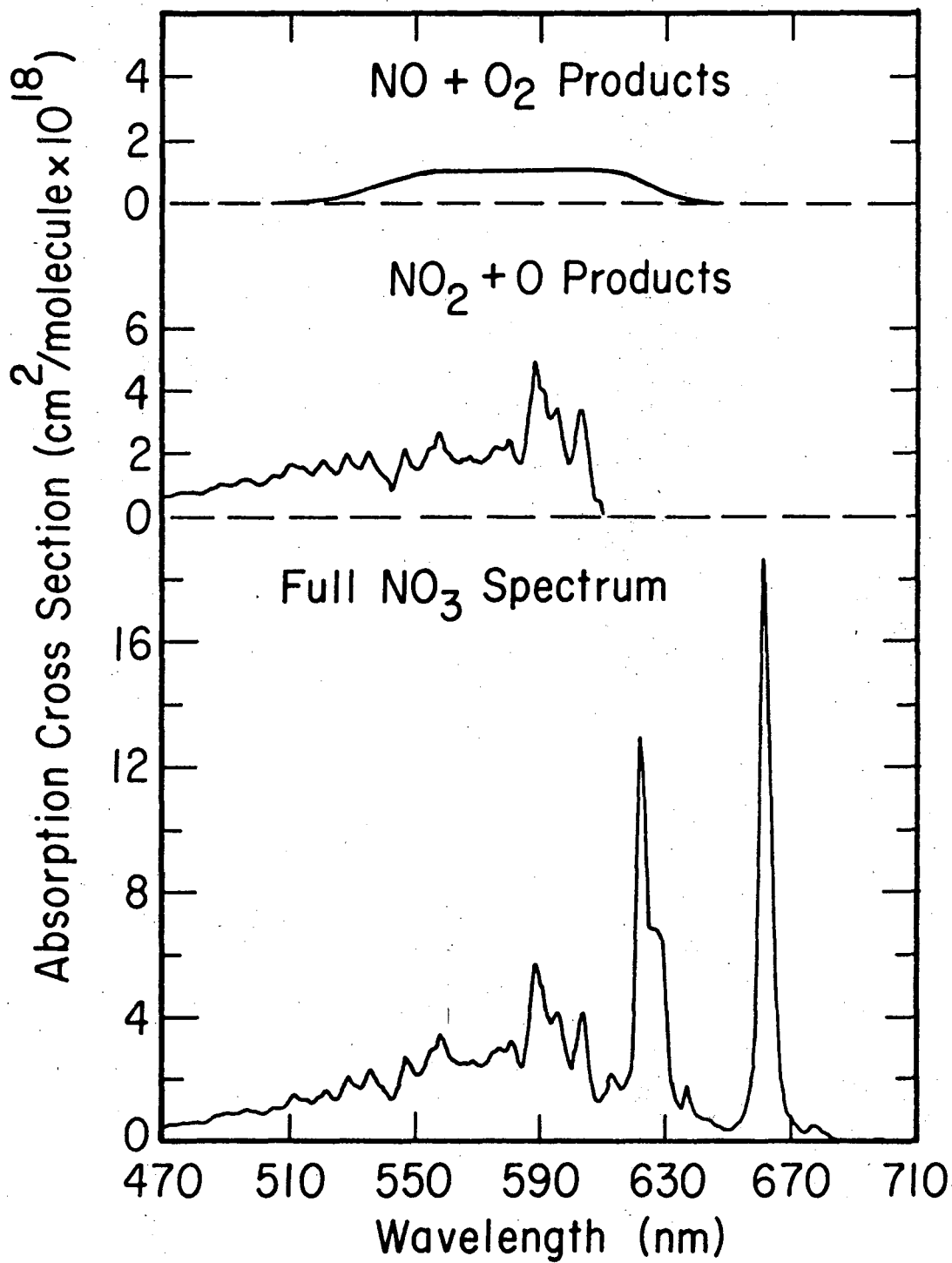
In order to determine the products of NO₃ photolysis, the apparent primary quantum yields in Table XIV must be combined with a detailed interpretation of the illuminated N₂O₅ catalyzed decomposition of ozone. The data for green and gold lamps at 298°K in Table IX were recalculated by Eq. (55) for several possible distributions of products in an effort to obtain the average $1/2(\text{Kh})^{2/3}(\text{2g})^{1/3}$ dark value. The quantum yields for red light photolysis were too small to yield information from this type of data treatment. All calculated values were corrected to 297.8°K by the activation energy of Eq. (74). The second set of values in Table XVII takes into account the lowered steady state concentration of NO₃ but does not make corrections for

Table XVII. Calculation of $\frac{1}{2}(Kh)^{\frac{2}{3}}(2g)^{\frac{1}{3}}$ for the illuminated reaction cell with all temperatures corrected to 297.8 K.

Run No.	Lamps	$\frac{1}{2}(Kh)^{\frac{2}{3}}(2g)^{\frac{1}{3}}$ (10^{-9} cm molecule $^{-\frac{1}{3}}$ sec $^{-1}$)				Reaction j_1 only	Reaction j_2 only	(Fitted to 0.484)	
		(No Corrections)	($[NO_3]_{ss}$ Corrections Only)						
24	Green	0.422	0.371	0.312	0.520	$j_1=0.11$ $j_2=0.90$	} $j_1:Q.Y. = 0.14 \pm 0.06$ $\sigma_{avg} = 2.99 \times 10^{-18}$ cm 2 molecule $^{-1}$		
26	Green	0.440	0.396	0.344	0.535	$j_1=0.17$ $j_2=0.80$			} $j_2:Q.Y. = 0.85 \pm 0.10$ $\sigma_{avg} = 1.88 \times 10^{-18}$ cm 2 molecule $^{-1}$
27	Gold	0.478	0.430	0.396	0.529	$j_1=0.25$ $j_2=0.60$	} $j_1:Q.Y. = 0.23 \pm 0.04$ $\sigma_{avg} = 3.11 \times 10^{-18}$ cm 2 molecule $^{-1}$		
29	Gold	0.472	0.423	0.391	0.524	$j_1=0.23$ $j_2=0.62$			} $j_2:Q.Y. = 0.63 \pm 0.06$ $\sigma_{avg} = 2.51 \times 10^{-18}$ cm 2 molecule $^{-1}$
30	Gold	0.468	0.429	0.387	0.521	$j_1=0.20$ $j_2=0.66$			

any ozone created or destroyed. The other calculated values also contain ozone corrections, and the total quantum yields for all the values are consistent with the apparent primary quantum yield data of Table XIV. The last column contains the quantum yields that result from fitting the data to the $1/2(Kh)^{2/3}(2g)^{1/3}$ dark value. Since the red light intensity below 600 nm was quite small, the red light quantum yield of 0.049 in Table XIV was assumed to be due to reaction j_1 . The quantum yields for red and green lamps in Table XIV were significantly lower at 329°K than at 298°K. Since the 329°K results suffered from large uncertainties in the calibration of the lamp intensities, this data was not used in the product analysis. The evidence for a temperature effect on the NO_3 quantum yield is not conclusive.

The quantum yields from the three sets of lamps at 298°K can be used to estimate the spectral distribution of photolysis products. Since only broad bands of light were used in this study, the actual details of band shapes cannot be determined. Figure 27 presents one possible separation of the NO_3 spectrum into photochemically active bands. Since the red light quantum yields are so low, the first two bands in the symmetric stretching sequence identified by Ramsay¹⁹ were assumed to be inactive. Although the threshold energy for the formation of NO_2 and oxygen atom was computed to be 580 ± 3 nm in the last section, vibrational and rotational energy could contribute to the dissociation process at higher wavelengths, as has been observed for NO_2 .⁷⁴ In Table XVIII, the products of average cross section and quantum yield deduced in Table XVII from experimental results are



XBL 759-7290

Fig. 27. Separation of the NO₃ spectrum into photochemically active bands with synthetic shapes.

Table XVIII. Comparison of experimental results with the synthetic spectra of Figure 27.

(σ_{avg} in units of $10^{-18} \text{ cm}^2 \text{ molecule}^{-1}$)						
	Experimental Results			Calculated Results		
	Green	Gold	Red	Green	Gold	Red
J₂:						
NO ₂ + O						
ϕ	0.85±0.10	0.63±0.06	---			
σ_{avg}	1.88	2.51	---			
$\phi \sigma_{\text{avg}}$	1.60±0.19	1.58±0.15	---	1.50	1.40	---
J₁:						
NO + O ₂						
ϕ	0.14±0.06	0.23±0.04	0.049±0.010			
σ_{avg}	2.99	3.11	2.17			
$\phi \sigma_{\text{avg}}$	0.42±0.13	0.71±0.05	0.11±0.02	0.40	0.67	0.10

compared with those calculated from the synthetic band shapes in Fig. 27. Although the calculated j -values are both slightly lower than the experimental results, almost all of the values fall within the error limits of the measurements. The wavelength averaged NO_3 cross sections from Table XII were used for the data analysis of Tables XVII and XVIII for convenience. The important kinetic parameter is the product of the quantum yield and absorption cross section, and although a different average cross section would be obtained from Fig. 27, the product would remain the same. By considering only the wavelength regions that were identified as being photochemically active, the results of Table XVII can be interpreted for a light flux constant with wavelength:

$$\begin{aligned} j_1: \text{Q.Y.} &= 0.24 \pm 0.05 & 520 \leq \lambda \leq 640 \text{ nm} \\ \sigma_{\text{avg}} &= 2.96 \times 10^{-18} \text{ cm}^2 \text{ molecule}^{-1} \\ j_2: \text{Q.Y.} &= 0.85 \pm 0.17 & 470 \leq \lambda \leq 600 \text{ nm} \\ \sigma_{\text{avg}} &= 2.00 \times 10^{-18} \text{ cm}^2 \text{ molecule}^{-1} \end{aligned}$$

Since the solar light flux from the green to red regions of the spectrum changes slowly with wavelength, the photolytic rates (cross section \times light flux \times quantum yield) calculated for NO_3 in the lower atmosphere have little dependence on the exact shape of the absorption bands that give the different products. Leighton¹ has tabulated solar light fluxes averaged over 100\AA intervals with corrections for ozone absorption, for the effects of particles in the atmosphere, and for Rayleigh scattering. These correction terms are not large in the region of the spectrum of the present work; the light fluxes for an

overhead sum were used to calculate j-values. If the entire NO_3 visible absorption band was photochemically active, the total j-value would be 0.27 sec^{-1} . The quantum yields of the present study give:

$$\begin{aligned} j_1 &= 0.040 \pm 0.008 \text{ sec}^{-1} \\ j_2 &= 0.099 \pm 0.020 \text{ sec}^{-1} \end{aligned} \quad (96)$$

The 20% error limits are an estimate of the overall uncertainties in these quantities. The only previously reported j-value⁵⁰ was an estimate of 0.07 sec^{-1} based on earlier cross section data⁷⁵ and an assumption of unit quantum yield.

C. Oxygen Atom Reactions

The interpretation of the rate data for the reactions of N_2O_5 and NO_3 with oxygen atom (reactions m and n, respectively) is highly dependent on the other kinetic parameters measured in this study. Computer simulations were carried out using the previously described quantum yields and rate constants to calculate the modulation contribution of reactions m and n for each set of conditions in Table XIX. The modulation amplitudes for reactions m and n in Table XIX are those calculated for the values of m and n assumed in the simulation. Some linear combination of these values must give the observed residual modulation amplitudes. Solving pairs of the data sets in simultaneous equations gives the multiples of these rate constants needed. A positive coefficient for reaction m would indicate that the products are NO_2 and O_2 , and a negative coefficient would indicate that NO_3 is produced. If both sets of products are formed, only the difference in magnitude of the two reaction paths would be observed. The results for reaction m in Table XIX indicate that the difference of the two

Table XIX. Data for reactions m and n from green lamp modulation.
 (Rate constants in $\text{cm}^3 \text{particle}^{-1} \text{sec}^{-1}$, concentrations in $10^{14} \text{molecules cm}^{-3}$)

Case No.	$\frac{[\text{N}_2\text{O}_5]}{[\text{NO}_3]}$	Measured Mod. Amp.	Residual Mod. Amp.	Mod. Amp. for $m = 2 \times 10^{-14}$	Mod. Amp. for $n = 9 \times 10^{-12}$	2 Simultaneous Equations			
						Cases	Multiples of m	Multiples of n	Reaction n only
(Modulation Amplitudes $\times 10^3$)									
<u>298 K</u>									
1	$\frac{15.45}{0.333}$	12.98	1.01	0.120	0.989	1 + 2	-1.77	1.24	1.025
2	$\frac{7.78}{0.270}$	10.41	0.86	0.060	0.778	1 + 3	-0.87	1.13	1.335
3	$\frac{2.96}{0.1953}$	7.26	0.57	0.022	0.521	2 + 3	0.27	1.08	$\frac{1.387}{1.25 \pm 0.12}$
<u>329 K</u>									
4	$\frac{12.03}{1.225}$	28.30	3.65	0.083	3.59	4 + 5	0.49	1.02	1.02
5	$\frac{4.85}{0.991}$	23.71	3.06	0.035	3.03	4 + 6	-9.2	1.23	1.01
6	$\frac{1.871}{0.753}$	18.51	2.62	0.013	2.23	5 + 6	-89.	1.69	$\frac{1.17}{1.07 \pm 0.07}$

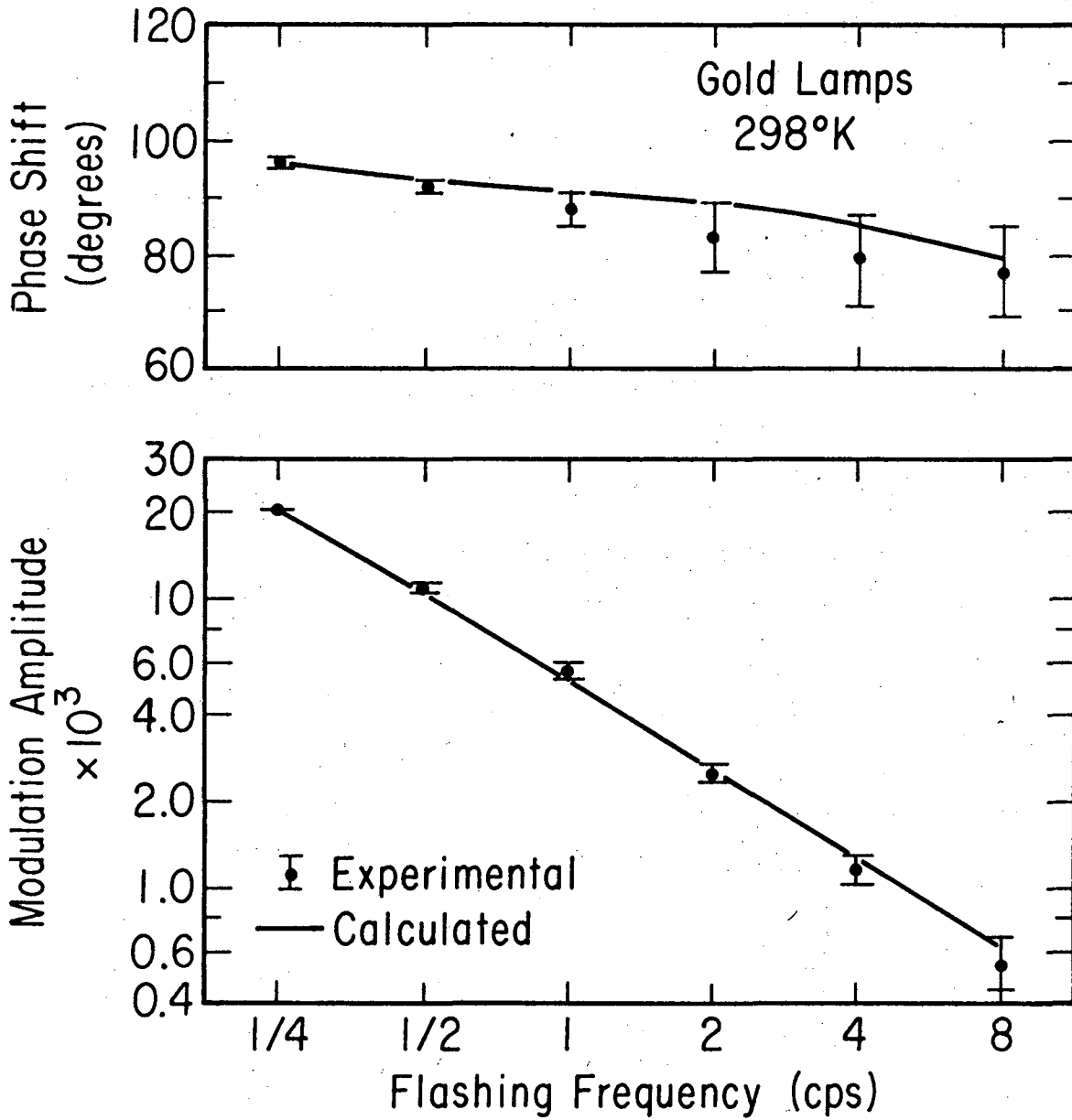
paths is too small to measure in the present system. If only one set of products is actually formed, these results constitute an upper limit for this reaction. The last column of Table XIX is calculated on the assumption that all of the residual amplitude is due to reaction n. Averaging the results for the 298 and 329°K data gives:

$$n = (1.0 \pm 0.2) \times 10^{-11} \text{ cm}^3 \text{ particle}^{-1} \text{ sec}^{-1} \quad (97)$$

The upper limit for m is estimated to be $2 \times 10^{-14} \text{ cm}^3 \text{ particle}^{-1} \text{ sec}^{-1}$, based on the assumption that only one set of products is formed. The large uncertainties in these rate constants is due to the low signal levels and the accumulation of uncertainties from the measured rate constants and quantum yields.

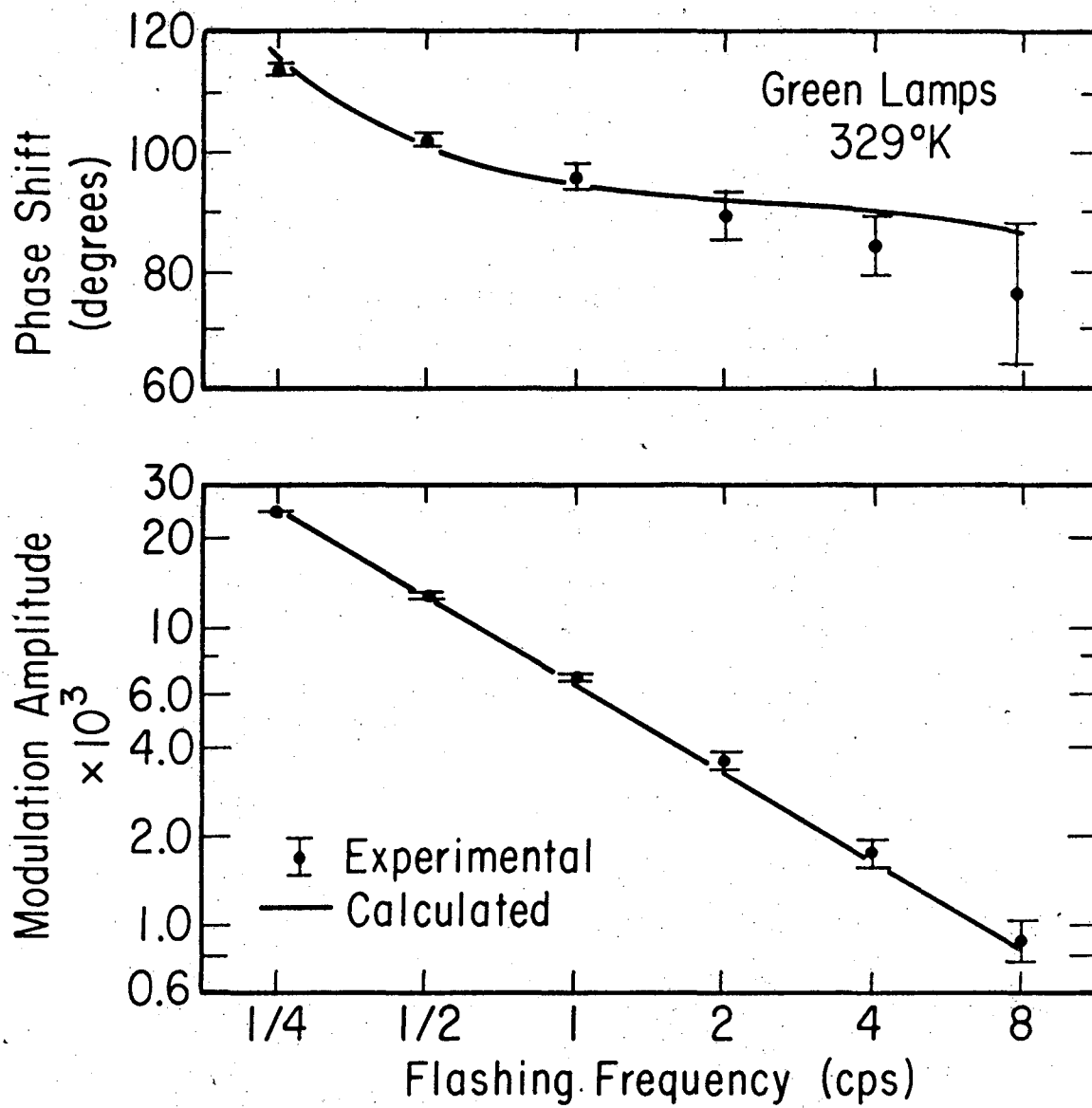
D. NO₃ Phase Shifts

The response of a chemical system to a periodic excitation provides information about the rate constants that determine its behavior. Since NO₃ had the largest modulation signal in the N₂O₅-O₃ system, its amplitude and phase shift were measured at flashing frequencies from 1/4 to 8 cps. The data for gold lamps at 298°K is presented in Fig. 28, and a study using green lamps at 329°K is presented in Fig. 29. Both studies used oxygen as a carrier gas, and the data is summarized in Table XX. The amplitude and phase shift profiles from the computer simulation fit the data within the experimental uncertainties in almost all cases. The amplitudes are inversely proportional to the frequency as is expected for a reactant being photolyzed. The complexity of this chemical system makes it difficult to give a physical interpretation to the variation of phase shift with



XBL 7510-7468

Fig. 28. Modulation amplitudes and phase shifts from Table XX for gold lamps.



XBL 759-7291

Fig. 29. Modulation amplitudes and phase shifts from Table XX for green lamp photolysis.

Table XX. Experimental change of modulation amplitude and phase shift with frequency compared to computer simulation.

Mod. Freq. (cps)	Experimental		Calculated	
	Mod. Amp. $\times 10^3$	Phase Shift (deg)	Mod. Amp. $\times 10^3$	Phase Shift (deg)
<p>(Gold Lamps 298 K</p> <p>$[O_3] = 6.2 \times 10^{16}$ $[NO_3] = 5.4 \times 10^{13}$ $[N_2O_5] = 1.22 \times 10^{15}$ $[O_2] = 2.46 \times 10^{19}$)</p> <p>(molecules/cm³)</p>				
1/4	20.61±0.18	96±1	20.58	96
1/2	10.85±0.21	92±1	10.42	93
1	5.58±0.25	88±3	5.25	91
2	2.45±0.19	83±6	2.63	89
4	1.16±0.13	79±8	1.30	85
8	0.53±0.11	77±8	0.62	79
<p>(Green Lamps 329 K</p> <p>$[O_3] = 2.4 \times 10^{16}$ $[NO_3] = 11.6 \times 10^{13}$ $[N_2O_5] = 7.5 \times 10^{14}$ $[O_2] = 2.23 \times 10^{19}$)</p> <p>(molecules/cm³)</p>				
1/4	24.47±0.30	114±1	24.22	117
1/2	12.88±0.22	102±1	12.91	101
1	6.75±0.20	96±2	6.56	95
2	3.60±0.21	89±4	3.30	92
4	1.75±0.17	84±5	1.64	90
8	0.89±0.14	76±12	0.82	86

flashing frequency. The quantitative agreement of these profiles, however, indicates that the system is well described by the results of the present study.

V. DISCUSSION

A. Absorption Cross Sections

The absorption cross sections for nitric acid vapor reported from this work⁶ agree well with the early work of Dalmon⁴ between 230 and 285 nm. His cross sections are higher than the present study at 290 and 300 nm, and this could be due to a 1.5% NO₂ impurity in his nitric acid. The cross sections reported by Biau⁷ for the 185 to 325 nm region show excellent agreement with the present study. Since pure nitric acid vapor is colorless, the large absorption reported by Schmidt et al.⁵ in the 320 to 440 nm region is probably in error.

The absorption cross sections for nitrous acid in Table V supersede some results reported earlier from this laboratory.⁷⁵ The position of the peaks in the spectrum agree to within 0.1 nm with those of King and Moule¹¹ whose high resolution study of the HNO₂ spectrum revealed no additional structure. Cox^{12,13} concluded from his photolysis studies of HNO₂ that the overall quantum yield of nitrous acid was unity if the average cross section in the 340 to 380 nm region was about $1.9 \times 10^{-19} \text{ cm}^2 \text{ molecule}^{-1}$. This is about four times higher than the average cross section from the present work for the same region, and would indicate a quantum yield of four. Insufficient information was provided about the spectral distribution of his photolysis light to determine the size of the disagreement accurately.

The absorption cross sections for NO₂ presented in Table V agree well with those of Hall and Blacet¹⁴ in the 370 to 420 nm region, but are lower at shorter wavelengths. Since Hall and Blacet¹⁴ had to

correct for a large N_2O_4 absorption below 370 nm, the present results in which the N_2O_4 concentration was too small to cause interference are probably more reliable. The NO_2 cross sections between 200 and 270 nm in the present research agree with those of Nakayama, Kitamura and Watanabe¹⁵ within their experimental error of 30%.

The NO_3 cross sections presented in this work are about four times higher than some previous reported values.⁷⁵ The earlier study used the values of K and g determined by Schott and Davidson¹⁸ to calculate the steady state concentration of NO_3 . Schott and Davidson¹⁸ extrapolated their 650 to 1050°K NO_3 cross sections determined in a shock tube to 300°K and obtained a value of $8.4 \times 10^{-19} \text{ cm}^2 \text{ molecule}^{-1}$ at 652 nm. The present study obtained a value of $3.9 \times 10^{-19} \text{ cm}^2 \text{ molecule}^{-1}$ at this wavelength and observed an increase in NO_3 cross section with temperature (Table XII). Since the wavelength chosen by Schott and Davidson lies between two strong absorption peaks, the possible variation in shape of both of these peaks with temperature makes their long extrapolation somewhat uncertain.

The N_2O_5 cross sections in Table V are based on concentrations determined by infrared absorptions. These values supersede some earlier data⁷⁵ based on a fairly crude NO_x mass balance. The present results are up to 40% higher than those of Jones and Wulf¹⁶ in the 290 to 310 nm region. The agreement is satisfactory, however, in view of the difficult experimental conditions in both studies.

The weak infrared absorption band from 1325 to 1375 cm^{-1} attributed to NO_3 by Cramarossa and Johnston²⁰ has been identified by a molecular modulation study in this research as N_2O_5 . Their study

used long path infrared monitoring of the species in the $N_2O_5-O_3$ system and subtracted off an overlying HNO_3 absorption. Part of their evidence for the band being NO_3 was an apparent one third power dependence of the absorption on the O_3 and N_2O_5 concentration. The present experimental conditions gave NO_3 to N_2O_5 ratios similar to the earlier study, and a residual absorption was observed when the HNO_3 absorption was subtracted from the spectrum. The band was identified as N_2O_5 by its phase shift.

B. $N_2O_5-O_3$ Kinetics

The early study by Schumacher and Sprenger²¹ of the N_2O_5 catalyzed decomposition of ozone used hundreds of torr of ozone and followed the reaction manometrically. Although the present research used only about 3 torr of ozone, the measurements of $1/2(Kh)^{2/3}(2g)^{1/3}$ in the two systems agree within the experimental errors. The results from the present study have a higher precision, a larger temperature range, and both N_2O_5 and O_3 were directly measured by their infrared absorptions. The high activation energy measured by Schumacher and Sprenger,²¹ 20,700 calories vs 19,700 calories in the present study, could be due to reactant self-heating. The high concentrations of reactants in their study gave such a large rate of heat release that the methods used to calculate self-heating effects in the present work^{69,70} can not be applied to their data.

The rate constant for the reaction of NO_2 with O_3 reported from this research³⁴ has been confirmed by the studies of Davis and co-workers³⁵ and Herron and Huie.³⁶ Since these other two works did not examine the mechanism of the reaction, the reason for the low reaction

stoichiometries observed in this research and in that of Wu et al.³³ remains undetermined. One possible explanation for the low stoichiometries is the heterogeneous reaction w observed in the $N_2O_5-O_3$ system. The conditions of the NO_2-O_3 experiments were quite different from the conditions in which w was measured (0.2 torr vs 760 torr total pressure), and thus no definite conclusions can be made about the role of reaction w.

Another possible explanation for the low stoichiometries has been suggested by Wu et al:³³



This alternate path for the NO_2-O_3 reaction would give a constant stoichiometry throughout the reaction. Since the reaction of ozone with nitric oxide is chemiluminescent,^{76,77} a chemiluminescence detection system using a large glass bulb at 298°K was employed to investigate this possible pathway for destruction of ozone. When the system was calibrated with 2 microns of NO, 20 microns of O_3 , and 100 microns of Ar, a strong chemiluminescent signal was observed. Nitrogen dioxide was substituted for the NO and less than 0.2% of the former emission was measured. This apparently eliminates NO as a possible gas-phase intermediate in reactions causing the low stoichiometry.

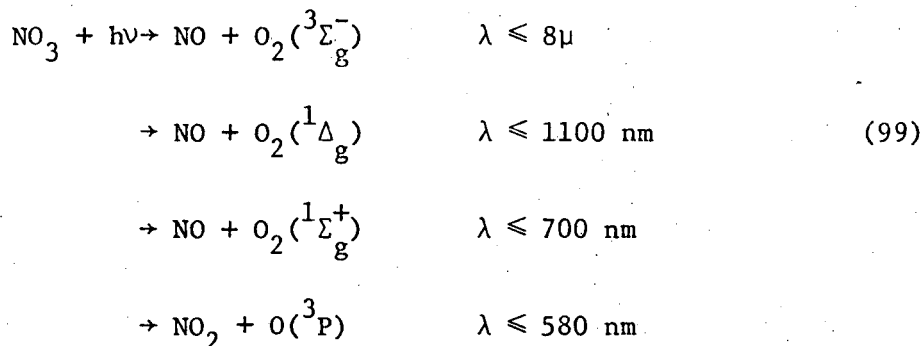
The equilibrium constant K determined in this research has been used with literature data^{40,46,47,49} to calculate rate constants for reactions B, e and f (Table XVI). In addition, the rate constants for the reaction of NO_3 with acetaldehyde and propylene measured by

Morris and Niki⁷⁸ can be revised to give $1.7 \times 10^{-15} \text{ cm}^3 \text{ molecule}^{-1} \text{ sec}^{-1}$ and $4 \times 10^{-15} \text{ cm}^3 \text{ molecule}^{-1} \text{ sec}^{-1}$, respectively.

C. NO₃ Photochemistry

The NO₃ free radical is important in several gas phase reaction mechanisms, but little is known about its structure or electronic states. Walsh⁷⁹ has predicted that the molecule has D_{3h} symmetry and a ²A₂' ground electronic state. Semi-empirical calculations by Olsen and Burnelle,⁸⁰ however, predict a Y-shaped structure with a ²B₂ ground state. Although the nitrate anion has absorptions in the 1350 to 1400 cm⁻¹ and 720 to 830 cm⁻¹ regions,⁸¹ no absorption bands for the NO₃ free radical have been observed.

Several reactions are energetically possible in the region of the strong NO₃ visible absorption spectrum:



The quantum yield results of this research indicate that both NO and NO₂ are formed by NO₃ photolysis, but the electronic states of the products were not identified. The proposed band shape for the NO₃ spectrum giving NO₂ as a product (Fig. 27) extends above the energetic wavelength threshold of 580 nm. This could be an effect analogous to that observed for NO₂ photolysis: Pitts, Sharp and Chan⁷⁴ found that the temperature dependence for NO₂ photolysis at 404.7 nm

(above its 398 nm threshold) could be predicted if part of the molecule's rotational energy was available for bond breaking. Small quantum yields for NO_2 photolysis have been observed at even higher wavelengths.⁸²

Reaction j_1 for NO_3 photolysis is part of a catalytic cycle for the destruction of ozone in the lower stratosphere (Eq. (12)). The rate constant for this reaction is important for calculating the global ozone balance and modeling the effects of NO_x injections from supersonic aircraft flying in the stratosphere.² Nitric oxide in the stratosphere is quickly oxidized by ozone to NO_2 when night falls, and NO_2 slowly reacts with ozone to form N_2O_5 during the night. The rate constants for reactions h and B determined in this study thus describe the most important nighttime NO_x reactions in the stratosphere. During the day, the accumulated N_2O_5 is slowly photolyzed and attacked by reactive intermediates such as oxygen atom. The rate constant for the reaction of N_2O_5 with $\text{O}(^3\text{P})$ is needed to predict how much N_2O_5 is converted to other forms of NO_x and thus determine how much NO and NO_2 is available for reactions destroying ozone. The upper limit of $2 \times 10^{-14} \text{ cm}^3 \text{ particle}^{-1} \text{ sec}^{-1}$ from this research is much lower than the upper limits established by Murphy⁵³ or Davis.⁵⁰

The rate constant for reaction n, $\text{O} + \text{NO}_3$, has not previously been reported. It is interesting to note that the value determined in this work, $(1.0 \pm 0.2) \times 10^{-11} \text{ cm}^3 \text{ particle}^{-1} \text{ sec}^{-1}$ is very similar to the literature value for the $\text{NO}_2 + \text{O}$ reaction,⁵⁰ $9.1 \times 10^{-12} \text{ cm}^3 \text{ particle}^{-1} \text{ sec}^{-1}$.

VI. CONCLUSIONS

This study measured a variety of absorption cross sections and kinetic parameters important in determining the role of the oxides of nitrogen in atmospheric photochemistry. The information from several spectroscopic techniques in this study was combined to give rate constants for the reactions important in the $N_2O_5-O_3$ system:

$$231 \text{ to } 298^\circ\text{K} \quad h = (1.34 \pm 0.11) \times 10^{-13} e^{-(4900 \pm 60)/RT} \text{ cm}^3 \text{ molecule}^{-1} \text{ sec}^{-1}$$

$$298 \text{ to } 329^\circ\text{K} \quad K = (8.4 \pm 1.8) \times 10^{26} e^{-(22210 \pm 200)/RT} \text{ molecules cm}^{-3}$$

$$298 \text{ to } 329^\circ\text{K} \quad g = (8.5 \pm 2.8) \times 10^{-13} e^{-(4870 \pm 200)/RT} \text{ cm}^3 \text{ molecule}^{-1} \text{ sec}^{-1}$$

The equilibrium constant K was used to calculate

$$\Delta H_{f,300^\circ\text{K}}(\text{NO}_3) = 17.6 \pm 0.2 \text{ kcal/mole}$$

Using literature data^{40,49} for K_e and K_f , the following rate constants were calculated:

$$298 \text{ to } 329^\circ\text{K} \quad e = (2.5 \pm 0.5) \times 10^{-14} e^{-(2440 \pm 200)/RT} \text{ cm}^3 \text{ molecule}^{-1} \text{ sec}^{-1}$$

$$297^\circ\text{K} \quad f = (1.87 \pm 0.41) \times 10^{-11} \text{ cm}^3 \text{ molecule}^{-1} \text{ sec}^{-1}$$

Molecular modulation studies of the strong NO_3 visible absorption spectrum combined with studies of the N_2O_5 catalyzed decomposition of O_3 with red, green and gold photolysis lamps revealed two sets of photolysis products:

$$j_1: \text{ Q.Y.} = 0.24 \pm 0.05 \quad 520 \leq \lambda \leq 640 \text{ nm}$$

$$j_2: \text{ Q.Y.} = 0.85 \pm 0.17 \quad 470 \leq \lambda \leq 600 \text{ nm}$$

The atmospheric j values derived from these quantum yields were 0.040 ± 0.008 and $0.099 \pm 0.020 \text{ sec}^{-1}$ for j_1 and j_2 , respectively. Molecular

modulation experiments also gave:

$$298^{\circ}\text{K} \quad m \leq 2 \times 10^{-14} \text{ cm}^3 \text{ particle}^{-1} \text{ sec}^{-1}$$

$$298 \text{ to } 329^{\circ}\text{K} \quad n = (1.0 \pm 0.2) \times 10^{-11} \text{ cm}^3 \text{ particle}^{-1} \text{ sec}^{-1}$$

The inequality for m is good if only one set of products ($\text{NO}_2 + \text{NO}_2 + \text{O}_2$ or $\text{NO}_3 + \text{NO}_3$) is formed; otherwise, the specified value refers to the difference in rate constants for the two reaction paths.

The rate constant for reaction h reported here disagrees substantially with that of Johnston and Yost,²⁷ but is in excellent agreement with the results of Davis and co-workers³⁵ and Herron and Huie.³⁶ The room temperature Arrhenius expressions for e , g and K from this research disagree significantly with the expressions Schott and Davidson¹⁸ obtained from an extrapolation of high temperature shock tube data.

ACKNOWLEDGEMENTS

I wish to thank Professor Harold S. Johnston for his guidance and encouragement throughout the course of this research. His patient and understanding approach to graduate research allows a student to develop resourcefulness and initiative. Both his enthusiasm and his wealth of knowledge have been invaluable resources in this research.

The assistance and encouragement of my co-workers Alan Harker, Peter Connell and John Girman have helped to make my work at Berkeley very enjoyable. Special thanks are due to Dr. Gary Whitten whose Gear program made the interpretation of my data tractable, and to Dolly Martin who assisted in the preparation of this manuscript.

I thank the personnel of the Department of Chemistry and of Lawrence Berkeley Laboratory for their assistance and support in many aspects of this research.

I especially wish to thank Lucy for her emotional support and assistance in this work.

I would like to thank the U. S. Atomic Energy Commission for their funding of this research through the Inorganic Materials Research Division of the Lawrence Berkeley Laboratory.

APPENDIX A: GEAR PROGRAM FOR CHEMICAL KINETICS

The following program is a Fortran II version of a chemical kinetics program written by Dr. G. Z. Whitten⁶² using the Gear method⁵⁶ for solving coupled ordinary differential equations. Information on the functions of the various subroutines can be found elsewhere.⁵⁶ This program was written in two overlays for use on a PDP 8/E computer. The first program (CHEMK) obtains the reactions and starting conditions from the operator in a conversational mode. The other overlay (DRIVES) is then loaded and executes the calculations. The program as listed utilizes 17K of core on a PDP 8/E computer and handles 30 reactions and 10 chemical species. Approximately 3 sec are required per time step for a calculation with 10 reactions and 10 species. Execution time goes up approximately as the square of the number of species.

```
C      CHEMK - GEAR PROGRAM FOR CHEMICAL KINETICS ON PDP 8-E

COMMON NO,N,NR,NP,NS,MF,KFLG1,KFLAG,JSTART,IP, ITYPE
COMMON RS,A,S,TITLE,PHTN,ZL,ABSE,TEMP,ERR,START,
1  STOPP,ABSP,PC,SIG,R,SPEC1,REACT
COMMON TTART,GUESS,HMIN,HMAX,EPS1
COMMON YMAX,ERROR,FZERO,C,FSAVE,PW,RT,KFL
DIMENSION IP(10),ITYPE(30)
DIMENSION RS(30,7),A(30),S(30),TITLE(7),SIG(10),R(30),
1  SPEC1(10),REACT(10),YMAX(10),ERROR(10),C(10,6),
2  FSAVE(20),PW(110),RT(30),KFL(10),NZT(30)

WRITE (1,302)
WRITE (1,302)
302  FORMAT(1X)
196  READ (1,301) INIT
301  FORMAT('INITIALIZE? (NO=0;YES=1):',15)

C  CONSTANTS FOR "M  ", "HV  ", "  "  " ,MORE REACT", "CONTINUE"
      RM='M      '
      RHV='HV    '
      RB='      '
      RMRT='MORE '
      RCONT='CONTIN'

      IF (INIT-1) 90,198,196
198  DO 200 I=1,601
200  RS(I)=0.
      DO 201 I=1,40
201  IP(I)=0
      JSTART=0
      KFLAG=0
      KFLG1=0
      NR=0
      NS=1
      FZERO=1.

      DO 119 I=1,210
119  RS(I)=RB
80  NS=NS-1

C  READ LAST REACTION NUMBER
      READ (1,1) NX
1  FORMAT('LAST REACTION NUMBER(15)=' ,15)
      WRITE (1,121)
121  FORMAT('/INPUT REACTIONS: (15,7A5,2E10.8)')
      WRITE (1,122)
122  FORMAT('<NO.>< R >< R >< R >< P >< P >< P >< P ><A-FACTOR',
1  '><E(CAL)/R>')

C  READ REACTIONS AND RATES
11  READ (1,3) NW,(FSAVE(I),I=1,9)
3  FORMAT (15,7A5,2E10.8)
      A(NW)=FSAVE(8)
      S(NW)=FSAVE(9)
      DO 205 I=1,7
205  RS(NW,I)=FSAVE(I)
      IF (NW-NR) 27,27,20
20  NR=NW
27  IF (NW-NX) 11,30,11
```


-151-

C FORM MATRIX OF SPECIES NUMBERS FROM THE REACTIONS

```

30      DO 81 I=1, NR
        IF (RS(I,1)-.9) 401, 81, 81
C 1ST REACTANT
401     IF (RS(I,1)-RB) 420, 402, 420
402     IF (RS(I,3)-RB) 404, 406, 404
404     RS(I,1)=RS(I,3)
406     RS(I,3)=RB
        IF (RS(I,1)-RB) 420, 408, 420
408     RS(I,1)=RS(I,2)
        RS(I,2)=RB
        IF (RS(I,1)-RB) 420, 410, 420
410     RS(I,1)=99.
C 2ND REACTANT
420     IF (RS(I,2)-RB) 430, 422, 430
422     IF (RS(I,3)-RB) 424, 430, 424
424     RS(I,2)=RS(I,3)
426     RS(I,3)=RB
C PRODUCTS
430     DO 434 K=4, 7
        IF (RS(I,K)-RM) 434, 432, 434
432     RS(I,K)=RB
434     CONTINUE
        IF (RS(I,4)-RB) 450, 436, 450
436     DO 438 K=1, 3
        IF (RS(I,8-K)-RB) 445, 438, 445
438     CONTINUE
        K=3
445     RS(I,4)=RS(I,8-K)
        RS(I,8-K)=RB
450     IF (RS(I,5)-RB) 460, 452, 460
452     IF (RS(I,7)-RB) 454, 456, 454
454     RS(I,5)=RS(I,7)
        RS(I,7)=RB
456     IF (RS(I,5)-RB) 460, 458, 460
458     RS(I,5)=RS(I,6)
        RS(I,6)=RB
460     RS7=RS(I,6)
        IF (RS7-RB) 465, 462, 465
462     RS(I,6)=RS(I,7)
        RS(I,7)=RS7
465     DO 79 J=1, 7
        RS6=RS(I,J)
        IF (J-3) 66, 66, 70
66     IF (RS6-RM) 68, 67, 68
67     RS(I,J)=RS(I,3)
        RS(I,3)=99.
68     IF (RS6-RHV) 71, 69, 71
69     RS(I,2)=99.
        GOTO 79
71     RS6=RS(I,J)
70     IF (RS6-RM) 72, 73, 72
72     IF (RS6-RB) 75, 73, 75
73     RS(I,J)=0.
        GOTO 79
75     IF (RS6-99.) 76, 79, 76
76     DO 78 L=1, NS
        IF (RS6-SPECI(L)) 78, 77, 78
77     RS(I,J)=FLOAT(L)
        GOTO 79
78     CONTINUE
        NS=NS+1
        SPECI(NS)=RS6
        RS(I,J)=FLOAT(NS)
79     CONTINUE

```

```
81     CONTINUE
      NS=NS+1
      SPECI(NS)=RM

      WRITE (1,123)
123     FORMAT(/'MATRIX OF REACTANTS')
      DO 210 J=1,NR
      IF (A(J)) 109,210,109
109     WRITE (1,110) J,(IFIX(RS(J,I)),I=1,7)
110     FORMAT(I3,4X,7I3)
210     CONTINUE

C READ TITLE CARD
90     WRITE (1,302)
      READ (1,306) (TITLE(I),I=1,7)
306     FORMAT('TITLE:',7A6)
      IF (TITLE(1)-RB) 93,196,93

C IS TITLE "MORE REACT"?
93     IF (TITLE(1)-RMRT) 94,280,94
C IS TITLE "CONTINUE"?
94     IF (TITLE(1)-RCONT) 95,98,95

C READ NUMBER OF INITIAL SPECIES
95     READ (1,134) N
134     FORMAT('NO. OF INITIAL SPECIES=',15)
      WRITE (1,314)
314     FORMAT('NAME (A5), MOLEC/CC (E10.8)')
      DO 319 I=1,N
      WRITE (1,315) I,
315     FORMAT(I3)
      READ (1,316) REACT(I)
316     FORMAT(' NAME:',A5)
      READ (1,318) C(I)
318     FORMAT('MOLEC/CC=',E10.8)
319     CONTINUE

97     WRITE (1,302)
      READ (1,340) FSAVE(1)
      READ (1,341) FSAVE(2)
      READ (1,342) FSAVE(3)
340     FORMAT('PRINT INTERVAL (SEC) (E10)=',E10.8)
341     FORMAT('PRINT AFTER N STEPS - (E10) N=',E10.4)
342     FORMAT('SPOT CHECK AFTER NTH PRINTOUT - (E10) N=',E10.4)
C READ INITIAL CONDITIONS: PHOTONS, CELL LENGTH, TEMPERATURE (K),
C ERROR TOLERANCE, T(0), T(LAST)
      WRITE (1,127)
127     FORMAT(/'INPUT: (6E10.8)'/ '<PHTN FLX><CELL(CM)><TEMP (K)>'
      1 '<ERR TOL.>< T(0) >< T(LAST)>')
      READ (1,320) PHTN,ZL,TEMP,ERR,START,STOPP
320     FORMAT(7E10.8)
      CALL RATES
      WRITE (1,101) (R(I),I=1,NR)
      GUESS=1.E-12
      TTART=START
      WRITE (1,102) (SPECI(I),I=1,NS)
      NO=NS
      MF=21
      CALL CHAIN('DRIV2')

C "MORE REACTIONS"
280     DO 286 I=1,NR
      IF (A(I)) 286,282,286
282     DO 286 J=1,7
      RS(I,J)=RB
```

-153-

```

286 CONTINUE
    C(NS)=0.
    GOTO 80

C "CONTINUE" CALCULATION
98 DO 99 I=1,NS
    REACT(I)=SPECI(I)
99 CONTINUE
    GOTO 97
101 FORMAT(/'THE RATE CONSTANTS USED WERE'/(6E12.4))
102 FORMAT(/5X,'TIME',6X,'INTERVAL ',4(6X,A5,1X)/
    1 6(6X,A5,1X))
END

```

SUBROUTINE RATES

C CHANGES IN VARIABLE NAMES: PC>SG

```

COMMON NO,N,NR,NP,NS,MF1,KFLG1,KFLAG,JSTRT,IP,ITYPE
COMMON RS,A,S,TITLE,PHTN,ZL,ABSB,TEMP,ERR,START,
1 STOPP,ABSP,SG,SIG,R,SPEC1,REACT,TTART,GUESS,
2 HMIN,HMAX,EPS1,YMAX,ERROR,FZERO,C,FSAVE,PW,RT
DIMENSION IP(10),ITYPE(30)
DIMENSION RS(30,7),A(30),S(30),TITLE(7),SIG(10),R(30),
1 SPECI(10),REACT(10),YMAX(10),ERROR(10),C(10,6),
2 FSAVE(20),PW(110),RT(30)
DO 10 I=1,10
    SIG(I)=0.
10 CONTINUE
    DO 30 I=1,N
        DO 20 J=1,NS
            IF (SPECI(J)-REACT(I)) 20,11,20
11 SIG(J)=C(I)
            GOTO 30
20 CONTINUE
            SPECI(NS+1)=SPECI(NS)
            SPECI(NS)=REACT(I)
            SIG(NS)=C(I)
            NS=NS+1
30 CONTINUE
            N=NS
            M=N-1
            C(N)=0.
            DO 40 I=1,M
                C(N)=C(N)+SIG(I)
                C(I)=SIG(I)
40 CONTINUE
                IF (SIG(N)) 401,402,401
401 C(N)=SIG(N)
402 NP=0
                DO 60 I=1,NR
                    IF (RS(I,1)) 41,60,41
41 ITYPE(I)=2
                    IF (RS(I,2)) 44,42,44
42 IF (RS(I,3)-99.) 44,43,44
43 RS(I,2)=FLOAT(N)
44 IF (RS(I,2)-FLOAT(N)) 47,45,47
45 IF (RS(I,3)-99.) 47,46,47
46 RS(I,3)=0.
47 IF (RS(I,2)) 49,48,49
48 ITYPE(I)=1
49 IF (RS(I,2)-99.) 51,50,51
50 ITYPE(I)=4

```

```
51 IF (RS(1,3)) 52,53,52
52 ITYPE(1)=3
53 IF (RS(1,3)-99.) 55,54,55
54 RS(1,3)=FLOAT(N)
55 IF (RS(1,2)-99.) 56,58,56
56 R(1)=A(1)*EXP(-S(1)/TEMP)
GOTO 60
58 NP=NP+1
SIG(NP)=A(1)
R(1)=A(1)
IP(NP)=IFIX(RS(1,1))
60 CONTINUE
SG=0.
ABSP=0.
IF (PHTN) 64,63,64
63 RETURN
64 NO=-1
T=START
CALL PEDERV
NO=NS
ABSP=100.*SG*ABSP/PHTN
RETURN
END
```

SUBROUTINE PEDERV

C CHANGE IN VARIABLE NAMES: A>B, PW>A, PC>SG, ABSP>PHOT, RT>RTA

```
COMMON NO,N,NR,NP,NS,MF1,KFLG1,KFLAG,JSTART,IP,ITYPE
COMMON RS,B,S,TITLE,PHTN,ZL,ABSB,TEMP,ERP,START,
1 STOPP,PHOT,SG,SIG,R,SPEC1,REACT,TTART,GUESS,
2 HMIN,HMAX,EPSI,YMAX,ERROR,FZERO,C,FSAVE,A,RTA
DIMENSION IP(10),ITYPE(30)
DIMENSION RS(30,7),B(30),S(30),TITLE(7),SIG(10),R(30),
1 SPEC1(10),REACT(10),YMAX(10),ERROR(10),C(10,6),
2 FSAVE(20),A(110),RTA(30)
DIMENSION RT(3)
F1=.16666667
F2=.41666667E-1
F3=.83333333E-3
F4=.13888888E-2
IF (NP) 1,17,1
1 SG=0.
DO 10 I=1,NP
K=IP(I)
SG=SG+SIG(I)*C(K)
10 CONTINUE
SG=SG*ZL
SS=SG*SG
IF (SG-.01) 12,12,11
11 PC=(1.-EXP(-SG))/SG
GOTO 13
12 PC=1.-SG*.5+SS*(F1-SG*F2+SS*F3)
13 PHOT=PHTN*PC
IF (NO) 110,14,14
14 IF (SG-.01) 16,16,15
15 PC=ZL*(1./PC-1.-SG)/SG
GOTO 17
16 PC=ZL*(SG*F1-.5-SS*(F2-SG*F3+SS*F4))/PC
17 DO 20 J=1,N
DO 20 I=1,N
```

-155-

```

A((J-1)*N+I)=0.
20 CONTINUE
DO 100 IR=1,NR
IF (RS(IR,1)) 21,100,21
21 IF (RS(IR,1)-99.) 28,100,28
28 MT=ITYPE(IR)
IF (MT-4) 22,70,22
22 DO 30 I=1,MT
MZ=I+1-I/3*3
J=IFIX(RS(IR,MZ))
MZ=I+2-I/2*3
K=IFIX(RS(IR,MZ))
RT(I)=C(J)*C(K)*R(IR)
30 CONTINUE
DO 60 K=1,MT
I=IFIX(RS(IR,K))
DO 40 L=1,MT
J=IFIX(RS(IR,L))
I5=(J-1)*N+I
A(I5)=A(I5)-RT(L)
40 CONTINUE
DO 50 L=4,7
J=IFIX(RS(IR,L))
IF (J) 42,60,42
42 I5=(I-1)*N+J
A(I5)=A(I5)+RT(K)
50 CONTINUE
60 CONTINUE
GOTO 100
70 J=IFIX(RS(IR,1))
RJ=R(IR)*S(IR)*PHOT
I5=(J-1)*N+J
A(I5)=A(I5)-RJ
RD=RJ*C(J)*PC
DO 75 L=1,NP
MT=IP(L)
I5=(MT-1)*N+J
A(I5)=A(I5)-RD*SIG(L)
75 CONTINUE
DO 90 K=4,7
I=IFIX(RS(IR,K))
IF (I) 76,100,76
76 I5=(J-1)*N+I
A(I5)=A(I5)+RJ
DO 80 L=1,NP
MT=IP(L)
I5=(MT-1)*N+I
A(I5)=A(I5)+RD*SIG(L)
80 CONTINUE
90 CONTINUE
100 CONTINUE
MT=N-1
DO 110 I=1,N
I5=(I-1)*N+N
A(I5)=0.
DO 110 J=1,MT
A(I5)=A(I5)+A((I-1)*N+J)
110 CONTINUE
RETURN
END

```

C DRIVES - DRIVER FOR DIFFERENTIAL EQUATION SOLVER

C CHANGES IN VARIABLE NAMES: START>TO, STOPP>TLAST,
C ERR>EPS, TTART>T, GUESS>H, ABSP>PHOT, C>Y
C KFLAG, ERR, NS ARE REDUNDANT

```
COMMON NO, N, NR, NP, NS, MF, KFLG1, KFLAG, JSTART, IP, ITYPE
COMMON RS, A, S, TITLE, PHTN, ZL, ABSB, TEMP, ERR, TO, TLAST, PHOT,
1 PC, SIG, R, SPEC1, REACT
COMMON T, H, HMIN, HMAX, EPS
COMMON YMAX, ERROR, FZERO, Y, FSAVE, PW, RT, KFL
DIMENSION IP(10), ITYPE(30)
DIMENSION RS(30, 7), A(30), S(30), TITLE(7), SIG(10), R(30),
1 SPEC1(10), REACT(10), YMAX(10), ERROR(10),
2 Y(10, 6), FSAVE(20), PW(10, 11), RT(30), KFL(30)
KFL(2)=0
N=NO
T=TO
HMIN=ABS(H)
HMAX=ABS(TO-TLAST)*.1
IF (HMIN-.1*HMAX) 3, 3, 2
HMIN=.1*HMAX
2 C NOTE: ONLY FIVE LETTERS IN VAR. NAME ARE UNIQUE
3 JSTART=0
EPS=ERR
KHFLAG=0
NHS=0
NTP=0
TOLD=0.
TPRNT=FSAVE(1)
MS=IFIX(FSAVE(2))
MT=IFIX(FSAVE(3))
MT1=MT
MS1=MS
TSTEP=TPRNT
GOTO 21
10 CALL STIFF
NQ=JSTART
KGO=1-KFLG1
GOTO (20, 100, 200, 300), KGO
20 CONTINUE
21 IF (T) 211, 333, 211
211 IF (T-TOLD) 10, 10, 22
22 TOLD=T
IF (MT1) 221, 221, 222
221 MT=IRDSW(0)
222 IF (MS1) 223, 223, 224
223 MS=IRDSW(0)
224 DO 26 I=1, N
IF (Y(I)-EPS) 23, 23, 26
23 IF (Y(I)) 626, 24, 24
24 IF (Y(I, 2)) 25, 25, 26
25 IF (Y(I)*EPS+Y(I, 2)) 626, 620, 620
620 IF (Y(I)-1.E-10) 626, 26, 26
626 DO 630 L=1, NR
DO 630 M=1, 3
IF (IFIX(RS(L, M))-1) 630, 628, 630
623 R(I)=0.
630 CONTINUE
```

```

DO 640 MP=1,6
640 Y(1,MR)=0.
26 CONTINUE
NHS=NHS+1
IF (NHS-MS) 30,32,32
30 IF (T-TLAST) 31,32,32
31 IF (T-TPRNT) 10,32,32
32 NHS=0
NTP=NTP+1
IF (T-TLAST) 33,333,333
33 IF (T-TPRNT) 333,50,50
333 WRITE (1,505) T,H,(Y(1),I=1,NS)
505 FORMAT(6E12.4)
WRITE (1,506)
506 FORMAT(1X)
IF (NTP-MT) 336,338,338
336 IF (T-TLAST) 10,338,338
338 NTP=0
WRITE (1,510) T
510 FORMAT(/'SPOT CHECK AT TOTAL TIME =',F10.2,' SEC')
CALL DIFFUN(0,60)
WRITE (1,315) (FSAVE(I),I=1,N)
315 FORMAT(/7X,'NET RATES=',7X,4E12.4/(6E12.4))
DO 40 I=1,NR
J=IFIX(RS(1,1))
K=IFIX(RS(1,2))
L=IFIX(RS(1,3))
IF (J) 35,34,35
34 FSAVE(I)=0.
GOTO 40
35 IF (J-99) 357,355,357
355 J=0
357 IF (K-99) 36,38,36
36 FSAVE(I)=Y(L)*R(I)*Y(J)*Y(K)
GOTO 40
38 FSAVE(I)=Y(J)*R(I)*S(I)*PHOT
40 CONTINUE
WRITE (1,320) (FSAVE(I),I=1,NR)
320 FORMAT(/'THE REACTION RATES ARE'/(6E12.4))
WRITE (1,520) (SPECI(I),I=1,NS)
520 FORMAT(/5X,'TIME',6X,'INTERVAL ',4(6X,A5,AX)/(6(6X,A5,AX)/))
IF (T-TLAST) 10,45,45
45 NHS=MS
NTP=0
IF (T-TLAST) 48,47,47
47 TPRNT=TLAST
48 DLT=TLAST-TOLD
TOLL=0.
50 PART=(TPRNT-T)/H
DO 52 I=1,N
52 FSAVE(I)=Y(I)
RR=1.
L=NQ+1
DO 54 J=2,L
RR=RR*PART
DO 54 I=1,N
54 FSAVE(I)=FSAVE(I)+Y(I,J)*RR
WRITE (1,505) TPRNT,H,(FSAVE(I),I=1,NS)
WRITE (1,506)
TPRNT=TPRNT+TSTEP
IF (NTP-MT) 56,38,38
56 IF (T-TLAST) 58,58,60
58 IF (T-TPRNT) 10,32,32
60 LO 64 I=1,N
64 Y(I)=FSAVE(I)
GOTO 700

```

```
100 WRITE(1,105) T
110 IF (KHFLAG-10) 112,150,112
112 KHFLAG=KHFLAG+1
    HMIN=HMIN*.1
    H=H*.1
    WRITE(1,115) H
    JSTART=-1
    GOTO 10
150 WRITE (1,155)
    GOTO 500
200 WRITE (1,205) T,H
    GOTO 500
300 WRITE (1,305) T
    GOTO 110
500 CONTINUE
105 FORMAT(//'KFLAG=-1 FROM STIFF AT T = ',E16.8/
1 'ERROR TEST FAILED WITH ABS(H) = HMIN'//)
115 FORMAT('H HAS BEEN REDUCED TO ',E16.8,
1 ' AND STEP WILL BE RETRIED'//)
155 FORMAT(//'PROBLEM UNSOLVABLE WITH GIVEN INPUT'//)
205 FORMAT(//'KFLAG=-2 FROM STIFF AT T = ',E16.8,' H = ',
1 E16.8/'REQUESTED ERROR IS SMALLER THAN CAN BE HANDLED'//)
305 FORMAT(//'KFLAG=-3 FROM STIFF AT T= ',E16.8/
1 ' CORRECTOR CONVERGENCE COULD NOT BE ACHIEVED'//)
700 CALL CHAIN('CHEMK')
    STOP
    END
```

SUBROUTINE STIFF

```
C CHANGES IN VARIABLE NAMES: EPSI>EPS,MFI>MF,KFLGI>KFLAG
C C>Y,TTART>T,KEX IS UNUSED
```

```
COMMON NO,N,NR,NP,NS,MF,KFLAG,KEX,JSTART,IP,ITYPE
COMMON RS,A,S,TITLE,PHTN,ZL,ALSB,TEMP,ERR,TO,
1 TLAST,PHOT,PC,SIG,R,SPECI,REACT
COMMON T,H,HMIN,HMAX,EPS
COMMON YMAX,ERROR,FZERO,Y,FSAVE,PW,EL,TQ,P,
1 METH,NQ,MAXDER,RT,KFL
DIMENSION IP(10),ITYPE(30)
DIMENSION RS(30,7),A(30),S(30),TITLE(7),SIG(10),R(30),
1 SPECI(10),REACT(10),YMAX(10),ERROR(10),Y(10,6),
2 FSAVE(20),PW(110),EL(6),TQ(4),P(5,3),RT(4),KFL(30)
```

```
IF (KFL(2)) 98,99,98
C DATA - DEFINE ONCE ONLY
99 ANOISE=1.E-7
    KFL(2)=1
    MITER=0
    EPSOLD=0.
    D1=0.
98 KFLAG=0
    TOLL=T
    IF (JSTART) 120,103,200
103 NSQ=NO*NO
    NSQ1=NSQ+1
    N1=NO+1
C CALL DIFF'N WITH Y AND FSAVE
    CALL DIFFIN(0,60)
    DO 110 I=1,N
    Y(1,2)=FSAVE(1)*H
```


-159-

```

AYI=ABS(Y(1,1))
IF (AYI) 105,104,105
104 AYI=ABS(Y(1,2))
105 IF (AYI) 107,106,107
106 AYI=1.
107 YMAX(1)=AYI
110 CONTINUE
NQ=1
L=2
RMAX=1.E4
EPSJ=SQRT(ANOISE)
CRATE=1.
OLDLO=1.
RC=0.
MFOLD=0
METH=0
HOLD=h
MF=21
120 IF (MF-MFOLD) 122,150,122
122 MEO=METH
METH=MF/10
MIO=MITER
MITER=MF-10*METH
MFOLD=MF
IF (MITER-MIO) 123,124,123
123 IVEVAL=MITER
124 IF (METH-MEO) 125,150,125
125 IDOUB=L+1
IRET=1
130 CALL COSET
RC=RC*EL(1)/OLDLO
OLDLO=EL(1)
140 ELN=(TQ(1)*EPS)**2
E=(TQ(2)*EPS)**2
EUP=(TQ(3)*EPS)**2
ENL=(TQ(4)*EPS)**2
GOTO (160,170,200),IRET
150 IF (EPS-EPSOLD)152,160,152
152 IRET=1
GOTO 140
160 LMAX=MAXDER+1
EPSOLD=EPS
IF (H-HOLD) 162,200,162
162 RH=H/HOLD
H=HOLD
170 IF (RH-hMIN/ABS(H)) 171,172,172
171 RH=hMIN/ABS(H)
172 IF (RH-hMAX/ABS(H)) 174,174,173
173 RH=hMAX/ABS(H)
174 IF (RH-RMAX) 176,176,175
175 RH=RMAX
176 RI=1.
DO 181 J=2,L
RI=RI*RH
DO 180 I=1,N
Y(I,J)=Y(I,J)*RI
180 CONTINUE
181 CONTINUE
H=h*RH
RC=RC*RH
IDOUB=L+1
IF (T-TOLD) 690,200,690
200 IF (ABS(RC-1.)-.3) 202,202,201
201 IVEVAL=MITER
202 T=T+h

```

```
      IDO=1
      CALL DOLLOOP(IDO)
220    DO 230 I=1,N
      ERROR(I)=0.
230    CONTINUE
      M=0

C CALL DIFFUN WITH Y AND FSAVE(N1)
      IS=60+N
      CALL DIFFUN(0,IS)
      IF (IWEVAL)360,360,232
232    CALL PEDERV
      RX=-EL(1)*H
      DO 250 I=1,NSQ
      PW(I)=PW(I)*RX
250    CONTINUE
      DO 305 I=1,N
      M8=I*N1-NO
      PW(M8)=PW(M8)+1.
305    CONTINUE
      IWEVAL=0
      RC=1.
      CALL DECOMP(IER)
      IF (IER) 420,360,420
360    DO 370 I=1,N
      IF (M) 361,365,361
361    M8=I+NO
      IF (-H*FSAVE(M8)*100.-Y(I,1)) 365,365,420
365    M8=I+NO
      FSAVE(M8)=FSAVE(M8)*H-Y(I,2)-ERROR(I)
370    CONTINUE
C CALL SOLVE WITH PW,FSAVE(N1),FSAVE,PW(NSQ1)
      CALL SOLVE
      D=0.
      DO 390 I=1,N
      ERROR(I)=ERROR(I)+FSAVE(I)
      D=D+(FSAVE(I)/YMAX(1))**2
      FSAVE(I)=Y(I,1)+EL(1)*ERROR(I)
390    CONTINUE
      IF (M) 391,394,391
391    IF (.9*CRATE-D/D1) 392,392,393
392    CRATE=D/D1
      GO TO 394
393    CRATE=CRATE*.9
394    IF (1.-2.*CRATE) 395,396,396
395    RAG=1.
      GO TO 397
396    RAG=2.*CRATE
397    IF (D*RAG-END) 450,450,398
398    D1=D
      M=M+1
      IF (M-3) 399,420,399
C CALL DIFFUN WITH FSAVE AND FSAVE(N1)
399    IS=60+N
      CALL DIFFUN(60,IS)
      GO TO 360
420    IF (IWEVAL+1) 424,440,424
424    T=TOLD
      RMAX=2.
      IDO=-1
      CALL DOLLOOP(IDO)
      IF (ABS(H)-HMIN*1.00001) 680,680,436
436    RH=.25
      GO TO 170
```

-161-

```

440 IWEVAL=MITER
      GOTO 220
450 D=0.
      DO 460 I=1,N
      D=D+(ERROR(I)/YMAX(I))**2
460 CONTINUE
      IF (MITER) 461,462,461
461 IWEVAL=-1
462 IF (D-E) 463,463,500
463 KFLAG=0
      DO 471 J=1,L
      DO 470 I=1,N
      Y(I,J)=Y(I,J)+EL(J)*ERROR(I)
470 CONTINUE
471 CONTINUE
      DO 480 I=1,N
      YM=ABS(Y(I,1))
      IF (YMAX(I)-YM) 472,473,473
472 YMAX(I)=YM
473 IF (YM-1.) 480,480,474
474 IF (YM-.01*YMAX(I)) 475,480,480
475 YMAX(I)=YM
480 CONTINUE
      IF (IDOUB-1) 481,520,481
      IDOUB=IDOUB-1
      IF (IDOUB-1) 482,482,700
482 IF (NQ-MAXDER) 483,700,483
483 DO 490 I=1,N
      Y(I,LMAX)=ERROR(I)
490 CONTINUE
      GOTO 700
500 KFLAG=KFLAG-1
      T=TOLD
      IDO=-1
      CALL DOL00P(IDO)
      RMAX=2.
      IF (ABS(H)-HMIN*1.00001) 660,660,513
513 IF (KFLAG+3) 640,640,514
514 PR3=1.E20
      GOTO 540
520 PR3=1.E20
      IF (NQ-MAXDER) 521,540,521
521 D1=0.
      DO 530 I=1,N
      D1=D1+((ERROR(I)-Y(I,LMAX))/YMAX(I))**2
530 CONTINUE
      ENQ3=.5/FLOAT(L+1)
      PR3=((D1/EUP)**ENQ3)*1.4+1.4E-6
540 ENQ2=.5/FLOAT(L)
      PR2=((D1/E)**ENQ2)*1.2+1.2E-6
      PR1=1.E20
      IF (NQ-1) 541,560,541
541 D=0.
      DO 550 I=1,N
      D=D+(Y(I,L)/YMAX(I))**2
550 CONTINUE
      ENQ1=.5/FLOAT(NQ)
      PR1=((D/EDN)**ENQ1)*1.3+1.3E-6
560 IF (PR2-PR3) 570,570,561
561 IF (PR3-PR1) 590,570,570
570 IF (PR2-PR1) 571,571,580
571 NEWQ=NQ
      RH=1./PR2
      GOTO 620
580 NEWQ=NQ-1

```

```

RH=1./PR1
GOTO 620
590 NEWQ=L
RH=1./PR3
IF (RH-1.1) 610,591,591
591 DO 600 I=1,N
KLAG=NEWQ+1
Y(I,KLAG)=ERROR(I)*EL(L)/FLOAT(L)
600 CONTINUE
GOTO 630
610 ILOUB=10
GOTO 700
620 IF (KFLAG) 628,621,628
621 IF (RH-1.1) 610,628,628
628 IF (NEWQ-NQ) 630,170,630
630 NQ=NEWQ
L=NQ+1
IRET=2
GOTO 130
640 IF (KFLAG+9) 641,670,641
641 RH=.1
IF (HMIN/ABS(H)-RH) 643,643,642
642 RH=HMIN/ABS(H)
643 H=H*RH
C CALL DIFFUN WITH Y AND FSAVE
CALL DIFFUN(0,60)
DO 650 I=1,N
Y(I,2)=H*FSAVE(I)
650 CONTINUE
IWEVAL=MITER
ILOUB=10
IF (NQ-1) 651,200,651
651 NQ=1
L=2
IRET=3
GOTO 130
660 KFLAG=-1
GOTO 700
670 KFLAG=-2
GOTO 700
680 KFLAG=-3
GOTO 700
690 RMAX=10.
700 HOLD=H
JSTART=NQ
RETURN
END
```

SUBROUTINE DOLOOP(IDO)

```

COMMON NO,N,JFILL,FILL1,Y,FILL2,METH,NQ,MAXDER,RT
DIMENSION JFILL(47),FILL1(372),Y(10,6),FILL2(155),RT(4)
RIDO=FLOAT(IDO)
DO 10 J1=1,NQ
DO 10 J2=J1,NQ
J=NQ-J2+J1
DO 10 I=1,N
Y(I,J)=Y(I,J)+RIDO*Y(I,J+1)
10 CONTINUE
RETURN
END
```

-163-

SUBROUTINE DIFFUN(KK1, KK2)

C NAME CHANGE: PC>PR (USED IN COMMON ST. ONLY), Y>X,
 C FSAVE>X(60+), FSAVE(N)>X(60+N+)

```

COMMON NO, N, NR, NP, JFILL, IP, ITYPE
COMMON RS, A, S, TITLE, PHTN, ZL, FILL1, PHOT, PR,
1 SIG, R, FILL2, T, H, FILL3, X
DIMENSION JFILL(5), IP(10), ITYPE(30)
DIMENSION RS(30, 7), A(30), S(30), TITLE(7), FILL1(5),
1 SIG(10), R(30), FILL2(20), FILL3(24), X(220)
DO 90 I=1, N
X(I+KK2)=0.
90 CONTINUE
IF (NP) 3, 30, 3
3 SG=0.
DO 10 I=1, NP
K=IP(I)+KK1
SG=SG+SIG(I)*X(K)
10 CONTINUE
SG=SG*ZL
SS=SG*SG
IF (SG-.01) 12, 12, 11
11 PC=(1.-EXP(-SG))/SG
GOTO 13
12 PC=1.-SG*.5+SS*(.16666667-SG*.041666667+SS*.83333333E-3)
13 PHOT=PHTN*PC
30 DO 70 IR=1, NR
I=FIX(RS(IR, 1))
IF (I) 31, 70, 31
31 J=FIX(RS(IR, 2))
IF (I-99) 312, 311, 312
311 I=0
312 IF (J-99) 32, 40, 32
32 K=FIX(RS(IR, 3))
RT=R(IR)*X(I+KK1)*X(J+KK1)
RT=RT*X(K+KK1)
IF (J) 33, 34, 33
33 IRG=J+KK2
X(IRG)=X(IRG)-RT
34 IF (K) 35, 50, 35
35 IRG=K+KK2
X(IRG)=X(IRG)-RT
GOTO 50
40 RT=R(IR)*S(IR)*PHOT
RT=RT*X(I+KK1)
50 IF (I) 501, 502, 501
501 X(I+KK2)=X(I+KK2)-RT
502 DO 60 K=4, 7
I=FIX(RS(IR, K))
IF (I) 51, 70, 51
51 IRG=I+KK2
X(IRG)=X(IRG)+RT
60 CONTINUE
70 CONTINUE
K=N-1
X(N+KK2)=0.
DO 80 I=1, K
IRG=N+KK2
X(IRG)=X(IRG)+X(I+KK2)
80 CONTINUE
RETURN
END

```

SUBROUTINE SOLVE

C NAME CHANGES: PW>RU, (PW(N*N)>PS), FSAVE>X, FSAVE(N)>X(N+)

```
COMMON NO,N,JFILL
COMMON FILL1,FILL2,X,RU,RT
DIMENSION JFILL(47),FILL1(280),FILL2(152),X(20),
1 RU(110),RT(30)
NPI=N+1
NSQ=NO*NO
4 IP=IFIX(RU(NSQ+1))
X(1)=X(N+IP)
DO 20 I=2,N
IP=IFIX(RU(NSQ+I))
K=I-1
S=0.
DO 10 J=1,K
S=S+RU((J-1)*N+IP)*X(J)
10 CONTINUE
X(I)=X(N+IP)-S
20 CONTINUE
X(N)=X(N)*RU((N-1)*N+IP)
DO 40 K=2,N
I=NPI-K
IP=IFIX(RU(NSQ+I))
IPI=I+1
S=0.
DO 30 J=IPI,N
S=S+RU((J-1)*N+IP)*X(J)
30 CONTINUE
X(I)=(X(I)-S)*RU((I-1)*N+IP)
40 CONTINUE
RETURN
END
```

```
SUBROUTINE COSET
COMMON JFILL, FILL1, EL, TQ, P, METH, NQ, MAXDER, RT
DIMENSION JFILL(49), FILL1(562), EL(6), TQ(4), P(5, 3), RT(4)
P(1)=1.
P(2)=1.
P(3)=.5
P(4)=.1667
P(5)=.04167
P(6)=2.
P(7)=4.5
P(8)=7.333
P(9)=10.42
P(10)=13.7
P(11)=3.
P(12)=6.
P(13)=9.167
P(14)=12.5
P(15)=1.
EL(2)=1.
MAXDER=5
GOTO (201, 202, 203, 204, 205), NQ
201 EL(1)=1
GOTO 900
202 EL(1)=6.6666667E-01
EL(3)=3.3333333E-1
GOTO 900
203 EL(3)=5.4545454E-1
EL(1)=EL(3)
EL(4)=9.0909090E-2
GOTO 900
204 EL(1)=.48
EL(3)=.7
EL(4)=.2
EL(5)=.02
GOTO 900
205 EL(1)=4.3795620E-1
EL(3)=8.2116788E-1
EL(4)=3.1021897E-1
EL(5)=5.4744525E-2
EL(6)=3.6496350E-3
900 LO 910 K=1, 3
TQ(K)=P(NQ, K)
910 CONTINUE
TQ(4)=.5*TQ(2)/FLOAT(NQ+2)
RETURN
END
```

```
      SUBROUTINE DECOMP( IER )  
C  CHANGES IN NAMES:  PW>RLU, ( PW(N*N)>RIPS ), FSAVE>SCALES  
  
      COMMON NO,N,JFILL  
      COMMON FILL1, SCALES, RLU, RT  
      DIMENSION JFILL(47), FILL1(432), SCALES(20), RLU(110),  
      1 RT(30)  
      NSQ=NO*NO  
      IER=0  
      DO 50 I=1,N  
      RLU(NSQ+I)=FLOAT(1)  
      ROWNR=0.  
      DO 20 J=1,N  
      IF (ROWNR-ABS(RLU((J-1)*N+I))) 11,20,20  
11  ROWNR=ABS(RLU((J-1)*N+I))  
20  CONTINUE  
      J=NO  
      IF (ROWNR) 21,95,21  
21  SCALES(1)=1./ROWNR  
50  CONTINUE  
      NMI=N-1  
      DO 170 K=1,NMI  
      BIG=0.  
      DO 110 I=K,N  
      IP=IFIX(RLU(NSQ+I))  
      SIZE=ABS(RLU((K-1)*N+IP))*SCALES(IP)  
      IF (SIZE-BIG) 110,110,55  
55  BIG=SIZE  
      IVROW=1  
110  CONTINUE  
      IF (BIG) 112,96,112  
112  IF (IVROW-K) 114,150,114  
114  J=IFIX(RLU(NSQ+K))  
      RLU(NSQ+K)=RLU(NSQ+IVROW)  
      RLU(NSQ+IVROW)=FLOAT(J)  
150  KP=IFIX(RLU(NSQ+K))  
      PIVOT=RLU((K-1)*N+KP)  
      PIVOT=1./PIVOT  
      RLU((K-1)*N+KP)=PIVOT  
      KPI=K+1  
      DO 160 I=KPI,N  
      IP=IFIX(RLU(NSQ+I))  
      EM=RLU((K-1)*N+IP)*PIVOT  
      RLU((K-1)*N+IP)=EM  
      DO 160 J=KPI,N  
      RLU((J-1)*N+IP)=RLU((J-1)*N+IP)-EM*RLU((J-1)*N+KP)  
160  CONTINUE  
170  CONTINUE  
      IP=IFIX(RLU(NSQ+N))  
      PIVOT=RLU((N-1)*N+IP)  
      IF (PIVOT) 25,96,25  
25  RLU((N-1)*N+IP)=1./PIVOT  
      RETURN  
95  IER=1  
      RETURN  
96  IER=2  
      RETURN  
      END
```


APPENDIX B. EXPERIMENTAL DATA FOR THE $N_2O_5-O_3$ REACTION

The measured rate constants, $1/2(Kh)^{2/3}(2g)^{1/3}$, for the N_2O_5 catalyzed decomposition of ozone were summarized in Tables VIII and IX. In the experiments the concentrations of HNO_3 , N_2O_5 and O_3 were measured for 5 to 10 time points in a given kinetic run. These time points for each species were least-squares fit to third-order polynomials. Table XXI contains the polynomial coefficients from which the rate constants were calculated. The concentration of each species was evaluated by the equation:

$$c = a_0 + a_1t + a_2t^2 + a_3t^3 \quad (100)$$

where t = time in tenths of minutes. The standard deviation refers to how well the polynomial curves fit the experimental points. The rate constants were calculated for each one minute interval between $T(0)$ and $T(\text{final})$, and the average rate constant and its per cent standard deviation are included in Table XXI for each run.

Table XXI . Polynomial coefficients for reaction species concentrations in the N_2O_5 catalyzed decomposition of ozone.

Species	a_0	a_1	a_2	a_3	Stan. Dev.
# 1	T(0)= 18	T(FINAL)= 84 MIN.		0.547E-9 +/- 1.48%	
HN03	0.169321E+16	0.109022E+13	-0.491253E+09	0.195711E+06 +/-	0.13E+14
N2O5	0.213460E+16	-0.651254E+12	0.246446E+09	-0.994851E+05 +/-	0.30E+13
O3	0.308328E+17	-0.102987E+14	0.281352E+09	0.101669E+07 +/-	0.48E+14
# 2	T(0)= 18	T(FINAL)= 84 MIN.		0.561E-9 +/- 1.60%	
HN03	0.121295E+16	0.104098E+13	-0.194008E+09	0.586307E+05 +/-	0.11E+14
N2O5	0.148207E+16	-0.475401E+12	0.531950E+07	-0.333348E+04 +/-	0.30E+13
O3	0.754904E+17	-0.168980E+14	0.386559E+10	-0.503323E+06 +/-	0.17E+15
# 3	T(0)= 84	T(FINAL)= 146 MIN.		0.547E-9 +/- 0.56%	
HN03	0.121295E+16	0.104098E+13	-0.194008E+09	0.586307E+05 +/-	0.11E+14
N2O5	0.148207E+16	-0.475401E+12	0.531950E+07	-0.333348E+04 +/-	0.30E+13
O3	0.754904E+17	-0.168980E+14	0.386559E+10	-0.503323E+06 +/-	0.17E+15
# 4	T(0)= 18	T(FINAL)= 64 MIN.		2.972E-9 +/- 2.14%	
HN03	0.708731E+15	0.326985E+13	-0.154408E+10	0.604509E+06 +/-	0.10E+13
N2O5	0.123039E+16	-0.160657E+13	0.460749E+09	-0.569092E+05 +/-	0.30E+13
O3	0.651694E+17	-0.593458E+14	0.266675E+11	0.324836E+07 +/-	0.15E+15
# 5	T(0)= 18	T(FINAL)= 92 MIN.		2.891E-9 +/- 0.45%	
HN03	0.648933E+15	0.273047E+13	-0.964224E+09	0.307903E+06 +/-	0.11E+14
N2O5	0.145212E+16	-0.124690E+13	0.566252E+08	0.797870E+05 +/-	0.20E+13
O3	0.540627E+17	-0.636380E+14	0.383335E+11	-0.879094E+07 +/-	0.85E+14
# 6	T(0)= 18	T(FINAL)= 86 MIN.		2.808E-9 +/- 1.20%	
HN03	0.660756E+15	0.220435E+13	-0.311401E+09	0.891114E+05 +/-	0.70E+13
N2O5	0.190106E+16	-0.103458E+13	-0.847971E+08	0.109553E+06 +/-	0.50E+13
O3	0.505657E+17	-0.735137E+14	0.465733E+11	-0.122725E+08 +/-	0.15E+15
# 7	T(0)= 18	T(FINAL)= 38 MIN.		12.407E-9 +/- 5.29%	
HN03	0.105383E+16	0.734494E+12	0.633312E+10	-0.853711E+07 +/-	0.70E+13
N2O5	0.672766E+15	-0.171692E+13	0.195683E+10	-0.158872E+07 +/-	0.30E+13
O3	0.413938E+17	-0.147071E+15	0.244262E+12	-0.154364E+09 +/-	0.13E+15
# 8	T(0)= 18	T(FINAL)= 40 MIN.		12.305E-9 +/- 3.91%	
HN03	0.657679E+15	0.160500E+13	0.476662E+09	-0.163053E+07 +/-	0.20E+13
N2O5	0.475666E+15	-0.997930E+12	0.413494E+09	0.111372E+06 +/-	0.50E+12
O3	0.179023E+17	-0.630573E+14	0.948290E+11	-0.515577E+08 +/-	0.98E+14

Species	a_0	a_1	a_2	a_3	Stan. Dev.
# 9	T(0)= 24	T(FINAL)= 46 MIN.	0.488E-9	+/- 1.78%	
HN03	0.535481E+15	0.298779E+13	-0.308126E+10	0.117006E+07	+/- 0.30E+13
N205	0.929305E+15	-0.194412E+13	0.238162E+10	-0.119381E+07	+/- 0.50E+12
03	0.550141E+17	-0.780850E+13	0.342930E+10	0.000000E+00	+/- 0.92E+14
# 10	T(0)= 18	T(FINAL)= 52 MIN.	0.482E-9	+/- 1.04%	
HN03	0.445739E+15	0.206804E+13	-0.197273E+09	-0.567159E+06	+/- 0.30E+13
N205	0.128181E+16	-0.114356E+13	-0.160375E+09	0.579618E+05	+/- 0.50E+13
03	0.605422E+17	-0.104133E+14	0.296733E+10	0.153911E+06	+/- 0.40E+14
# 11	T(0)= 18	T(FINAL)= 84 MIN.	0.462E-9	+/- 1.34%	
HN03	0.422191E+15	0.153886E+13	0.809281E+08	-0.133960E+06	+/- 0.24E+14
N205	0.155654E+16	-0.101330E+13	0.639919E+08	0.585640E+05	+/- 0.30E+13
03	0.696977E+17	-0.135841E+14	0.507668E+10	-0.135101E+07	+/- 0.93E+14
# 12	T(0)= 18	T(FINAL)= 60 MIN.	0.504E-9	+/- 2.52%	
HN03	0.333935E+15	0.155544E+13	-0.106548E+09	-0.102114E+06	+/- 0.60E+13
N205	0.144287E+16	-0.880614E+12	-0.346798E+08	0.913959E+05	+/- 0.10E+13
03	0.329138E+17	-0.657700E+13	-0.237306E+10	0.369561E+07	+/- 0.32E+14
# 13	T(0)= 18	T(FINAL)= 64 MIN.	0.499E-9	+/- 2.14%	
HN03	0.365468E+15	0.151042E+13	-0.469879E+09	0.207856E+06	+/- 0.40E+13
N205	0.128942E+16	-0.127702E+13	0.127124E+10	-0.747377E+06	+/- 0.50E+13
03	0.671012E+17	-0.117839E+14	0.250325E+10	0.581892E+06	+/- 0.38E+14
# 14	T(0)= 18	T(FINAL)= 46 MIN.	0.479E-9	+/- 1.67%	
HN03	0.329697E+15	0.154350E+13	-0.847288E+09	0.914833E+05	+/- 0.10E+13
N205	0.690619E+15	-0.771795E+12	0.380205E+09	0.246478E+05	+/- 0.10E+13
03	0.413597E+17	-0.570984E+13	0.209919E+10	0.000000E+00	+/- 0.13E+15
# 15	T(0)= 20	T(FINAL)= 56 MIN.	2.558E-9	+/- 3.41%	
HN03	0.703342E+15	0.216259E+13	-0.961426E+09	0.160507E+06	+/- 0.70E+13
N205	0.862340E+15	-0.994688E+12	0.258299E+09	0.655498E+05	+/- 0.10E+13
03	0.360191E+17	-0.345708E+14	0.265600E+11	-0.915131E+07	+/- 0.14E+15
# 16	T(0)= 18	T(FINAL)= 60 MIN.	2.632E-9	+/- 2.04%	
HN03	0.533865E+15	0.154140E+13	-0.103172E+09	-0.142133E+06	+/- 0.60E+13
N205	0.915486E+15	-0.715109E+12	-0.308786E+08	0.114734E+06	+/- 0.10E+13
03	0.283821E+17	-0.297613E+14	0.179942E+11	-0.429826E+07	+/- 0.47E+14
# 17	T(0)= 18	T(FINAL)= 56 MIN.	2.597E-9	+/- 1.66%	
HN03	0.472730E+15	0.153163E+13	-0.590785E+09	0.358991E+06	+/- 0.60E+13
N205	0.891078E+15	-0.758179E+12	0.299827E+09	-0.178333E+06	+/- 0.10E+13
03	0.367824E+17	-0.349230E+14	0.224466E+11	-0.754092E+07	+/- 0.12E+15

Species	a_0	a_1	a_2	a_3	Stan. Dev.
# 18	T(0)= 18	T(FINAL)= 34 MIN.	10.986E-9	+/- 2.47%	
HN03	0.369742E+15	0.198933E+13	-0.177495E+10	0.619479E+06	+/- 0.40E+13
N205	0.393738E+15	-0.953736E+12	0.926317E+09	-0.384456E+06	+/- 0.10E+13
03	0.543664E+17	-0.107835E+15	0.137744E+12	-0.712854E+08	+/- 0.33E+14
# 19	T(0)= 18	T(FINAL)= 40 MIN.	10.818E-9	+/- 4.28%	
HN03	0.375325E+15	0.224987E+13	-0.199415E+10	0.938322E+06	+/- 0.80E+13
N205	0.605516E+15	-0.995185E+12	0.654214E+09	-0.199019E+06	+/- 0.20E+13
03	0.479075E+17	-0.130844E+15	0.163348E+12	-0.774428E+08	+/- 0.14E+15
# 20	T(0)= 18	T(FINAL)= 40 MIN.	11.089E-9	+/- 3.89%	
HN03	0.335371E+15	0.207573E+13	-0.108953E+10	0.572157E+06	+/- 0.20E+13
N205	0.972375E+15	-0.851553E+12	0.168457E+09	0.337127E+05	+/- 0.10E+13
03	0.623000E+17	-0.219733E+15	0.293923E+12	-0.143510E+09	+/- 0.12E+15
# 21	T(0)= 18	T(FINAL)= 44 MIN.	0.546E-9	+/- 6.80%	
HN03	0.463098E+15	0.195412E+13	-0.431716E+09	0.190360E+06	+/- 0.50E+13
N205	0.113877E+16	-0.974807E+12	0.142330E+09	-0.283576E+05	+/- 0.10E+13
03	0.840991E+17	-0.156530E+14	0.952028E+10	-0.511475E+07	+/- 0.64E+14
# 22	T(0)= 18	T(FINAL)= 50 MIN.	0.484E-9	+/- 2.46%	
HN03	0.613279E+15	0.122342E+13	0.652151E+09	-0.799744E+06	+/- 0.60E+13
N205	0.117267E+16	-0.667732E+12	-0.162499E+09	0.246421E+06	+/- 0.12E+13
03	0.768241E+17	-0.137972E+14	0.692767E+10	-0.278627E+07	+/- 0.64E+14
# 23	T(0)= 38	T(FINAL)= 60 MIN.	0.494E-9	+/- 2.30%	
HN03	0.442201E+15	0.220675E+13	-0.103909E+10	0.535687E+06	+/- 0.60E+13
N205	0.127422E+16	-0.105433E+13	0.385268E+09	-0.173276E+06	+/- 0.20E+13
03	0.764915E+17	-0.210119E+14	0.196440E+11	-0.101697E+08	+/- 0.43E+14
# 24	T(0)= 18	T(FINAL)= 68 MIN.	0.436E-9	+/- 1.03%	
HN03	0.264901E+16	0.266926E+13	-0.173884E+10	0.777982E+06	+/- 0.14E+14
N205	0.105323E+16	-0.142584E+13	0.914925E+09	-0.399208E+06	+/- 0.31E+13
03	0.829575E+17	-0.100274E+14	0.363792E+10	-0.164719E+06	+/- 0.45E+14
# 25	T(0)= 30	T(FINAL)= 62 MIN.	0.494E-9	+/- 2.24%	
HN03	0.244037E+16	0.157951E+13	-0.387319E+09	-0.091914E+05	+/- 0.91E+10
N205	0.110219E+16	-0.120445E+13	0.528744E+09	-0.191728E+06	+/- 0.20E+13
03	0.837520E+17	-0.139356E+14	0.436902E+10	-0.525243E+05	+/- 0.15E+14
# 26	T(0)= 18	T(FINAL)= 46 MIN.	0.445E-9	+/- 1.91%	
HN03	0.251354E+16	0.170593E+13	0.344130E+09	-0.721530E+06	+/- 0.57E+13
N205	0.111919E+16	-0.989570E+12	0.305072E+09	-0.115390E+06	+/- 0.12E+13
03	0.816871E+17	-0.103781E+14	0.177311E+10	0.533267E+06	+/- 0.99E+14

<u>Species</u>	<u>a₀</u>	<u>a₁</u>	<u>a₂</u>	<u>a₃</u>	<u>Stan. Dev.</u>
# 27	T(0)= 18	T(FINAL)= 56 MIN.		0.476E-9 +/- 1.52%	
IN03	0.385707E+16	0.261129E+13	-0.137911E+10	0.993287E+06 +/-	0.22E+14
N205	0.164574E+16	-0.129553E+13	0.331092E+09	-0.942437E+05 +/-	0.59E+12
03	0.823730E+17	-0.161654E+14	0.551171E+10	-0.314866E+06 +/-	0.57E+14
# 23	T(0)= 18	T(FINAL)= 58 MIN.		0.487E-9 +/- 1.80%	
IN03	0.329514E+16	0.191651E+13	-0.601733E+09	0.480776E+06 +/-	0.13E+14
N205	0.197896E+16	-0.102903E+13	0.208899E+09	-0.464329E+05 +/-	0.26E+13
03	0.793321E+17	-0.162275E+14	0.180701E+10	0.607356E+06 +/-	0.53E+14
# 29	T(0)= 20	T(FINAL)= 56 MIN.		0.472E-9 +/- 2.50%	
IN03	0.379145E+16	0.174504E+13	0.449050E+09	-0.365192E+06 +/-	0.17E+14
N205	0.165402E+16	-0.116823E+13	0.334295E+09	-0.145596E+06 +/-	0.75E+12
03	0.744395E+17	-0.157347E+14	0.621577E+10	-0.933922E+06 +/-	0.52E+14
# 30	T(0)= 18	T(FINAL)= 58 MIN.		0.460E-9 +/- 1.42%	
IN03	0.351490E+16	0.175912E+13	0.217502E+09	-0.258496E+06 +/-	0.11E+14
N205	0.153003E+16	-0.100221E+13	0.211042E+09	-0.121964E+06 +/-	0.72E+12
03	0.858253E+17	-0.162405E+14	0.694003E+10	-0.231640E+07 +/-	0.59E+14
# 31	T(0)= 26	T(FINAL)= 60 MIN.		0.484E-9 +/- 0.68%	
IN03	0.247250E+16	0.173219E+13	-0.417206E+09	0.216996E+06 +/-	0.15E+14
N205	0.193666E+16	-0.903711E+12	0.234856E+09	-0.125711E+06 +/-	0.49E+13
03	0.771922E+17	-0.185311E+14	0.751392E+10	-0.346046E+07 +/-	0.48E+14

REFERENCES

1. Philip A. Leighton, Photochemistry of Air Pollution (Academic Press, NY, 1961), pp. 26-71.
2. Harold Johnston, Science 173, 517 (1971).
3. D. G. Murcray, T. G. Kyle, F. M. Murcray and W. J. Williams, J. Opt. Soc. Amer. 59, 1131 (1969).
4. R. Dalmon, Mem. Serv. chim. etat. 30, 141 (1943).
5. S. C. Schmidt, R. C. Amme, D. G. Murcray, A. Goldman and F. S. Bonomo, Nature (London), Phys. Sci. 238, 109 (1972).
6. Harold Johnston and Richard Graham, J. Phys. Chem. 77, 62 (1973).
7. F. Biauume, J. Photochem. 2, 139 (1973/74).
8. G. S. Beddard, D. J. Giachardi and R. P. Wayne, J. Photochem. 3, 321 (1974/75).
9. G. Porter, J. Chem. Phys. 19, 1278 (1951).
10. P. Tarte, Bull. Soc. Chim. Belges 59, 365 (1950).
11. G. W. King and D. Moule, Can. J. Chem. 40, 2057 (1962).
12. R. A. Cox, J. Photochem. 3, 175 (1974).
13. R. A. Cox, J. Photochem. 3, 291 (1974/75).
14. T. C. Hall and F. E. Blacet, J. Chem. Phys. 20, 1745 (1952).
15. T. Nakayama, M. Y. Kitamura, and K. Watanabe, J. Chem. Phys. 30, 1180 (1959).
16. E. J. Jones and O. R. Wulf, J. Chem. Phys. 5, 873 (1937).
17. G. Sprenger, Z. Elektrochem. 37, 674 (1931).
18. Gary Schott and N. Davidson, J. Am. Chem. Soc. 80, 1841 (1958).
19. D. A. Ramsay, Proc. Colloq. Spectroscopy Int., 10th, 583 (1962).
20. F. Cramarossa and H. S. Johnston, J. Chem. Phys. 43, 727 (1965).

21. H. J. Schumacher and G. Sprenger, Z. Physik. Chem. 2B, 266 (1929).
22. H. S. Johnston, Gas Phase Reaction Rate Theory (Ronald Press Co., NY, 1966), p. 14-32.
23. M. E. Nordberg, Science 70, 580 (1929).
24. T. M. Lowry and R. V. Seddon, J. Chem. Soc., 1461 (1938).
25. D. J. Wuebbles and J. S. Chang, J. Geophys. Res. 80, 2637 (1975).
26. O. R. Wulf, F. Daniels and S. Karrer, J. Am. Chem. Soc. 44, 298 (1922).
27. H. S. Johnston and D. M. Yost, J. Chem. Phys. 17, 386 (1949).
28. H. S. Johnston, Ph. D. Thesis, California Institute of Technology (1948).
29. H. W. Ford, G. J. Doyle and N. Endow, J. Chem. Phys. 26, 1336 (1957).
30. D. H. Stedman and H. Niki, J. Phys. Chem. 77, 2604 (1973).
31. J. A. Ghormley, R. L. Ellsworth and C. J. Hochanadel, J. Phys. Chem. 77, 1341 (1973).
32. P. M. Scott, K. F. Preston, R. J. Andersen and L. M. Quick, Can. J. Chem. 49, 1808 (1971).
33. C. H. Wu, E. D. Morris, Jr. and H. Niki, J. Phys. Chem. 77, 2507 (1973).
34. R. A. Graham and H. S. Johnston, J. Chem. Phys. 60, 4628 (1974).
35. D. D. Davis, J. Prusaczyk, M. Dwyer and P. Kim, J. Phys. Chem. 78, 1775 (1974).
36. J. T. Herron and R. E. Huie, Int. J. Mass Spectrom. Ion Physics 16, 125 (1975).
37. F. Daniels and E. H. Johnston, J. Am. Chem. Soc. 43, 53 (1921).
38. R. A. Ogg, Jr., J. Chem. Phys. 15, 337, 613 (1947).
39. R. A. Ogg, Jr., J. Chem. Phys. 18, 572 (1950).

40. H. S. Johnston and Yu-sheng Tao, *J. Am. Chem. Soc.* 73, 2948 (1951).
41. J. H. Smith and F. Daniels, *J. Am. Chem. Soc.* 69, 1735 (1947).
42. R. L. Mills and H. S. Johnston, *J. Am. Chem. Soc.* 73, 938 (1951).
43. H. S. Johnston and R. L. Perrine, *J. Am. Chem. Soc.* 73, 4782 (1951).
44. H. S. Johnston, *J. Am. Chem. Soc.* 75, 1567 (1953).
45. D. J. Wilson and H. S. Johnston, *J. Am. Chem. Soc.* 75, 5763 (1953).
46. R. L. Mills, Ph. D. Thesis, Stanford University (1951).
47. H. S. Johnston, private communication.
48. I. C. Hisatsune, B. Crawford, Jr. and R. A. Ogg, Jr., *J. Am. Chem. Soc.* 79, 4648 (1957).
49. Alan B. Harker and H. S. Johnston, *J. Phys. Chem.* 73, 1153 (1973).
50. D. Garvin and R. F. Hampson, ed., Chemical Kinetics Data Survey, NBSIR 74-430 (1974).
51. S. W. Benson, The Foundations of Chemical Kinetics (McGraw-Hill Book Co., Inc., NY, 1960), pp. 408-418.
52. D. D. Wagman, W. H. Evans, V. B. Parker, I. Halow, S. M. Bailey and R. H. Schumm, NBS Technical Note 270-3, 1968.
53. R. F. Murphy, Ph. D. Thesis, University of California, Los Angeles (1969).
54. E. Castellano and H. J. Schumacher, *J. Chem. Phys.* 36, 2238 (1962).
55. E. Castellano and H. J. Schumacher, *Z. Physik Chem.* 34, 198 (1962).
56. A. C. Hindmarsh, Lawrence Livermore Laboratory Report UCID-30001 Rev., 1 (1972).
57. A. B. Harker, Reaction Kinetics of the Photolysis of NO_2 , and the Spectra and Reaction Kinetics of the Free Radicals in the Photolysis of the $\text{Cl}_2\text{-O}_2\text{-CO}$ System (Ph. D.), LBL-1114, Sept. 1972.

58. T. T. Paukert, Spectra and Kinetics of the Hydroperoxyl Free Radical in the Gas Phase (Ph. D.), UCRL-19109, November 1969.
59. E. D. Morris, Jr., Ph. D. Thesis, University of California, Berkeley (1968).
60. E. D. Morris, Jr. and H. S. Johnston, Rev. Sci. Instrum. 39, 620 (1968).
61. R. A. Graham, submitted to DECUS.
62. G. Z. Whitten, Rate Constant Evaluations Using a New Computer Modelling Scheme, paper presented at ACS National Meeting (Spring, 1974).
63. A. P. Altshuller, J. Phys. Chem. 61, 251 (1957).
64. D. M. Waldorf and E. L. Balb, J. Chem. Phys. 39, 432 (1963).
65. F. H. Verhoek and F. Daniels, J. Am. Chem. Soc. 53, 1250 (1931).
66. E. D. Morris, Jr. and H. Niki, J. Phys. Chem. 77, 1929 (1973).
67. A. C. Jenkins, Laboratory Techniques for Handling High-Concentration Liquid Ozone in Ozone Chemistry and Technology--Advances in Chemistry No. 21 (1959), p. 13.
68. M. Griggs, J. Chem. Phys. 49, 857 (1968).
69. T. Boddington and D. Gray, Proc. Roy. Soc. Lond. A. 320, 71 (1970).
70. P. G. Ashmore, B. J. Tyler and T. A. B. Wesley, 11th Int. Symp. on Combustion, 1133 (1967).
71. R. C. L. Bosworth, Heat Transfer Phenomena (John Wiley & Sons, Inc., NY, 1952), p. 99.
72. J. C. DeVos, Physics XX, 690 (1954).
73. G. A. W. Rutgers and J. C. DeVos, Physics XX, 715 (1954).

74. James N. Pitts, Jr., James H. Sharp and Sunney I. Chan,
J. Chem. Phys. 42, 3655 (1964).
75. Harold S. Johnston and Richard Graham, Can. J. Chem. 52, 1415 (1974).
76. J. C. Greaves and D. Garvin, J. Chem. Phys. 30, 348 (1959).
77. M. A. A. Clyne, B. A. Thrush, and R. P. Wayne, Trans. Faraday
Soc. 60, 359 (1964).
78. E. D. Morris, Jr. and H. Niki, J. Phys. Chem. 78, 1337 (1974).
79. A. D. Walsh, J. Chem. Soc., 2306 (1953).
80. John F. Olsen and Louis Burnelle, J. Am. Chem. Soc. 92, 3659 (1970).
81. K. Nakamoto, Infrared Spectra of Inorganic and Coordination
Compounds (John Wiley & Sons, Inc., NY, 1963), p. 92.
82. I. T. N. Jones and Kyle D. Bayes, J. Chem. Phys. 59, 4836 (1973).

LEGAL NOTICE

This report was prepared as an account of work sponsored by the United States Government. Neither the United States nor the United States Energy Research and Development Administration, nor any of their employees, nor any of their contractors, subcontractors, or their employees, makes any warranty, express or implied, or assumes any legal liability or responsibility for the accuracy, completeness or usefulness of any information, apparatus, product or process disclosed, or represents that its use would not infringe privately owned rights.

TECHNICAL INFORMATION DIVISION
LAWRENCE BERKELEY LABORATORY
UNIVERSITY OF CALIFORNIA
BERKELEY, CALIFORNIA 94720